2024-07

Petrographic and Geochemical Characteristics of Medium to Highgrade Metamorphic and Associated Intrusive Rocks in the Konso Zone (Kholme Cluster Tebelana & Quchele Kebele)

Mulatu, Hana

BAHIR DAR UNIVERSITY

GRADUATE STUDIES OFFICE

SCHOOL OF EARTH SCIENCES

DEPARTMENT OF GEOLOGY

PETROGRAPHIC AND GEOCHEMICAL CHARACTERISTICS OF MEDIUM TO HIGH-GRADE METAMORPHIC AND ASSOCIATED INTRUSIVE ROCKS IN THE KONSO ZONE (KHOLME CLUSTER TEBELANA & QUCHELE KEBELE)

By

Hana Mulatu Afeta

July, 2024

Bahir Dar, Ethiopia

BAHIR DAR UNIVERSITY

SCHOOL OF EARTH SCIENCES

DEPARTMENT OF GEOLOGY

PETROGRAPHIC AND GEOCHEMICAL CHARACTERISTICS OF MEDIUM TO HIGH-GRADE METAMORPHIC AND ASSOCIATED INTRUSIVE ROCKS IN THE KONSO ZONE (KHOLME CLUSTER TEBELANA & QUCHELE KEBELE)

A THESIS SUBMITTED TO THE SCHOOL OF EARTH SCIENCES, BAHIR DAR UNIVERSITY, IN PARTIAL FULFILLMENT OF THE REQUIREMENTS FOR THE DEGREE OF MASTERS OF SCIENCE IN PETROLOGY

By

Hana Mulatu Afeta

Advisor

Minyahl Teferi (Ph.D.)

July, 2024

Bahir Dar, Ethiopia

BAHIR DAR UNIVERSITY

SCHOOL OF EARTH SCIENCES

DEPARTMENT OF GEOLOGY

Thesis Approval for Defense

I hereby certify that I have supervised, read, and evaluated this thesis/dissertation entitled "**PETROGRAPHIC AND GEOCHEMICAL CHARACTERISTICS OF MEDIUM TO HIGH-GRADE METAMORPHIC AND ASSOCIATED INTRUSIVE ROCKS IN THE KONSO ZONE (KHOLME CLUSTER TEBELANA & QUCHELE KEBELE**)" by Hana Mulatu prepared under my guidance. I recommend the thesis/dissertation be submitted for oral defense.

Minyahl Teferi (Ph.D.) ____________________ ____________________ ____________

Advisor Name Signature Date

BAHIR DAR UNIVERSITY

SCHOOL OF EARTH SCIENCES

DEPARTMENT OF GEOLOGY

Approval of the thesis for defense result

We hereby certify that we have examined this dissertation/thesis entitled "Petrographic and geochemical characteristics of medium to high-grade metamorphic and associated intrusive rocks in the Konso zone (Kholme cluster Tebelana & Quchele kebele)" by Hana Mulatu, we recommend that the thesis is approved for the degree of "Masters in petrology".

Board of Examiners

Prof.Gezahagn Yirgu

______________________	________________	_____________
External examiner's name	Signature	Date

Mr. Gshaw wudie
(Asst prof)

______________________	________________	_____________
Internal examiner's name	Signature	Date

Mr. Ayenachew Alemayehu

______________________	________________	_____________
Chairperson name	Signature	Date

DECLARATION OF ORIGINALITY

I hereby declare that this thesis is my original paper entitled "**Petrographic and geochemical characteristics of medium to high-grade metamorphic and associated intrusive rocks in the Konso zone (Kholme cluster Tebelana & Quchele kebele)**" which was prepared by me, with the supervision of Dr. Minyahl Teferi, school of Earth Science, Bahir Dar University during the year 2023/2024. This thesis is my original work and has not been presented for any qualification in any other university or institute, and all sources of data used for the thesis work have been properly acknowledged.

Hana Mulatu	____________	_____________
M.Sc Candidate	Signature	Date

ACKNOWLEDGMENT

First and foremost, I am deeply grateful to my Almighty God. My faith has been a constant source of inspiration and strength throughout this journey. With God's grace, I believe anything is achievable.

My sincere and immense gratitude goes to my advisor, Dr. Minyahl Teferi. Throughout this entire project, Dr. Minyahl Teferi has provided invaluable support. His consistent advice, guidance, and encouragement were instrumental in shaping my research. He generously dedicated his time to following my progress, offering valuable suggestions, and helping me navigate every stage of my thesis work. I am deeply indebted to his mentorship and dedication.

I am grateful to Arba Minch University for the opportunity to pursue my Master of Science degree and for providing financial assistance that made it possible.

My sincere appreciation goes to my exceptional team members: Mr. Gosaye B., Mr. Habtamu W., Mr. Asmamaw H., Mr. Muleken F., and Mr. Talema M. Their willingness to participate and collaborative spirit during field data collection were crucial to the success of this work. I am fortunate to have worked alongside such dedicated individuals.

I would like to extend my appreciation to the personnel of the School of Earth Science at Bahir Dar University for their contributions to the foundational knowledge that underpinned this research.

Also, I would like to acknowledge my friends Ms. Kidist Tesfa, Mr. Gezeadis Tesfa, Mr. Atinkut Kelemu, Mr. Ayene Yilak, Ms. Awokech Abebaw, and Ms. Hana Abera for their insightful suggestions and support in developing this thesis work.

Finally, I am deeply grateful to my entire family and my husband Endalkachew Abebaw for their unwavering support and their constant well wishes. They have been a source of strength throughout my academic journey.

ABSTRACT

This study investigated the petrographic and geochemical characteristics of metamorphic and intrusive rocks in the Kholme Cluster, Konso Zone, Southwestern Ethiopia. Fieldwork, petrographic analysis, and geochemical evaluations were employed to achieve this objective. The dominant geological units in the study area are high- to medium-grade metamorphic rocks, including granitic gneiss, amphibole gneiss, and biotite gneiss. Additionally, intrusive granite rocks are present. Petrographic analysis revealed compositional banding within the gneiss units. Hornblende, plagioclase, biotite, and quartz were identified as the primary mineral assemblage, with minor amounts of opaque minerals. Field observations and structural measurements indicated various geological structures, such as foliation, folds, joints, dikes, boudinage, veins, and veinlets. These structures are attributed to multi-phase deformation events and play a significant role in the metamorphic processes. Geochemical analysis revealed that most granitic gneiss units fall within the calc-alkaline series on the AFM ternary diagram, except for amphibole gneiss, which plots within the tholeiitic series. All studied rocks, except one sample, displayed geochemical signatures indicative of igneous origins. And exhibited geochemical characteristics suggestive of a sedimentary source. The enrichment of large-ion lithophile elements (LILE) relative to high-field-strength elements (HFSE) in both gneisses and granitoids points towards subduction zone enrichment and crustal contamination of the source region. Harker diagrams for the granite units did not reveal a clear geochemical trend, although they suggested the influence of crystal fractionation processes. The scattered trends are likely due to the pervasive metamorphic alteration within the area. Geochemically, the granites are characterized as high-potassium, calc-alkaline, and peraluminous, indicating magma activity derived from mixed sources. The rare earth element (REE) patterns displayed a slight enrichment in heavy rare earth elements (HREEs), reflecting the acidic nature of the rocks. The negative europium anomaly observed in the granites suggests plagioclase fractionation. Discrimination diagrams utilizing Rb-(Y+Nb), Ta-Yb, Rb-(Y+Nb), and Nb-Y ratios suggest that the granites formed in a volcanic arc or syn-collisional granite (syn-COLG) tectonic setting. However, one sample was plotted within the within-plate granite (WPG) field.

Keywords: Kholme cluster, Protolith, Geochemistry, Granite, Petrogenesis

TABLE OF CONTENTS

ACKNOWLEDGMENT iv
ABSTRACT v
TABLE OF CONTENTS vi
LIST OF FIGURES ix
LIST OF TABLE xi
LIST OF ACRONYMS xii
CHAPTER ONE 2
1. INTRODUCTION 2
1.1. Background 2
1. 2. Description of the study area 3
1.2.1. Location and Accessibility 3
1.2.2. Physiography and Climate 4
1.3. Statement of the Problem and Research Questions 5
1.4. Objectives of the study 7
1.4.1. General Objective 7
1.4.2. Specific Objectives 7
1.5. Scope of the Study 7
1.6. Methodology 7
1.6.1. Field investigation 8
1.6.2. Petrographic analysis 8
1.6.3. Geochemical analysis 8
1.7. Relevance of the Study 10
CHAPTER TWO 12
2. REGIONAL GEOLOGICAL SETTING 12
2.1. Introduction 12
2.2. Geodynamic Evolution of East African Orogeny 12
2.2.1. Arabian-Nubian Shield (ANS) 13
2.2.2. Mozambique belt (MB) 15
2.3. Precambrian Geological Evolution of Southern Western Ethiopia 15
2.3.1. Moyale-Sololo complex 17
2.3.2. Adola complex 17
2.3.3. Genale-dolo complex 18
2.3.4. Burji–Finchaa complex 18

CHAPTER THREE 20
3. GEOLOGY OF THE AREA: FIELD AND PETROGRAPHIC AND METAMORPHISM 20
3.1. Introduction 20
3.2. Field description of rocks in the study area 20
3.2.1. Biotite gneiss 20
3.2.2. Amphibole gneiss 21
3.2.3. Granitic gneiss 22
3.2.4. Mica schist 23
3.2.5. Granite 24
3.3. Petrographic description of rocks in the study area 25
3.3.1. Amphibole gneiss 25
3.3.2. Granitic gneiss 26
3.3.3. Granite 29
3.3.4. Mica schist 31
3.3.5. Biotite gneiss 33
3.4. Geological Structures of the area 34
3.4.1. Foliation 34
3.4.2. Fold 35
3.4.3. Joint 37
3.4.4. Boudinage 38
3.4.5. Ductile shear sense indicators 38
3.5. Metamorphism 41
CHAPTER FOUR 42
4. GEOCHEMISTRY OF THE AREA 42
4.1. Introduction 42
4.2. Geochemistry of Rocks 43
4.2.1. Major Elements Geochemistry and Rock Classification 43
4.2.2. Trace Elements of Geochemistry 48
4.2.3. Rare Earth Elements Geochemistry 51
4.2.4. Protoliths of Metamorphic Rocks 53
4.2.5. Tectonic Setting of Intrusive Rock 55
CHAPTER FIVE 58
5. DISCUSSION 58
5.1. Fractional Crystallization 58

5.2. Mantle Source Characteristics 58
5.3. Degree of Partial Melting and Depth of Melting 59
5.4. Crustal Contamination 59
CHAPTER SIX 61
6. CONCLUSION AND RECOMMENDATION 61
6.1. Conclusion 61
6.2 Recommendation 62
REFERENCE 63
APPENDICES 68

LIST OF FIGURES

Figure 1: Location map of the study area....4
Figure 2: Physiographic map of the study area....5
Figure 3: Geological map of Precambrian basement rocks in Southern Ethiopia adopted from Asrat et.al. (2001)....6
Figure 4: Generalized flow chart showing overall methodological approaches that will be employed in the study area....10
Figure 5: A Thematic sketch of the tectonic evolution of the East African Orogen that resulted in the greater Gondwana Supercontinent (adopted from Stern et al., 2006)....13
Figure 6: Map of the East African orogen showing the location of the Arabian-Nubian shield relative to theMozambique Belt and adjacent cationic margins (adopted from Abdelsalam et al., 2011; Stern et al., 2012)....14
Figure 7: Geological map of Ethiopia (adopted from EIGS, 1996)....17
Figure 8: Field photograph of Biotite gneiss exposed at the hillside and river cut....21
Figure 9: Amphibole genesis exposed on the hilltop and stream cut....22
Figure 10: Field photograph of Granitic gneiss exposed at the hillside and stream cut. 23
Figure 11: Representative Field photographs of Mica schist exposed at hilltop and river cut.. 24
Figure 12: Field photograph of granite exposed at stream cut and hillside 25
Figure 13: Representative Photomicrograph of Amphibolite gneiss in XPL and PPL under 4x magnification....26
Figure 14: Representative Photomicrograph of granite gneiss in XPL and PPL 29
Figure 15: Representative Photomicrograph of granite in XPL and PPL under 4x magnification....31
Figure 16: Representative photomicrographs under (XPL & PPL) of Mica schist....32
Figure 17: Photograph that shows quartz inclusion in poikilitic texture....34
Figure 18: Shows **A)** foliation, **B)** Stereo plots of planes to the foliation, **C)** Stereo plots of the pole to foliation and rose diagram **D)** Kamb counters plot foliation of data....35
Figure 19: **A)** Red arrow shows ptygmatic fold and red arrows small scale M fold, **B)** Synformal fold, and **C)**Recumbent fold....36
Figure 20: Fold structure shows **A)** Antiformal fold and **B)** Recumbent fold....36
Figure 21: A) Point data of lineation and B) Rose diagram of lineation....37
Figure 22:A) Field photograph of Joint structure B) Sstereonetplot of a plane to joint and C) Rose diagram of joint....37
Figure 23: Boudinage structure....38

Figure 24: A) Mica fish structure showing dextral shearing, B and C) Small scale S fold structure showing sinistral shearing 39
Figure 25: Geological map of the study area 40
Figure 26: Harker variation diagram of SiO_2 vs major oxides for the studied rock 45
Figure 27: The AFM triangular diagram used to differentiate calc-alkaline series (CA) to tholeiitic series (TH) of orthogneiss rock of the study area 46
Figure 28: **(A)** Chemical classification diagram for granite rock of the study area based on TAS (after Peccerillo and Taylor, 1976). 48
Figure 29: Variation diagram of SiO_2 vs selected trace elements for the studied rocks. 50
Figure 30: **A)** Primitive mantle-normalized trace elements diagrams from McDonough and Sun (1995). **B)** Chondrite-normalized REE spider diagrams used by Boynton (1984) of the studied rocks. 53
Figure 31: Element mobility and protolith reconstruction diagrams for the Kolme metamorphic rocks.. 55
Figure 32: Y+Nb vs Rb; Y vs Nb; Ta+Yb vs Rb, and Yb vs Ta tectonic discrimination diagrams of Pearce et al. (1984) 57

LIST OF TABLE

Table 1: Chemical analysis of the selected samples where Major and minor oxides expressed in wt% and trace elements in ppm.. 42

LIST OF ACRONYMS

ALS	Australian Laboratory Science
ANS	Arabian-Nubian Shield
EAO	East African Orogen
GCD	Geochemical data kit tool
GPS	Global Positioning System
HFSE	High Field Strength Elements
HREE	Heavy Rare Earth Elements
ICP-AES	Inductively Coupled Plasma Atomic-Emission Spectrometry
ICP-MS	Inductively Coupled Plasma Mass Spectrometry
LILEs	Large Ion Lithophile Elements
LOI	Loss on Ignition
LREE	Light Rare Earth Elements
MB	Mozambique Belt
ME-ICP06	Multi-Element Inductively Coupled Plasma 06
ME-MS81	Multi-Element Mass Spectrometry 81
ME-4ACD81	multi-element four acid digestion 81
PPL	Plane Polarized Light
REEs	Rare Earth Elements
SNNRP	South nation nationality representative people
Syn-COLG	Syn-Collisional Granite
VAG	Volcanic arc Granite
WPG	Within Plate Granite
wt.%	Weight percent
XPL	Cross polarized Light

CHAPTER ONE

1. INTRODUCTION

1.1. Background

The East African Rift divides Ethiopia's plateau into two halves, resulting in a diverse geology and spectacular topography (Abbate et al.,2015). A Precambrian basement rock underlies the Ethiopian Oligocene plateau and Paleozoic-Mesozoic sedimentary rocks at depth, which is considered to be a continuation of two belts (Ayalew, 1997): the Mozambique belt and the Arabian-Nubian shield of gneissic rocks. The two mobile belts together form the East African Orogen (EAO), which represents a plate tectonic cycle spanning a period of 150 Ma, beginning at about 800 Ma with rifting and continental breakup and ending at 650 Ma after a continent-to-continent convergence between East and West Gondwana (Vail, 1985; Berhe; 1990; Stern,1994; and Abdelsalam,1996). Based on the reconnaissance review of geochronological, geochemical, and metamorphic data, Asrat et al. (2001) concluded that the ANS and MB were formed coevally with the Pan-African Orogeny (650-500Ma).

The Precambrian basement rocks have been divided into three groups based on their lithological and structural mapping. The oldest group is called the Lower complex and is made up of high-grade biotite-amphibole gneisses with minor quartz feldspathic genesis, calc silicates, and amphibolite affected by faulting and folding. The Middle complex is made up of clastic metasediments. The Upper complex is composed of lower-grade metamorphic rocks and includes ophiolitic rocks, andesitic metavolcanic, and various types of metasediments such as clastic and carbonate (Kazmin et al.,1978). The Precambrian has been historically classified into lower, middle, and upper complexes. (Asrat et al.,2001) applied Pb-Pb age dating to these complexes. While the complex classification might still be applicable, their research suggests a revision of the age assignments. Notably, rocks previously assigned to the lower complex (Konso, Alghe, Awata, and Yavelo gneisses) are not older than 885 Ma and as young as 560 Ma, whereas rocks from the middle complex (Wadera group) contain zircons as old as 1657 Ma. The Proterozoic Eon of Precambrian metamorphic rocks and associated intrusive rocks constitute various high-grade gneisses, schist, and associated syn to post-tectonic plutonic rocks (Davidson, 1983; Gichile, 1991). These rocks are originally related to the pan-African orogenic event, particularly in a part of the Mozambique belt (Kazmin, 1971). The Precambrian (Proterozoic metamorphic rocks) are exposed in Ethiopia in the North, West, Southwest, South, and East parts (Asrat et al., 2001).

In the Precambrian basement of Southern Ethiopia, metamorphic and associated granitic intrusive rocks outcrop in the Konso highlands, west of the main Ethiopian rift (Davidson, 1983).

Therefore, this paper presents preliminary data on the petrographic, and geochemistry of metamorphic and associated intrusive igneous rocks in southwestern Konso Ethiopia. The constraints that the data can impose on the origin, protolith, and probable tectonic setting are considered based on comparative regional geology. This thesis can address the present field observations and investigation related to geological mapping, alterations, petrography, and new major and trace element data of the basement rock collected from several representative outcrops in the study area. With this in mind, the study area is situated in a region of the Mozambique belt in Ethiopia's southwest Precambrian metamorphic terrains. This area is composed of a variety of metamorphic rocks as well as related intrusive rocks, and to the west of it are Cenozoic volcanic and sedimentary deposits connected to the Main Ethiopian Rift System. With this in mind, the study area is situated in a region of the Mozambique belt in Ethiopia.

As a result, the goal of this study is to analyze and report the results of a thorough petrological and geochemical investigation of metamorphic rocks and related intrusive igneous rocks. In addition, this study can determine which mineral assemblages are present in a given rock and explore the tectonic setting, the protolith. In addition, an in-depth 1:25,000 geological map of the research region is provided in this work.

1. 2. Description of the study area

1.2.1. Location and Accessibility

This study is carried out in the South Nation Nationality Peoples Representative (SNNPR) region of Ethiopia, in the Konso Zone and Kholme Cluster (Tebelana and Quchele Kebele), which are situated in the southwest Ethiopian Precambrian Shield. Geographically, it is bounded between 291430 to 305049m Easting and 577215 to 580595m Northing as shown in (Fig. 1).

The total area coverage of the study is 54 km^2. Karat Town, which is the capital of Konso Zone, is located at a distance of about 355 and 630km from Hawassa and Addis Ababa City respectively. The study area from Karat town is accessible via a 30km asphalted road towards Jinka and the remaining 65km inter-sites are gravel roads/dry season roads. The area can be easily accessed through the asphalted roads which run from Hawassa-Morocho-Wolayta Soddo-Arbaminch-Karat to Kholme Cluster.

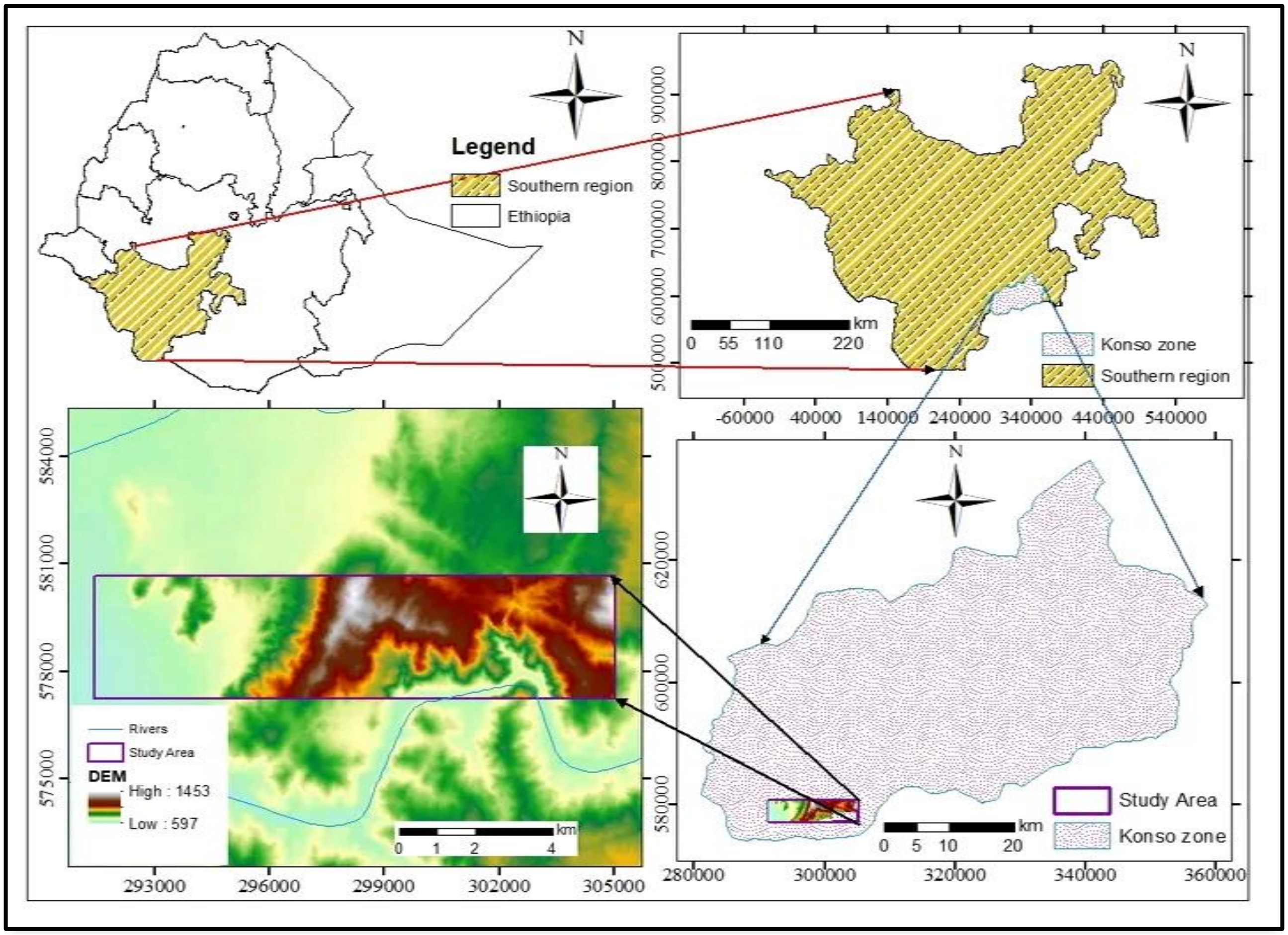

Figure 1: Location map of the study area

1.2.2. Physiography and Climate

The study area is characterized by an undulating topographic feature consisting of several elevated cliffs, folded mountain chains, deep valleys, and gorges. Where a large flat to gently sloping plain is located along the river banks in the Western low-land portion of the area. However, an extensive area of gently rolling to hilly upland (steep-slope) is observed in the ridges, from the center to the East part of the area. The highest elevation is about 1453m in the central to Eastern part of the study and the lowest elevation is 597m in the Western part of the study (Fig. 2).

According to Alemayehu (2006), The climate of Ethiopia ranges from hot lowlands to cool highlands with an altitude ranging from around 120m below sea level in the Dallol depression up to 4620 m.a.s.l on the Semien Mountain highlands. Based on altitudinal range and temperature Ethiopian climate can be classified into five climatic zones. The Bereha zone is very hot having less than 500 m.a.s.l and above $25^0{}_C$ temperature, The Kola zone is also a hot and arid region ranging between 500-1500 m.a.s.l. altitudes with $20\text{-}25^0{}_C$, Woina-Dega from 1500-2300 m.a.s.l and $15\text{-}20^0{}_C$, Dega from 2300-3300 m.a.s.l with $10\text{-}15^0{}_C$, and Kur zones are found in highland regions having more than 3300 m.a.s.l and $10^{0}{}_{C}$ or less temperature. Accordingly, the study area has an altitude between 597m and 1453m m.a.s.l, and it falls under the Kola zone with a mean annual temperature of 20.05 ^{0}C and rises to $29.7^{0}{}_{C}$ during March month.

In Ethiopia, RF has uneven distribution both in time and space. The spatial and temporal variation of RF in Ethiopia is strongly controlled by the inter-annual movement of the position of the Inter Tropical Convergence Zone (ITCZ) (National Atlas of Ethiopia, 1981). The mean annual rainfall of the study area ranges between 821mm-1129mm.

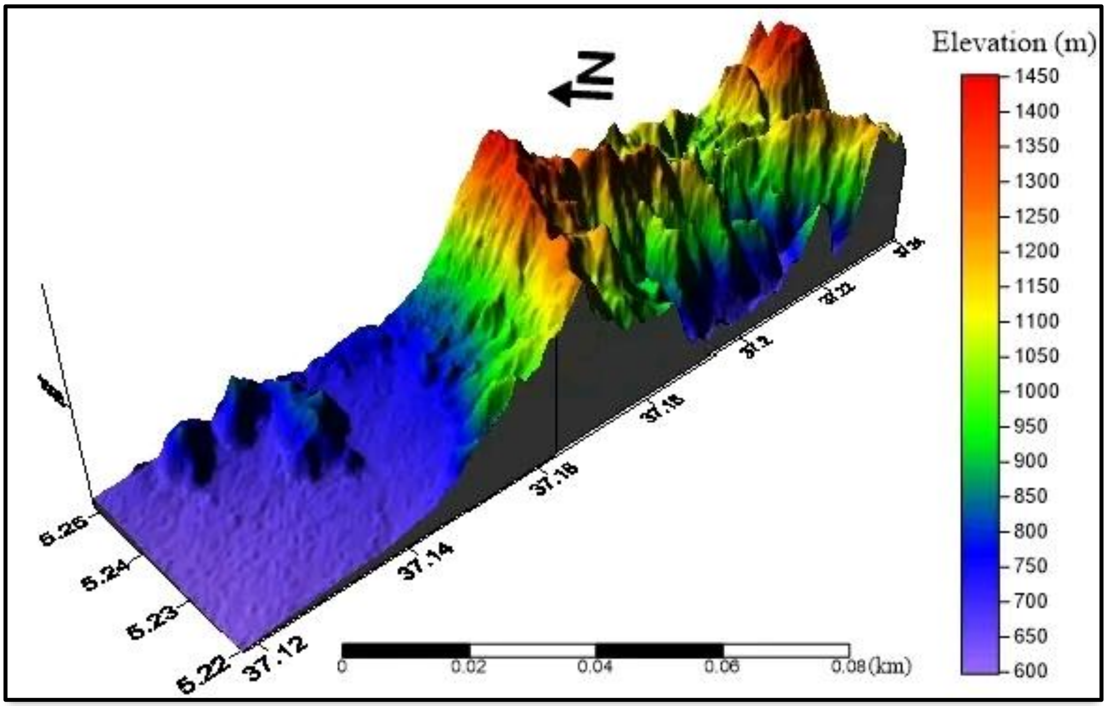

Figure 2: Physiographic map of the study area

1.3. Statement of the Problem and Research Questions

A lot of research has been conducted on the basement rocks of Ethiopia to understand the geodynamic and temporal evolution using geochemical and geochronological methods regionally (e.g., Kazmin et al. 1978; De Wit and Chewaka 1981; Davidson 1983; Ayalew et al. 1990; Alene and Barker, 1993, and Asrat and Barbey, 2003). The Precambrian rocks of Southern Ethiopia as shown in (Fig. 3) are extensively studied particularly in the Southwestern area regarding geology, geochronological, petrographic, geochemical analysis, structural geology, economic geology, and tectonic setting (e.g., Gichile, 1992; Asrat and Barbey, 2003; Alene and Barker, 1993).

Even though, there are many parts of metamorphic terrains in Southwestern Ethiopia, the basement rock in the Konso area requires further study concerning lithologic unit identification, determination of local geology, petrology, and geochemical analysis. Thus, the Konso area is one part of

Southwestern Ethiopia that has basement rock units where a detailed survey related to geological mapping, petrography, alterations, and geochemistry has not yet been studied in detail. To reduce this gap, the present work has been designed to study the petrography and geochemistry of metamorphic and associated intrusive rocks in the Konso zone, Kholme cluster: Tebelana-Quchale kebele area. This study has been done using detailed local geology, petrographic description, and geochemical analysis along with field investigation, to have a brief understanding of the tectonic setting, protolith of the metamorphic rocks, the mineral assemblages, detailed geological map at the scale of 1:25,000, and geochemical and petrographic characteristics of the rocks. Furthermore, the study compares and contrasts the petrogenesis of the basement rock of the study area with the previous regional work. Accordingly, the findings of this research can help to have a much better conceptualization and model of the overall petrological and geochemical variability of lithological units within the study area.

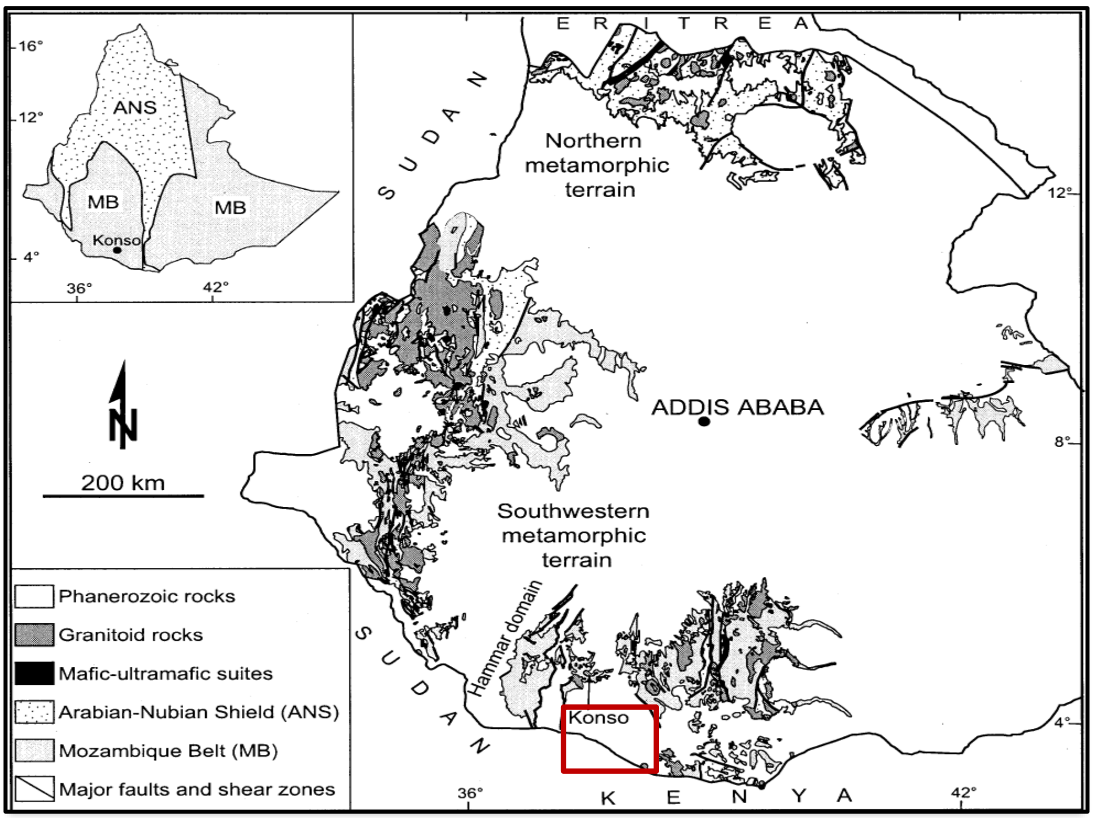

Figure 3: Geological map of Precambrian basement rocks in Southern Ethiopia (adopted from Asrat et.al. 2001). The rectangle inset indicates the study area.

The following research questions are relevant to this work and have been examined and answered.

- What is the protolith of the metamorphic rocks in the study area?
- How do the mineral assemblages look?
- How does the tectonic setting of the area?
- What do the petrography and geochemistry of the rocks look like?

1.4. Objectives of the study

1.4.1. General Objective

The goal of the current study is to examine and evaluate the petrographical and geochemical properties of metamorphic and related intrusive rocks in the Tebelana and Quchele kebele, Kholme cluster, Konso zone, Southwestern Ethiopia.

1.4.2. Specific Objectives

The following are the specific objectives that have been done through the research work:

- Characterizing and interpreting the petrography and geochemistry of metamorphic and associated intrusive rocks in the target area.
- Identifying and evaluating the nature of the protolith (parent rock) of the area.
- Characterizing and identifying the metamorphic mineral assemblages.
- Determining and investigating the tectonic setting of the area.

1.5. Scope of the Study

This research is designed to characterize the petrography and geochemistry of metamorphic and associated intrusive rocks in the study area. Besides, the characterization, the study is dedicated to identifying and evaluating the protolith (parent rock) of the area and relating the different metamorphic mineral assemblages with a degree of metamorphism in the area. This study also intended to investigate the tectonic settings of the area based on field investigation, and petrographic, and geochemical analysis of rocks in the study area.

1.6. Methodology

To realize the objective and the specific tasks of this thesis work the method of field investigation, petrographic studies, and geochemical data analysis have been done. All the collected field and laboratory data were organized, analyzed, and interpreted using GCDkit 4.1, Microsoft Excel 2019, ArcMap 10.3, and Surfer 10 software programs. The methods have been classified into three phases for procedural study namely: pre-field, fieldwork, and post-fieldwork phase.

During the pre-fieldwork phase: the collection, compilation, and review of previous and related work, identifying the problem, deciding the objectives, preparation of a topographic map of the study area, Collection of geological field equipment or materials, and selecting and tracing of traverse lines on topographic maps have been done. The second phase is fieldwork and data collection; in this phase, detailed description and characterization, sampling (1kg from each rock unit), labeling, and packing of representative fresh samples from the outcrops, describing and measuring structures, and taking GPS locations of the outcrop are the main activities that were employed. The third phase incorporates sample preparation, analyzing, synthesizing, interpreting, and presenting the petrographic microscope and geochemical powder of the rock, producing a detailed geological map, and writing this thesis. Sample preparation involves removing the weathered parts and cutting them to the appropriate size.

1.6.1. Field investigation

As part of the investigation, we conducted a field study to characterize, sample, map, measure, and photograph outcrops and geological structures. The fieldwork duration has been conducted from May 17 to 26/2022. For ten consecutive days in the field, two days were visited in the overall area in order to know the exposure of the outcrop, while the rest eight days were spent in the area to collect the representative and fresh rock samples for petrographic and geochemical analysis. I followed a systematic approach to sample fresh rocks for petrographic and geochemical analysis through field traverses. I examined all rock units and descriptive geological structures through road cuts and quarry sites. Additionally, I recorded the precise location of rock samples, gradational contacts, and geological structures to aid in geological mapping and characterization.

1.6.2. Petrographic analysis

Petrographic analysis of metamorphic rock helps to examine the texture and mineral assemblages in a particular rock. For the purpose of petrographic studies, a total of twelve representative samples (nine metamorphic samples and three intrusive rock of granite samples) were prepared for a thin section on a standard thickness of 0.03mm at the Mineralogy and Petrographic Laboratory of the Geological Survey of Ethiopia (GSE). These thin sections were prepared by cutting the fresh part of the rock sample into an appropriate size by slicing each specimen with diamond saws. Then attach it to a glass slide and make it smooth and flat using progressively finer abrasive gravel until the exposed surface of the rock is gradually lapped down to 0.03 mm thickness. Regularly quartz is used as a measurement to determine the thickness since it is one of the most plenteous minerals, cemented it to microscope slides. While, the analysis was performed at Bahir Dar University, School of Earth Sciences petrology, and geochemistry laboratory using a transmitted light microscope. The petrographic study/thin section including the identification of minerals, mineral assemblages, modal percentage of minerals in the rock, textural description, grain size, grain shape, and naming of rocks has been conducted.

1.6.3. Geochemical analysis

Based on spatial and lithological variation a total of eleven fresh samples from the study area were selected for whole-rock geochemical analysis using Inductively Coupled Plasma-Atomic Emission Spectroscopy (ICP–AES) for major elements and Inductively Coupled Plasma-Mass Spectrometry

(ICP–MS) for trace and rare earth elements. These are done by disintegrating the sample by lithium metaborate ($LiBO_2$) fusion at the Australian Laboratory Service (ALS), Ireland. Sample preparation of the selected samples was done at the ALS laboratory branch in Addis Ababa, Akaki Kaliti, Ethiopia, and the samples were sent for geochemical analysis to Ireland.

The samples were prepared in a powdered form after removing the weathered part from the surface of the rock sample and then breaking the samples into desirable sizes and crushing the broken fresh sample in a jaw crusher. The crushed sample has been milled down to micron-size particles in an agate ball automatic milling machine. To minimize cross-contamination of samples, the Jaw crusher was washed out to remove any possible contaminant after it crushed and milled every single rock sample, then dried to continue with the second sample. Samples were dried, crushed to 76.9% passing 2mm, slit, and passed through a splitter to get a 300-gram sample which was then pulverized to 93.3% passing 75 µm used for geochemical analysis.

As a result, the concentration of major oxides was calculated from the determined elemental concentration and finally, the concentration of major oxides and trace elements i.e. the geochemical result was reported in Excel format (2017). Major oxides (SiO_2, Al_2O_3, Fe_2O_3, CaO, MgO, Na_2O, K_2O, TiO_2, MnO, and P_2O were analyzed with ICP-AES whole-rock package. Trace elements (Ba, Ce, Cr, Cs, Dy, Sm, Sn, Sr, Ta, Tb, Th, Tm, U, V, W, Y, Yb, Zr, Er, Eu, Ga, Gd, Hf, Ho, La, Lu, Nb, Nd, Pr, Rb) were analyzed with a whole-rock package of Lithium Borate Fusion by ICP-MS. Besides, base metals (Ag, As, Cd, Co, Cu, Li, Mo, Ni, Pb, Sc, Ti, and Zn) were analyzed by ICP-AES acid digestion. The reproducibility of the analyzed results was checked using blank, AMIS0304, and OREAS 102a duplicated samples. The accuracy of major oxides is<3%; those of trace elements are <5%. Finally, after the geochemical analysis of the rock sample is completed, the result is interpreted, analyzed, and presented in different graphs using the Excel sheet, GCDkit, and Arc Map. The overall methodological approaches that are used for doing the thesis are shown in (Fig. 4).

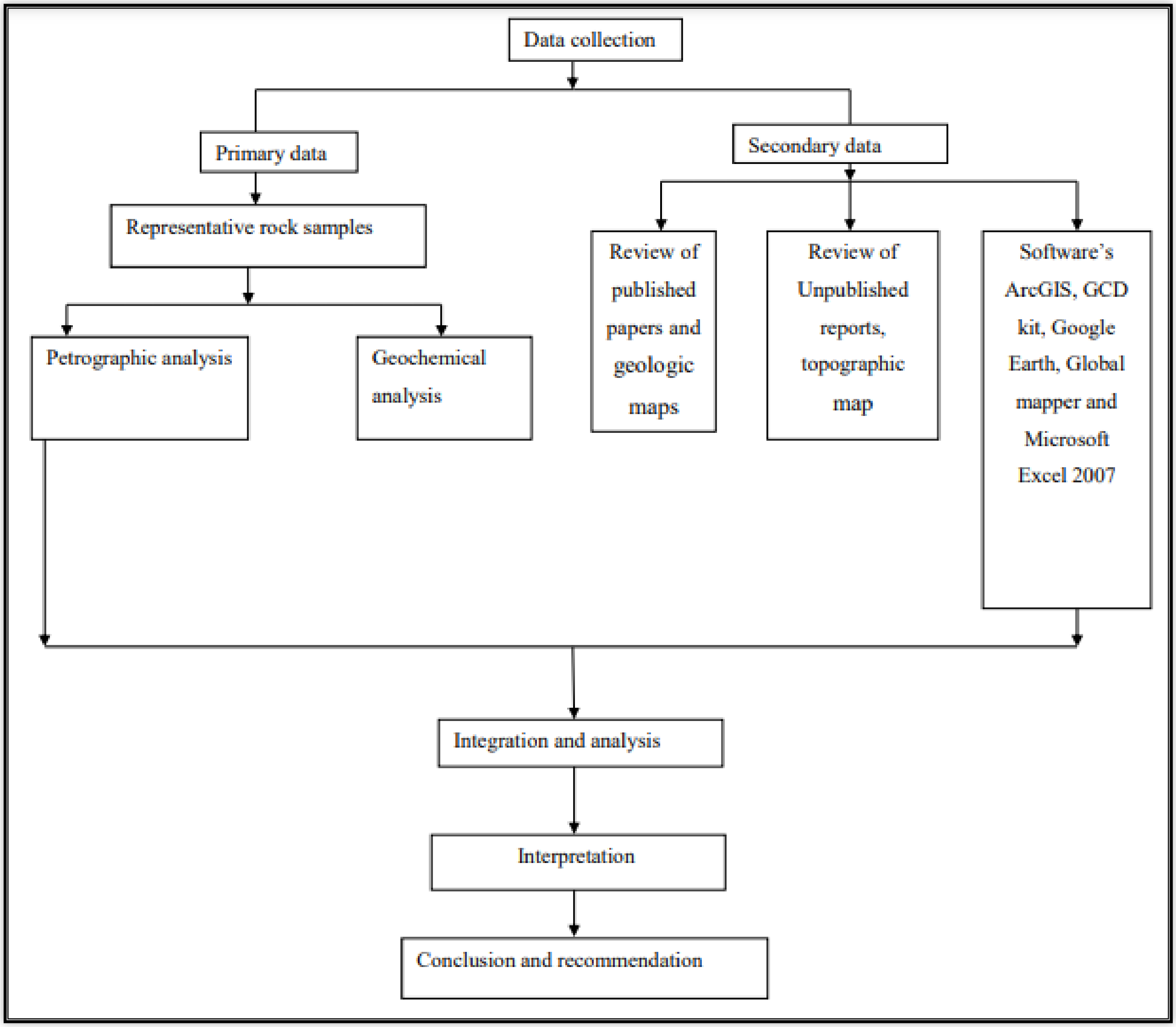

Figure 4: Generalized flow chart showing overall methodological approaches that will be employed in the study area

For the work of the thesis, the following materials and software were used.

- Topographic map
- Geological hammer, geological compass, and global positioning system (GPS)
- GCDkit, Microsoft Excel 2019, and Arc Map software were used for petrographically and geochemical data plotting.

1.7. Relevance of the Study

The petrography and geochemistry of the Kholme cluster Tebelana & Quchale kebele, Konso zone, have not been detailed studied yet. Thus, this research is very relevant to the scientific community and provides the following significance:

- To understand the geochemical and petrographic characteristics of the rock and the process that derived magmatic genesis and protolith.
- To know the parent rock and a systematic classification of the rocks using petrographic and geochemical data.
- It provides information about the geological background of the area for companies, public interest groups, and private sectors that work with mineral exploration issues and infrastructural developments.
- It contributes some datasets, for the ongoing study of petrology and geochemistry in metamorphic areas.

To this end, the study gives a better answer to the petrological and geochemical problems in the area by providing new first-hand information and fundamental knowledge on petrology, geochemistry, and metamorphic mineral assemblage. It can also be used as a reference for petrologists who will be conducting research in a similar geological or environmental setting.

CHAPTER TWO

2. REGIONAL GEOLOGICAL SETTING

2.1. Introduction

Southern Ethiopia boasts a rich geological history, evident in its Precambrian rocks. These rocks form a crucial part of the East African Orogeny (EAO), a vast zone of mountain building encompassing the Pan-African Mozambique Belt and the Arabian-Nubian Shield (Stern, 1994). To the west, younger volcanic rocks and sediments, associated with the Main Ethiopian Rift System, overlay this ancient terrain (Yibas et al., 2000b; Yibas et al., 2003).

Southern Ethiopia's Precambrian geology can be broadly divided into two distinct terrains, each characterized by unique rock types, structural features, and metamorphic intensity (Yibas, 2000; Yibas et al., 2000a):1. Granite-Gneiss Terrain: This terrain is dominated by high-grade gneisses, formed from both sedimentary and igneous rocks (Para- and Ortho-gneisses). Intercalated within these gneisses are amphibolites (metamorphosed volcanic rocks), sillimanite-kyanite-bearing schists (highly metamorphosed sedimentary rocks), marbles (metamorphosed limestone), and deformed and metamorphosed granitic rocks. This terrain extends into Northern Kenya, with its Para-gneisses bearing a strong resemblance to those found there (Yibas, 2000; Yibas et al., 2000a).2. Ophiolitic Fold and Thrust Belts: In contrast, these belts are composed of low-grade metamorphic rocks derived from mafic and ultramafic igneous rocks (rich in iron and magnesium) alongside sedimentary assemblages. These two contrasting terrains are separated by major shear zones, which are zones of intense deformation within the Earth's crust (Yibas, 2000). These shear zones often exhibit evidence of multiple episodes of deformation.

2.2. Geodynamic Evolution of East African Orogeny

The East African Orogen (EAO) stands as a testament to Earth's dynamic past. Formed during the Neoproterozoic to early Cambrian period (890 to 550 million years ago), this vast zone of deformation arose from a process known as collision-accretion orogeny. This process played a critical role in the assembly of the supercontinent Gondwana (Stern et al., 2006). The EAO's formation involved a complex interplay of tectonic movements, magmatic activity (molten rock intrusion and extrusion), and metamorphic processes (rock transformation under high pressure and temperature), as illustrated in (Fig. 5). The EAO essentially marks the boundary where two ancient landmasses collided: the Arabian-Nubian Shield (ANS) to the north and the Mozambique Belt (MB) to the south. A significant portion of the EAO is composed of a newly formed (juvenile) Neoproterozoic crust (Avigad and Gvirtzman, 2009). The northern segment generally exhibits low to medium metamorphic grade. In contrast, the southern portion is characterized by high-grade metamorphic rocks, remnants of the older Paleoproterozoic crust known as the Mozambique Belt (Hargrove et al., 2006; Fritz et al., 2013). The southern EAO is essentially the Mozambique Belt, formed through a forceful collision between two continents, akin to the creation of the Himalayan Mountains in the Phanerozoic era (Dawit & Chewaka, 1981). This belt is characterized by the presence of high-grade gneisses, migmatites (partially melted rocks), and schists (highly foliated metamorphic rocks) (Asrat et al., 2001). The Mozambique Belt extends further south, west, and east into Ethiopia (Berhe, 1990; Asrat et al., 2001).

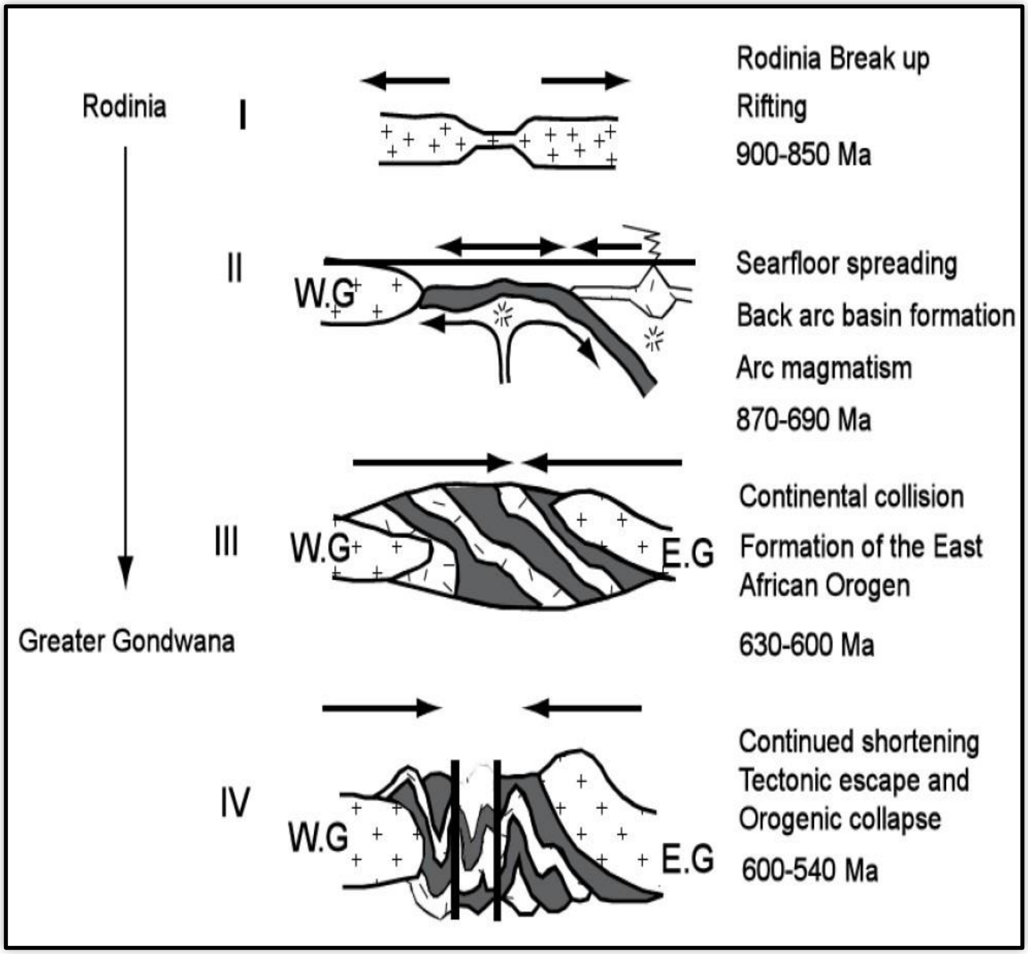

Figure 5: Thematic sketch of the tectonic evolution of the East African Orogen that resulted in the greater Gondwana Supercontinent (adopted from Stern et al., 2006). W. G=West Gondwana and E. G=East Gondwana.

2.2.1. Arabian-Nubian Shield (ANS)

The Ethiopian portion of the Arabian-Nubian Shield (ANS) is dominated by juvenile (newly formed) landmasses (terranes) that originated as island arcs, back-arc basins, and oceanic plateaus during the Pan-African Orogeny (900 to 500 million years ago) (Stern, 1994; Almond, 1983). These terranes are frequently interspersed with abundant ophiolites, fragments of oceanic crust. As depicted in (Fig. 6), the ANS in Ethiopia intricately combines with the Mozambique Belt, forming the southern half of the East African Orogen (EAO). This region witnessed the most intense collision between fragments of the ancient supercontinent Gondwana (Stern, 1994). The western margin of the ANS is characterized by the presence of volcano-sedimentary sequences alongside juvenile Neoproterozoic Island arc magmatic rocks, all decorated with ophiolites. These bodies form linear belts and are interpreted as remnants of dismembered ophiolites (Teklewold Ayalew et al., 1990; Abdelsalam and Stern, 1996). Additionally, the ANS is characterized by the presence of variously deformed and intruded granites, gabbros (coarse-grained igneous rocks), and dikes (intrusive igneous features).

The timing of magmatic events within the ANS multifaceted occurred before 630 million years ago, there is evidence of later high-magnesium andesite intrusions (schistose dykes) in southern Israel around 630 million years ago (Kroner and Stern, 2004). several studies (Warden and Horkel, 1984; Ghebreab, 1992; Worku and Yifa, 1992) suggest that subduction did not occur in the ANS's history.

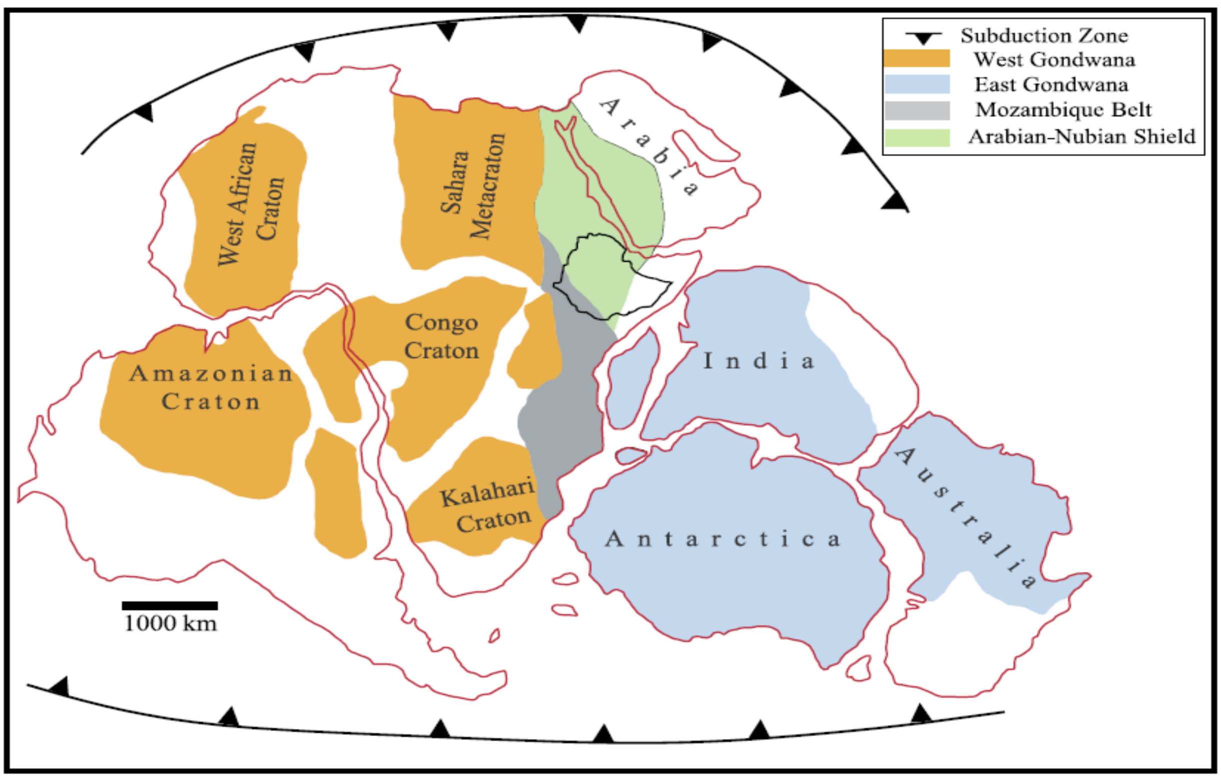

Figure 6: Map of the East African orogen showing the location of the Arabian-Nubian shield relative to the Mozambique Belt and adjacent cationic margins (adopted from Abdelsalam et al., 2011; Stern et al., 2012).

It is dominated by low-grade volcano-sedimentary rocks with associated plutons and ophiolitic remnants (Robinson et al., 2014; Blades et al., 2015). According to Abdelsalam and Stern, (1996), the deformation belt has divided the ANS into two deformation belts: (1) Related to arc-arc and arc-continent collisions, which are both associated with sutures. The arc-arc deformation belts are manifested by the occurrence of E-W and N-S verging ophiolites in the northern and southern parts of the ANS, respectively.

2.2.2. Mozambique belt (MB)

The Mozambique Belt (MB) is a remarkable geological entity, formed from much older continental crust (Meert, 2003; Blades et al., 2015). It exposes high-grade metamorphic rocks, revealing features from deep within the Earth's crust (middle to lower levels). According to (Stern ,1994), the MB's story began around 900-850 million years ago with the rifting (splitting) of the supercontinent Rodina. Geochronological data (dating rocks) from the MB in Kenya (Key et al., 1989) suggests these rocks are not significantly older than those of the Arabian-Nubian Shield (ANS). This study also proposes two distinct periods of deformation: the initial collision event and a subsequent one resulting in upright folds and shear zones.

In Ethiopia, the MB is exposed in the southern and southwestern regions, where it borders the ANS (Asrat and Barbey, 2003). The ANS is a lower-grade (greenschist facies) terrain composed of volcanic and sedimentary rocks with a strong influence of calcium and alkali metals (calc-alkaline). Kazmin (1975) divided Ethiopia's metamorphic complexes into three: Lower and Middle Complexes correlating with the MB, and an Upper Complex linked to the ANS. The Mozambique Belt's rocks are well-exposed in various regions, including Kenya, southern, eastern, and western Ethiopia, northern Somalia, and to a lesser extent, northern Ethiopia (Kazmin et al., 1978; Alemu and Abebe, 2007). Overall, the Mozambique Belt is a Neoproterozoic collisional belt, stretching along and underlying the eastern edge of much of Africa (Shackleton, 1979). It's characterized by folds and metamorphic features trending north-northeast to north-northwest. The belt is dominated by high-grade metamorphic rocks, ranging from amphibolite to granulite facies (Gichile, 1992), forming a complex of gneisses and migmatites (partially melted rocks).

2.3. Precambrian Geological Evolution of Southern Western Ethiopia

The Precambrian basement complex in southwestern Ethiopia offers into the ancient geological history of the region (Kazmin, 1972). This complex is characterized by dark-colored, high-pressure metamorphic rocks called granulites that outcrop in two distinct areas within the Segen half-graben. These areas lie along the southernmost extension of the Main Ethiopian Rift (Mohr, 1967) and the Konso West Highland (Davidson, 1983).

The crystalline basement rocks, formed deep within the Earth's crust, are exposed in various regions of southwestern Ethiopia, including Illubabor, southwest of Kafa, southwest of Gamo Gofa, and southwest of Sidamo (Fig. 7). These rocks can be further classified into several distinct geological units based on their characteristics. Some of the key units include the Medium to High-Grade Adola-Moyale Belt: This belt is composed of metamorphic rocks that have undergone moderate to intense metamorphism (Worku and Schandelmeier, 1996; Yibas et al., 2002). High-Grade Akobo, Surma, and Hammar Domains: These domains are dominated by rocks that have been significantly metamorphosed at high temperatures and pressures, resulting in the formation of schists and gneisses. Additionally, these domains are intruded by various igneous rock types ranging from gabbros granites (Davidson, 1983). The Akobo domain is dominated by schists and gneisses that have undergone less intense metamorphism compared to the other two domains. (De Wit and Chewaka ,1981), Observed that the boundaries between different rock types and the overall structural trends in southwestern Ethiopia cut across the boundaries defined by the metamorphic grade. Their findings suggest that the high-grade metamorphism might be a younger event compared to the earlier metamorphic events that affected the region.

Furthermore, geochronological data obtained through radiometric dating techniques (Amenti et al., 1992; Worku, 1996; Teklay et al., 1998; Yibas et al., 2002; Tadesse, 2003) suggests that the high-grade gneisses and granulites are not necessarily older than the low-grade volcanic and sedimentary rocks found in the region. Based on recent observations (Yibas, 2000), the geology of southern Ethiopia can be divided into two distinct geological terranes. These terranes are Granite-Gneiss Terrane: This terrane is composed of highly metamorphosed rocks, including parageneses, orthogneisses, and deformed and metamorphosed granitoid rocks. Ophiolitic Fold and Thrust Belts: This terrane comprises low-grade metamorphic rocks composed of various proportions of mafic and ultramafic rocks, along with sedimentary assemblages.

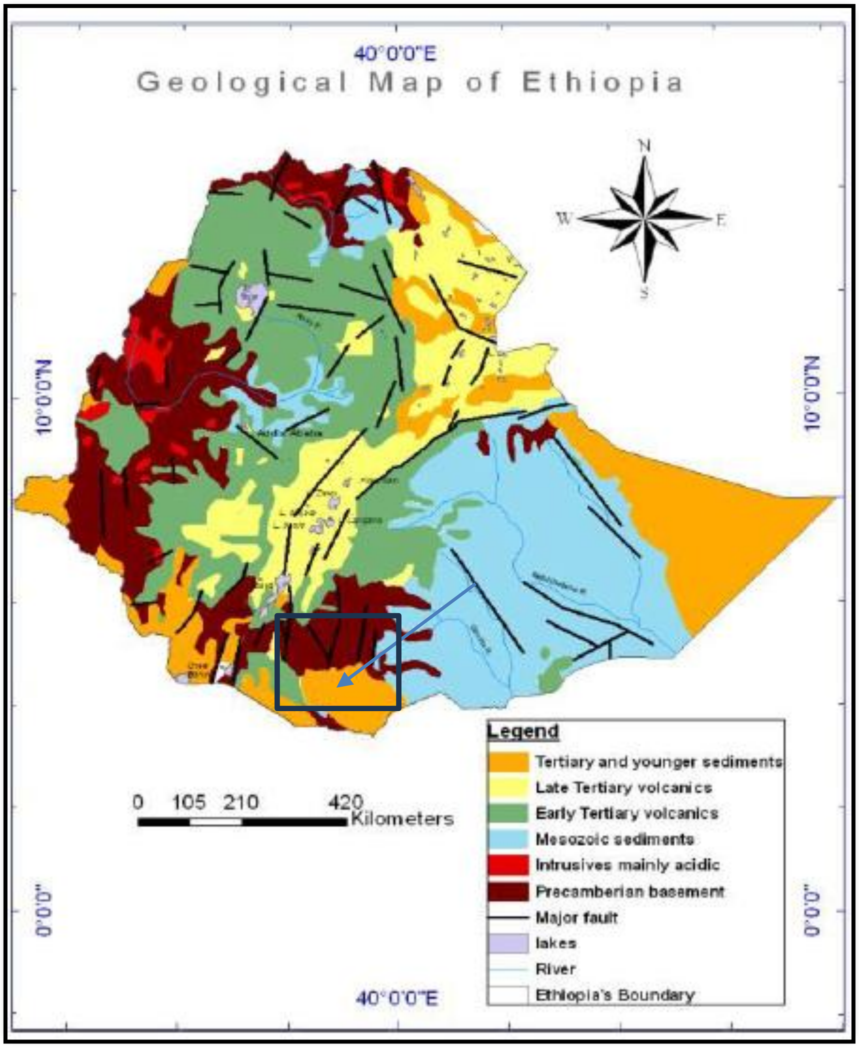

Figure 7: Geological map of Ethiopia (adopted from from EIGS, 1996). The blue arrow line indicates approximately the study area.

2.3.1. Moyale-Sololo complex

The Moyale–Sololo granite-gneiss complex comprises mainly granitic and granodioritic gneisses and subordinate parageneses (biotite gneiss, mylonitic quartz-feldspathic-gneiss, and muscovite-quartz-feldspar gneiss). Geochemical investigation of the complex confirms the dominance of orthogneisses ranging from monzonitic to Monzo-dioritic-granitoid of both volcanic-arc and within-plate tectonic activity (Yibas, 2000; Yibas et al., 2000d). Lithological, the biotite-hornblende gneisses in the Western part of the Moyale-Sololo granite-gneiss complex and the Burji gneisses in the North are similar, suggesting that these gneisses might belong to the same facies. The Moyale-Sololo para-gneisses are also extended Southwards into Kenya (Key et al., 1989).

2.3.2. Adola complex

Although the orthogneisses in the Adola granite-gneiss complex are dominant, significant amounts of parageneses and schists also occur (Worku, 1996; Yibas, 2000; Yibas et al., 2000b). The Adola gneisses have been classified into five formations (Kozyrev et al., 1985): (1) Zembaba, (2) Aflata, (3) Kenticha, (4) Buluka and (5) Bore Formations. However, as (Yibas,2000) and (Yibas et al.,2000a) argued, both the Buluka and Bore formations are dominated by migmatitic and granitoid gneisses, which are similar to the Awata migmatitic and granitoid gneisses, and, hence, these units together mapped as the Awata-Bulbul granitoid-migmatitic assemblage. The Zembaba Formation occupies the Eastern part of the Adola Complex and forms the lowest stratigraphic unit in this complex. The Zembaba Formation consists mainly of quartzo-feldspathic gneisses, with a minor amount of leucocratic biotite gneiss, which is intercalated with biotite-muscovite schists. (Kazmin ,1972), (Kazmin et al,1978), and (Kozyrev et al,1985) regarded that most of these rocks are para-gneisses, but Worku (1996) and Yibas (2000) emphasized the presence of a significant proportion of ortho-gneisses in addition to para-gneisses.

2.3.3. Genale-dolo complex

The Genale-Dolo granite-gneiss complex forms the largest segment of the Alghe gneiss as described above. Kazmin (1972, 1975) characterized these rocks as biotite and biotite-amphibole gneisses grading into banded migmatites and grey granodioritic rocks. The parageneses of the Genale-Dolo granite-gneiss complex in the central, Western, and Northeastern regions are classified into three major assemblages, which are intruded by different phases of orthogneisses (Yibas, 2000; Yibas et al., 2000d). However, the mylonitic gneisses that widely developed throughout the complex are regarded to be the result of the Wadera shearing event at about 580 Ma (Yibas et al., 2000a, b). The equilibrium paragenesis that is commonly observed in the gneissic rocks of Southern Ethiopia is representative of the medium-temperature part of the amphibolite facies (Chater, 1971; Worku, 1996; Yibas, 2000).

2.3.4. Burji–Finchaa complex

The Kholme cluster, located in southwestern Ethiopia, lies within the Burji-Finchaa complex. This complex includes a rich geological history characterized by two major rock groupings (Davidson, 1983; Yibas, 2000; Yibas et al., 2000d). The first group is an older, highly deformed rock assemblage known as the gneissic complex. This complex comprises various rock types, including mafic (rich in iron and magnesium), intermediate (mixtures of minerals), felsic (light-colored, rich in silicon), and even metasedimentary gneisses and granulite (highly metamorphosed rocks). These gneisses experienced intense metamorphism under high-pressure and high-temperature conditions, ranging from middle to upper amphibolite facies and locally reaching granulite facies.

The gneissic rocks are intensely folded and exhibit a dominant foliation (layered structure) trending north-northwest to south-southeast, typically dipping steeply northeast. The second group consists of intrusive igneous rocks that cut through the older gneisses. These plutonic rocks occur as distinct bodies of gabbros (coarse-grained, dark igneous rocks), diorites (intermediate igneous rocks), and granites (light-colored, coarse-grained igneous rocks). The granites can be further categorized based on their timing of intrusion relative to deformation events: syn-tectonic (emplaced during deformation), late-tectonic, and post-tectonic. Additionally, the complex is laced with dikes of leucogranite, aplite, and pegmatite. Particularly, the granitic rocks in the Burji-Finchaa complex are predominantly high-potassium (K) granites, although minor occurrences of shoshonitic, peralkaline, tonalites (intermediate, rich in plagioclase feldspar), and granodiorites (intermediate, with plagioclase and potassium feldspar) are also present (Yibas, 2000; Yibas et al., 2000d).

CHAPTER THREE

3. GEOLOGY OF THE AREA: FIELD AND PETROGRAPHIC AND METAMORPHISM

3.1. Introduction

The key aim of this chapter is to describe the lithological units cropping out on the study area based on the field investigation and petrographic thin sections. The study area is predominantly covered by medium- to high-grade metamorphic rocks and associated intrusive. Twelve representative samples were taken from different localities in the study area including nine metamorphic rocks and three granite rocks, to account for the variety of rock lithologies. The study of rocks at a microscopic level provides valuable insight into metamorphism, including their mineralogy, texture, color, and grain boundary. Through petrographic analysis of metamorphic rocks, it is also possible to determine the conditions of the metamorphic facies by examining the mineral assemblages present.

The study area consists of a high-grade metamorphic rock of, granitic gneiss, amphibole gneiss, granite, and biotite gneiss, which are mainly found in the East Central, Southeast, and Southwest regions (Fig. 25). The Precambrian intrusive rock is represented by granite and is mostly found in the Western, Northwest, and Southwest parts of the study area. The largest portion of the study area is covered by amphibole gneiss rock units. Most of the rocks in the study area have been affected by secondary structures, including joints, folds, faults, quartz veins, pegmatite dikes, and veins and fractures. These structures are exposed in a relatively low-lying and very rugged topography. Below, you will find a description of the different types of lithology and their corresponding petrography and metamorphism details.

3.2. Field description of rocks in the study area

3.2.1. Biotite gneiss

Biotite gneiss is relatively not widely exposed in the study area. This rock exhibits a fresh, dark-gray color that weathers to a lighter gray. Its texture ranges from medium-grained to coarse-grained, with a prominent layering or banding known as foliation (Fig. 8A**)**. The contact between biotite gneiss and the surrounding amphibolite gneiss unit appears gradational, meaning the transition is smooth rather than abrupt. The dominant minerals in biotite gneiss are mafic (rich in iron and magnesium), including biotite (black mica) and hornblende (dark green or black amphibole). Additionally, felsic minerals like quartz (light-colored) are present, contributing to the medium to coarse-grained texture. The strong, flaky nature of the dark minerals, particularly biotite, allows them to align in different directions, creating the characteristic banded appearance of gneiss. The variations in composition within this rock unit are a result of metamorphic differentiation, a process that occurs during high-grade metamorphism accompanied by intense deformation. Biotite gneiss displays evidence of significant deformation through the presence of structures like folds and foliation. Ptygmatic folds, characterized by their distinctive zigzag pattern, are also observed within this rock unit (Fig. 8B). These folds are believed to form when pre-existing rocks partially melt during metamorphism. This type of rock is typically found in areas with exposed bedrock due to stream erosion or on hillsides.

Figure 8: Field photograph of Biotite gneiss exposed at the hillside and river cut. A) rock shows small-scale M-type fold and ptygmatic fold and B) Rock shows foliation

3.2.2. Amphibole gneiss

Dominantly the study area is covered by exposed amphibolite rock, found at stream cuts and hilltops. It has a dark grey weathered appearance with a mixture of dark and minor light colors when fresh, as shown in (Fig. 9). The rock has a distinct foliation consisting of alternating layers of dark-colored amphibole minerals and felsic minerals, Plagioclase feldspar, and k-feldspar. The dark color of the rock is primarily caused by the amphibole minerals. The compositional variation and banding pattern observed in this rock unit are a result of metamorphic differentiation that occurred during the progressive deformations of high-grade metamorphism. This rock unit has a gradational contact with adjacent units and can be classified as a high-grade metamorphic rock due to its coarse grain size.

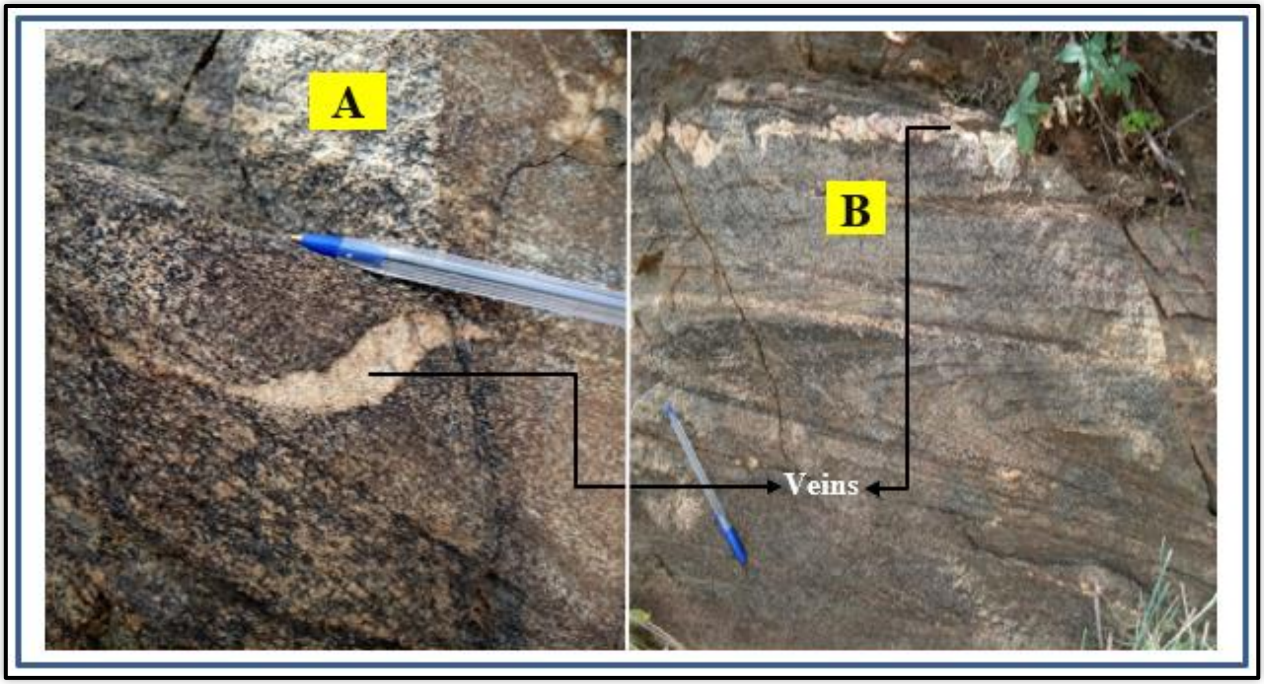

Figure 9: Amphibole genesis exposed on the hilltop and stream cut. A) Rock shows S types of fold B) Rock shows an isoclinal recumbent fold.

3.2.3. Granitic gneiss

This rock is a coarse-grained**,** gneissose rock characterized by alternating light and dark mineral bands (Fig. 10). Both the light and dark minerals exhibit a distinct preferred orientation, contributing to the overall gneissose structure. The weathered surface appears light grey, while the fresh outcrop is light pink. The lighter bands are dominated by quartz and feldspar. The darker bands primarily consist of biotite. Plagioclase feldspar, likely a sodium-rich member of the plagioclase feldspar series, is present and characterized by a gray color and elongated form. Additionally, K-feldspar contributes to the light-colored bands, with a slightly light pink color.

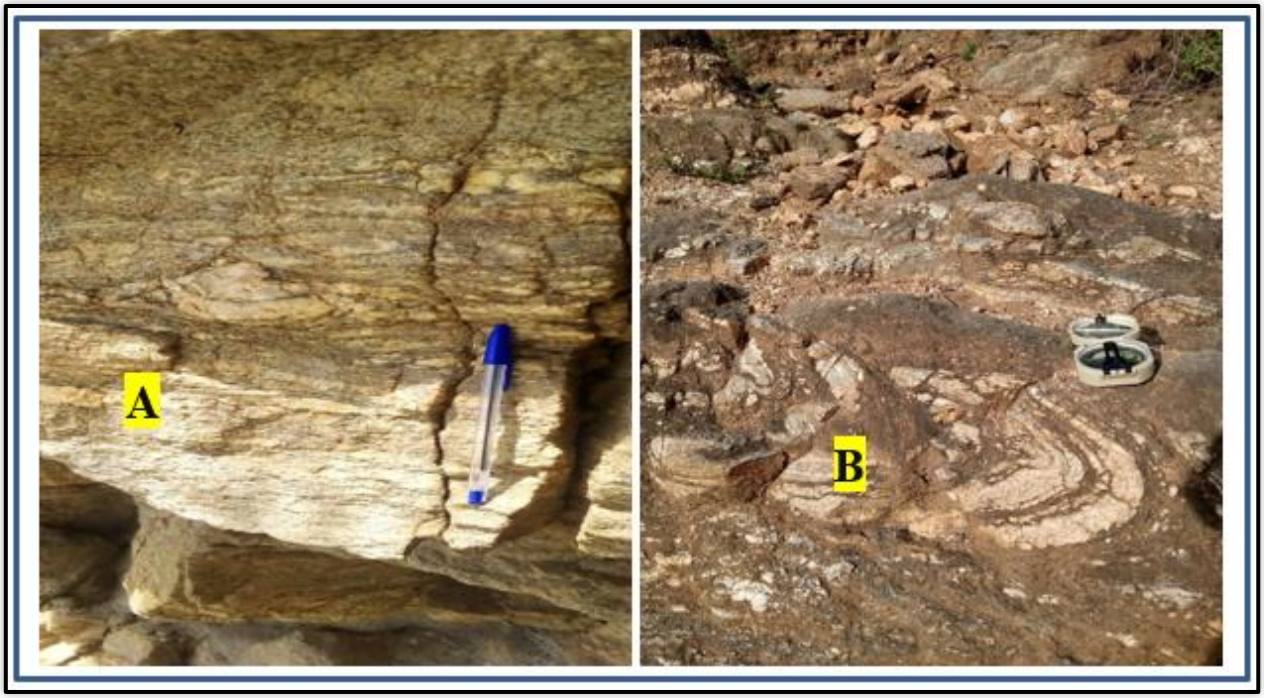

Figure 10: Field photograph of Granitic gneiss exposed at the hillside and stream cut. A) Rock shows a small joint and B) Rock shows a recumbent fold.

3.2.4. Mica schist

The Mica Schist rock unit in the study area cannot be mapped at a 1:25,000 scale and, hence, covers a very small area. However, it can be spotted in road cuts and hillsides. This rock unit comprises quartz, plagioclase, muscovite biotite, and opaque minerals. It also has a schistose fabric and medium to coarse grain sizes. Just like the biotite gneiss found in the top right side of the study area, this rock unit is associated with granitic gneiss. It is also characterized by the presence of foliation due to the parallel alignment of micaceous minerals (Fig. 11A & B). It has different colors depending on the colors of the constituent minerals ranging from brownish to grayish fresh color and has gray weathered color. The boudinage structure is clearly shown in the (fig.11B) and it is formed by extensional tectonics, where a rigid tabular body such as hornfels, is stretched and deformed within less competent surroundings. The presence of boudinage indicates the rock is exposed in a shear/weak zone.

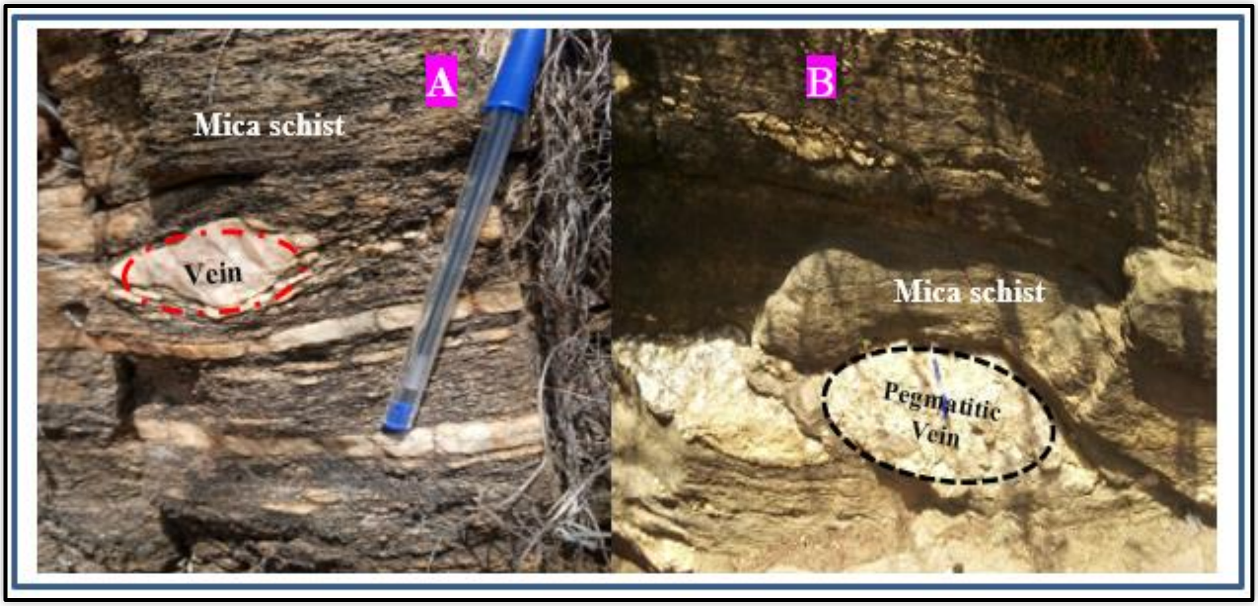

Figure 11: Representative Field photographs of Mica schist exposed at hilltop and river cut. **A)** Rock shows mica-like fish structure and **B)** pegmatitic rich boudinage-like structure.

3.2.5. Granite

The primary minerals present in this rock include K-feldspar (microcline), quartz, mica, and biotite. It exhibits a range of colors including grayish, pinkish, and whitish. Weathered outcrops appear brownish to reddish, while fresh outcrops display a pink and gray color as depicted in (Fig. 12A & B). It is relatively less weathered compared to the other types of lithologic units due to the presence of weathering-resistant minerals. However, in some localities, it has been fractured, weathered, and altered due to the percolation of the water through fracture and the presence of less weathering-resistant minerals like mica minerals. It is dissected by one systematic joint and its strike S30°E and its dip 65°NE. It has an estimated thickness of ~100m.

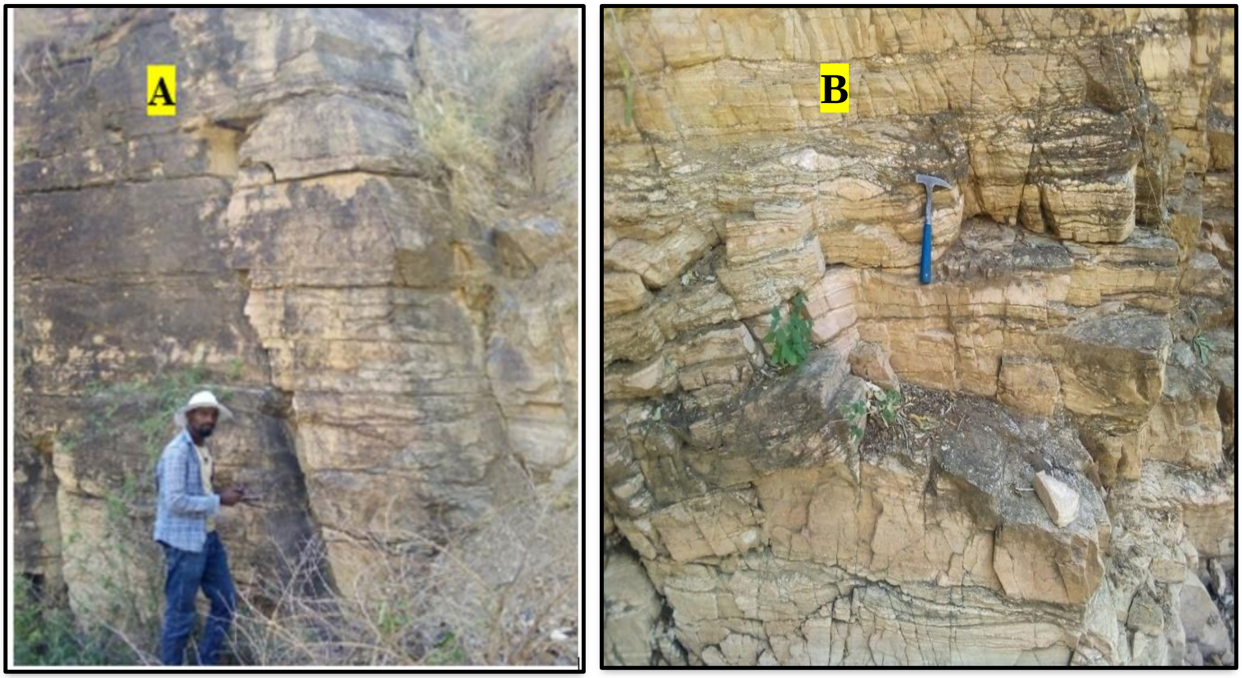

Figure 12: Field photograph of granite exposed at stream cut and hillside A) Rock shows one systematic joint approximately 1.5 cm space and B) rock shows highly fractured.

3.3. Petrographic description of rocks in the study area

Studying the petrographic characteristics of a rock helps to describe its nature and systematic classification of rocks. The representative samples are analyzed using two main methods: plane-polarized light (PPL) and cross-polarized light (XPL) view of transmitted light microscopy. This allows for a thorough examination and interpretation of the rock's features.

3.3.1. Amphibole gneiss

The microscopic examination or petrographic analysis reveals that KSAM11 and KSAM12 are medium- to coarse-grained rocks. Their primary mineral composition consists of approximately 30% quartz, 8% biotite, 50% hornblende, 10% chlorite, and 2% opaque minerals. Most mineral grains exhibit irregular and elongated shapes, with some, like hornblende, quartz, and biotite, displaying a preferential alignment within the plane of foliation. However, despite this alignment, a well-developed foliation is not always readily apparent. The mineral-like hornblende, biotite, and quartz grains form aggregates with a strong parallel orientation (nematoblastic texture), but distinct mineral banding is minimal. The mineral grains in these samples range from subhedral to anhedral. Hornblende is the most abundant mineral, followed by chlorite, quartz, and biotite. Interestingly, rounded quartz grains can be observed within the hornblende crystals, sometimes forming small inclusions (poikiloblastic texture). Additionally, significant alteration of hornblende to chlorite is evident under both polarized light (XPL) (Fig. 13B**)** and plane-polarized light (PPL) refer to (Fig.

13A). The quartz grains exhibit subhedral to anhedral shapes and display a wavy extinction pattern, which is indicative of deformation they experienced. In some areas, fine-grained chlorite flakes and minor hornblende partially replace these larger, pre-existing quartz crystals. These larger crystals may have formed during a later stage of retrograde metamorphism.

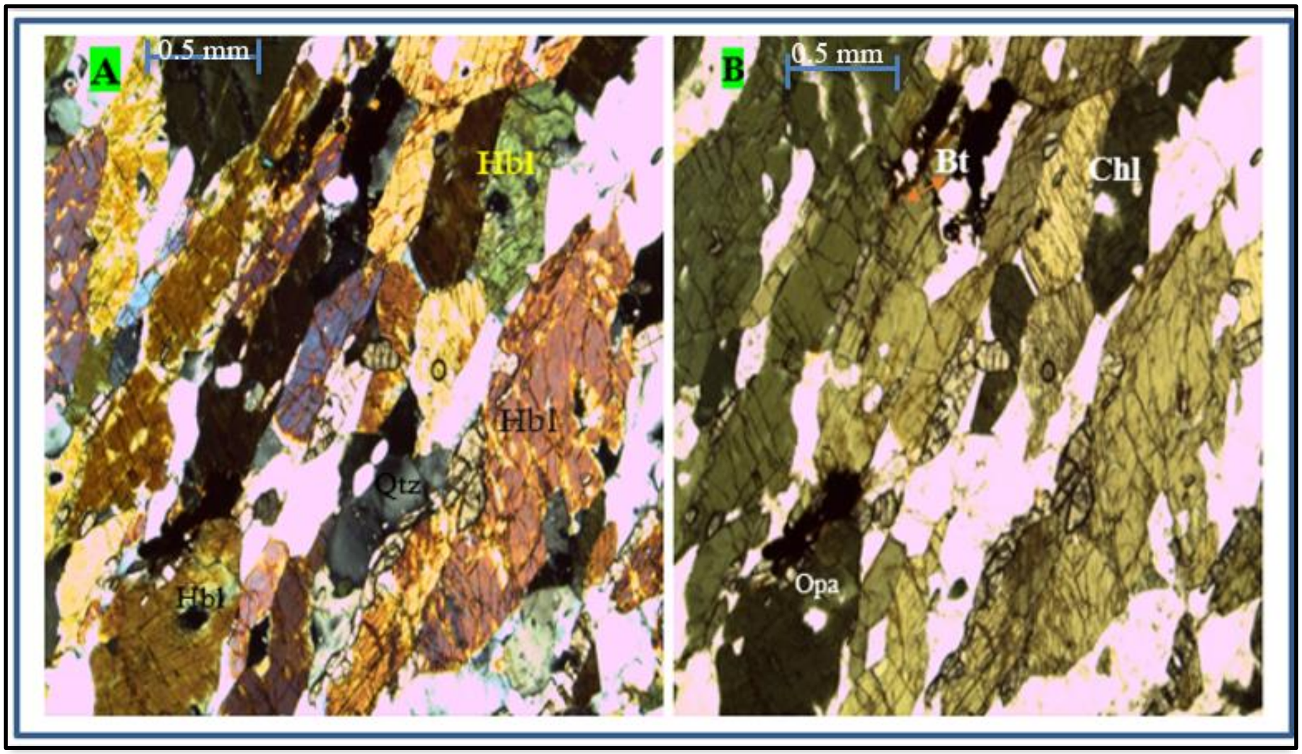

Figure 13: Representative Photomicrograph of Amphibolite gneiss in XPL and PPL under 4x magnification. (A) Photomicrograph of Amphibolite gneiss under PPL view; elongated xenoblastic grains of quartz, hornblende, chlorite, and opaque with a strong preferred orientation. (B) Photomicrograph of Amphibolite gneiss under XPL view; in-equidimensional xenoblastic to hypidioblastic plagioclase grains interlocked with hornblende crystals. The labels of the identified minerals are (Qtz-Quartz, Pl-plagioclase, Hbl-Hornblende, Chl-chlorite, and Opa-opaque

3.3.2. Granitic gneiss

The microscopic examination of the rock samples representing KSGN1, KSGN2, KSGN3, and KSGN5 is coarse-grained with a weakly developed foliation, giving them a semi-schistose texture. Their primary mineral composition consists of approximately 40% quartz, 30% microcline, 12% plagioclase feldspar, 14% biotite, 2% albite, and 2% opaque minerals. The rocks are characterized by alternating light and dark bands that reflect variations in mineral composition. Lighter bands are dominated by quartz and feldspars, while darker bands are enriched in biotite. This banded appearance is indicative of a weak foliation. The quartz grains exhibit wavy extinction, suggesting they experienced deformation. They also display irregular grain boundaries and sometimes occur as small, rounded inclusions within microcline and plagioclase that show poikilitic texture. The quartz grains exhibit wavy extinction, suggesting they experienced deformation. They also display irregular grain boundaries and sometimes occur as small, rounded inclusions within microcline and plagioclase feldspar (poikilitic texture). The biotite grains are present with a pronounced parallel to a sub-parallel arrangement in one direction, to which the foliation of the rock is shown in (Fig. 14**)**. Microcline and potassium feldspar, is a major component and locally form a granoblastic texture with quartz and plagioclase. Where the mineral alignment is not as prominent as in strongly foliated gneisses. In this case, the presence of weak foliation alongside some granoblastic texture is formed.

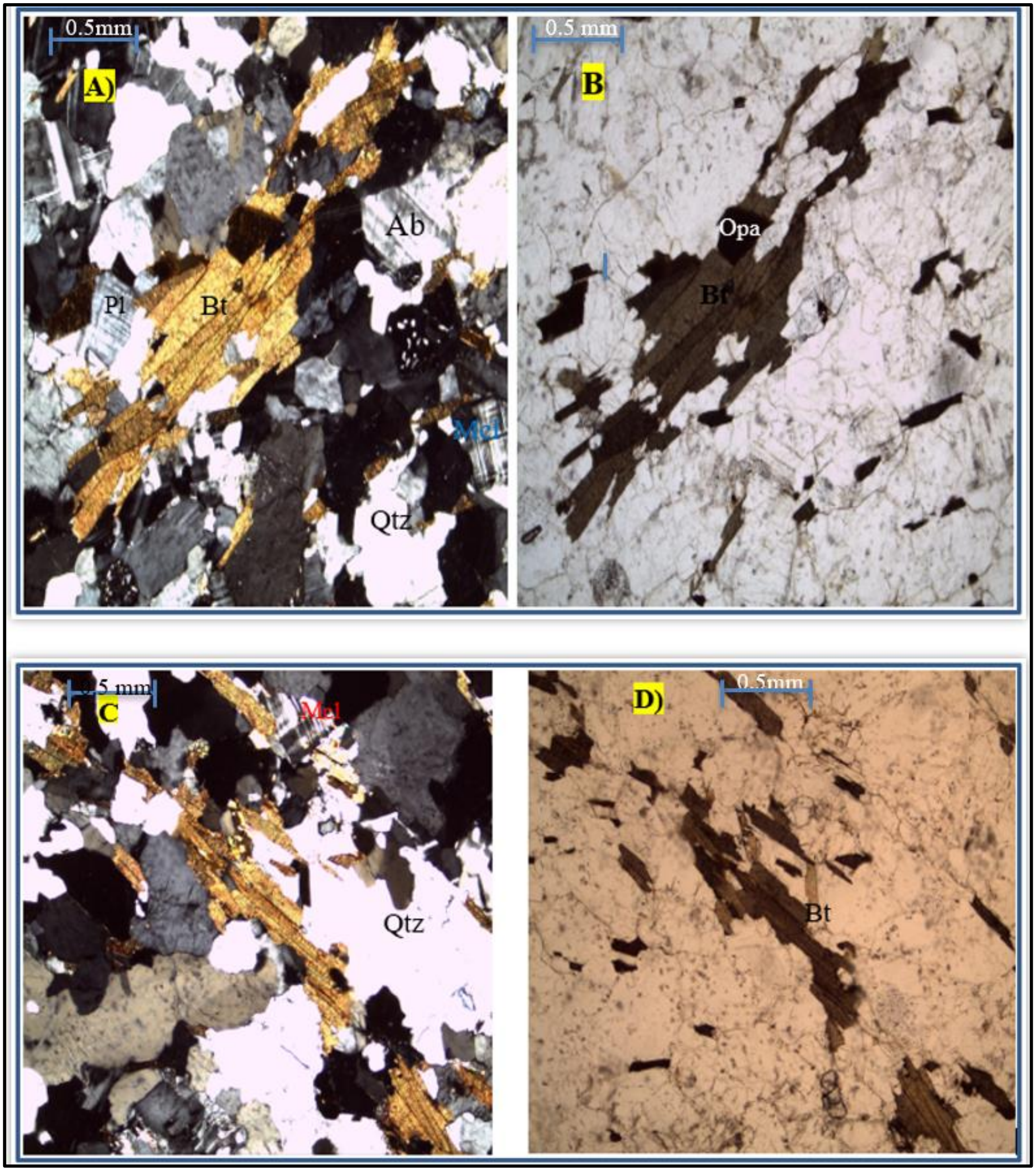
0.5mm
A)
Ab
Pl
Bt
Mcl
Qtz
0.5 mm
B
Opa
Bt
C
Mcl
Qtz
D)
0.5mm
Bt

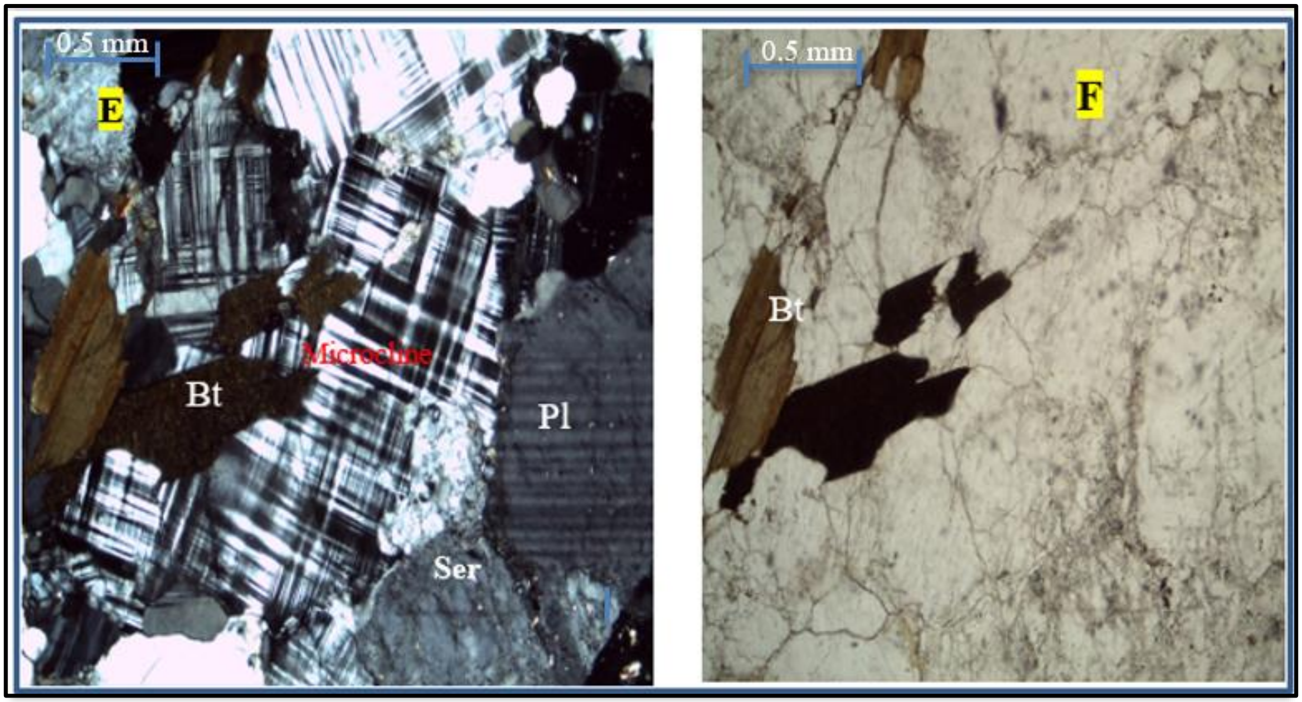

Figure 14: Photomicrograph of Granitic gneiss 4x magnification Elongated biotite crystals with a strong preferred orientation forming a dark layer under XPL view **(**A**)** and PPL view **(**B**)**. A photograph that exhibits a large grain of Quartz surrounded by parallel aliment biotite grain under XPL view **(**C) and PPL **(**D**)** view. Well-developed microcline crystal and clear alteration plagioclase to sericite under XPL **(**E**)** view and PPL **(**F**)** view. The labels of the identified minerals are (Bt-Biotite, Qtz-Quartz, Pl-plagioclase, and Ser-sericite).

3.3.3. Granite

The microscopic examination reveals this rock unit sample for KSG8, KSG9, and KSG10 consists of mineral assemblages of plagioclase (25%), alkali pyroxene (5%), microcline (12%), biotite (20%), quartz (35%), and opaque (3%) minerals. Some of the quartz crystals show little undulose extinction and it occurs as an anhedral to subhedral crystal habit. The quartz grains occur as clusters between the plagioclase and worm-like structure also common as shown in (Fig. 15B). Reaction textures are defined by the intergrowth of two minerals such as feldspar and quartz (granophyric texture or worm-like structure, shown in (Fig. 15C**)**, and alterations are also quite common due to the highly jointed nature of the rock unit. The microcline grows larger characterized by cross-hatch twinning that occurs in sub-hederal to anhedral shape. The alkali pyroxene minerals observed in the rock range between anhedral and subhedral crystal shapes with some visible euhedral grain shapes. And they have higher relief than the other minerals that constitute the granite unit. There is also chemical oscillatory zoning that helps to understand the fractional crystallization mineral. A cluster of subsequent crystals of microcline is abundant in the granites as shown in (Fig. 15D**)**. Some of the pyroxene grains contain inclusions of opaque and biotite. In the thin section view, both albite and microcline appear cloudy due to alteration product development (sericite) as a secondary mica.

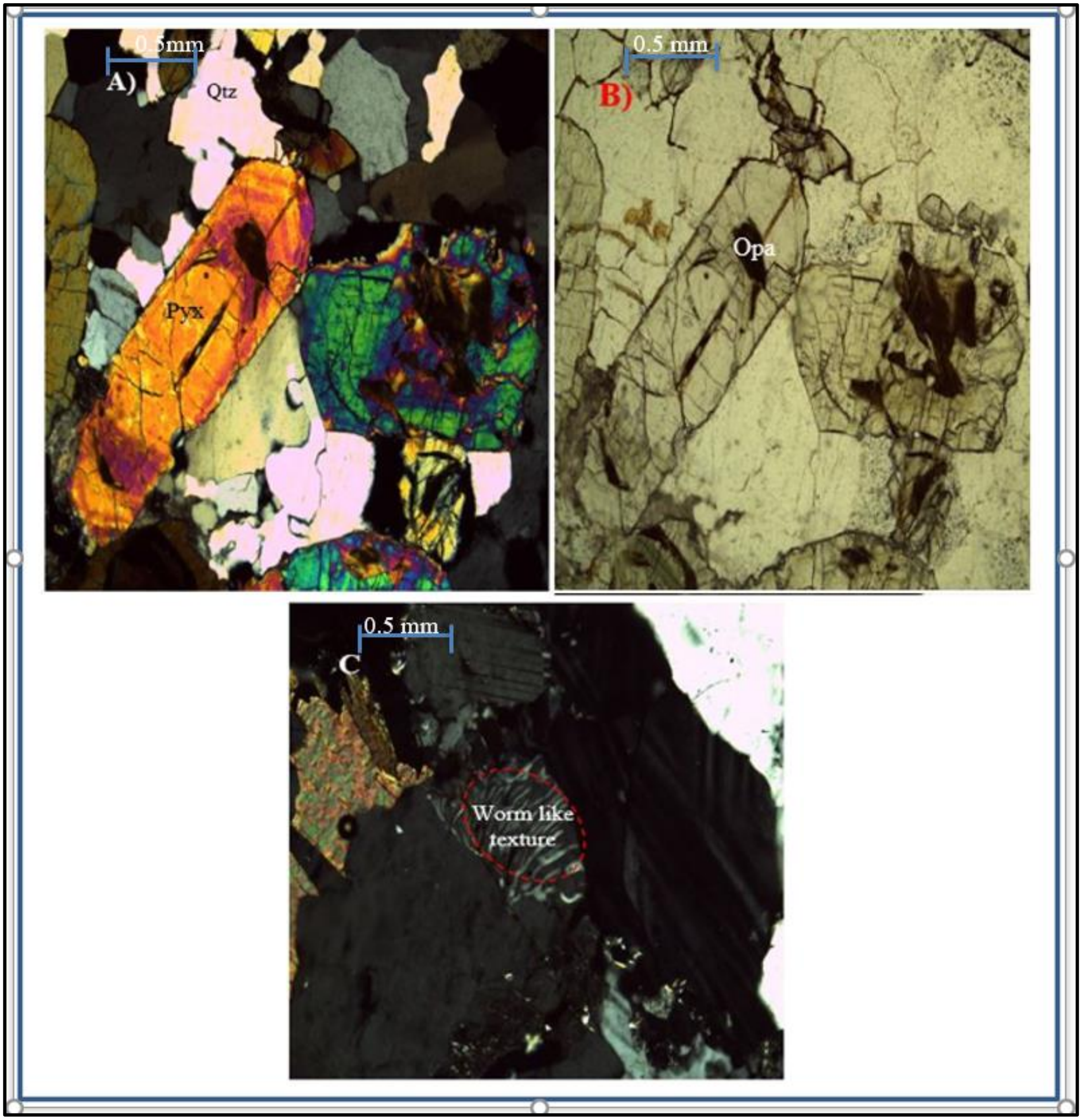

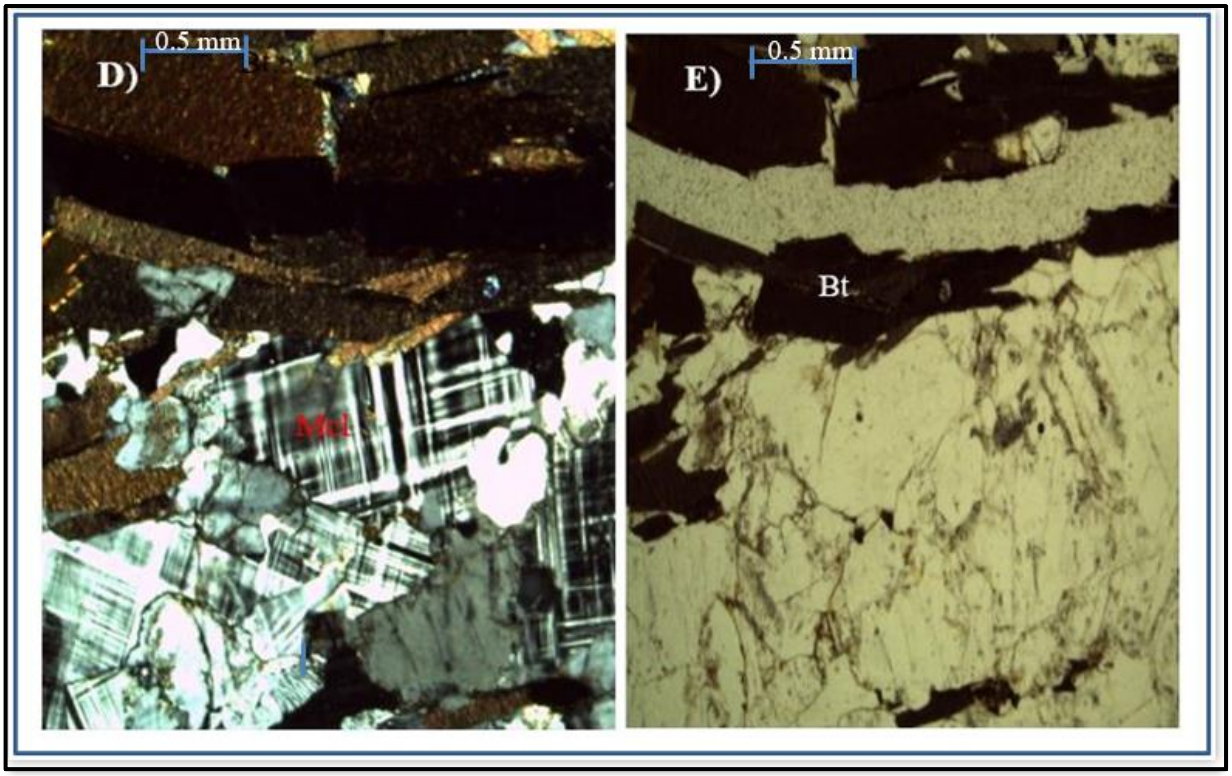

Figure 15: Representative Photomicrograph of granite in XPL and PPL under 4x magnification. A) pyroxene clearly shows oscillatory zoning, B**)** some pyroxene crystal inclusion of opaque and biotite under ppl view C**)** worm-like structure under XPL. Microcline clearly shows cross-hatched twining under XPL view (D**)** and PPL view **(**E**)**. The labels of the identified minerals are (Qtz-Quartz, Bt-Biotite, Mcl- microcline, Pyx-pyroxene, and Opa-opaque).

3.3.4. Mica schist

In the petrographic analysis, the KSMS13 mica-schist rock sample was found to have a schistose type of foliation, with muscovite dominating the parallelism of the mica flakes. Platy minerals aligned in this sample have resulted in crenulation cleavage. The rock is composed of minerals such as muscovite (40%), biotite (25%), quartz (17%), plagioclase (13%), and some opaque (5%) minerals. In certain instances, the quartz and biotite grains exhibit boudinage shape due to the deformation of minerals to Augen texture, with their longest axis penetrating in the direction of foliation, as can be seen in (Fig. 16C and D).

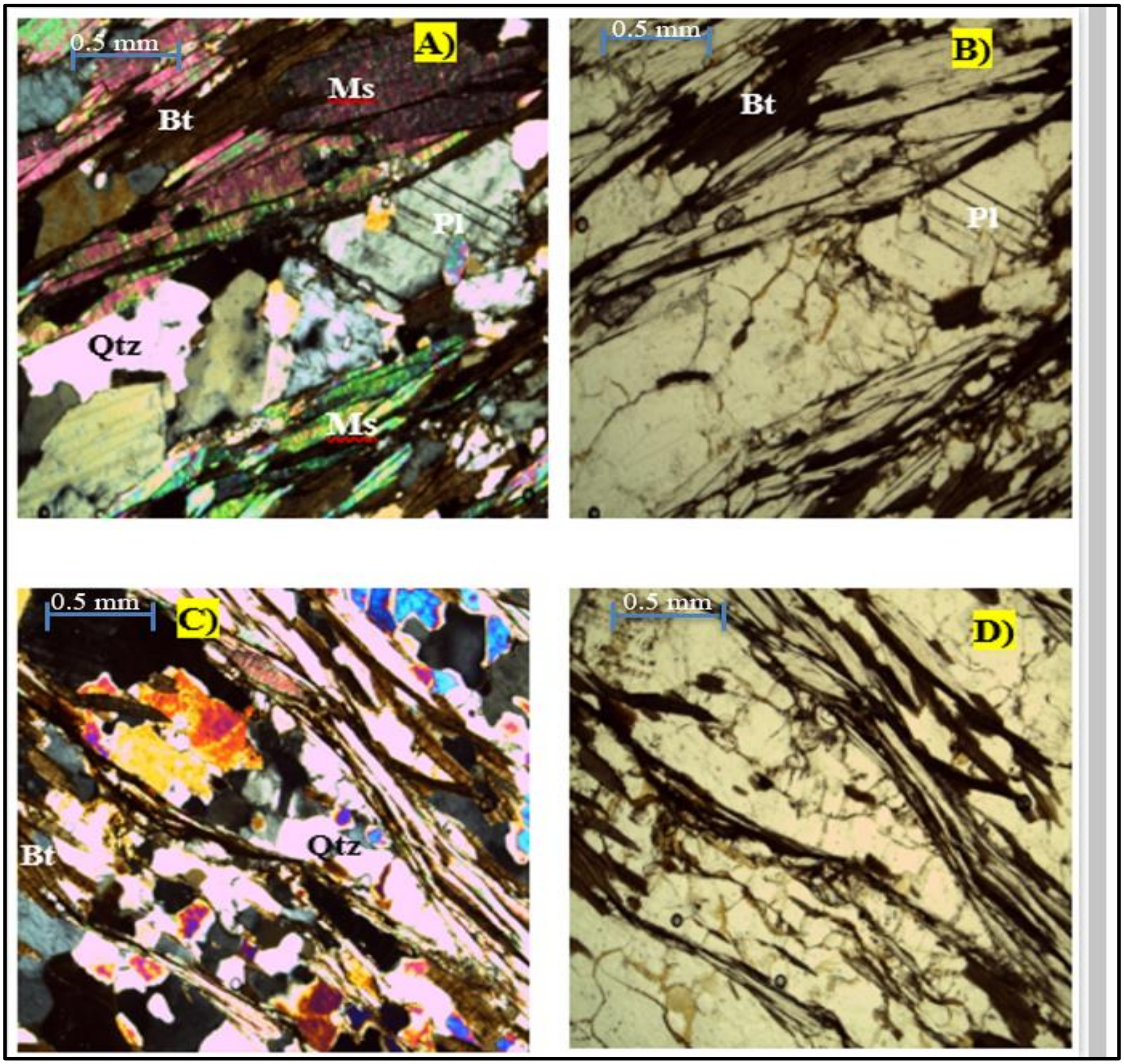

Figure 16: Representative photomicrographs under (XPL & PPL) of Mica schist. **(**A**)** Photomicrograph of Mica schist under XPL view; hypidioblastic biotite flakes with a strong preferred orientation forming foliation. **(**B**)** Photomicrograph of Mica schist under PPL view; grains of xenoblastic quartz and xenoblastic to hypidioblastic plagioclase surrounded by hypidioblastic muscovite flakes, forming schistose structure **(**C**)** quartz displays clear aggregate up and down in biotite grain **(**D**)** biotite and quartz crystals grain clearly shows Augen shape. The labels of the identified minerals are (Bt-Biotite, Qtz-Quartz, Pl-plagioclase, and Ms-Muscovite.

3.3.5. Biotite gneiss

As shown in (Fig. 17**)**, the KSBN4 and KSBN6 biotite gneiss samples are mostly composed of quartz (30%), plagioclase (17%), albite (13%), biotite (35%), and opaque (5%) minerals. The rock displays alternating light-colored layers of quartz and feldspar, and dark layers rich in biotite. The quartz grains reveal undulated extinction and irregular crystal shapes, with inclusions of quartz grains found in plagioclase. Meanwhile, the plagioclases are xenoblastic to hypidioblastic in anhedral to sub-hederal shape, exhibiting albite twinning. The biotite forms lath-shaped crystals with perfect cleavages in one direction, and together with elongated plagioclase and quartz, defines the foliations of the rocks. Lastly, the opaque minerals are mostly present as irregularly shaped crystals.

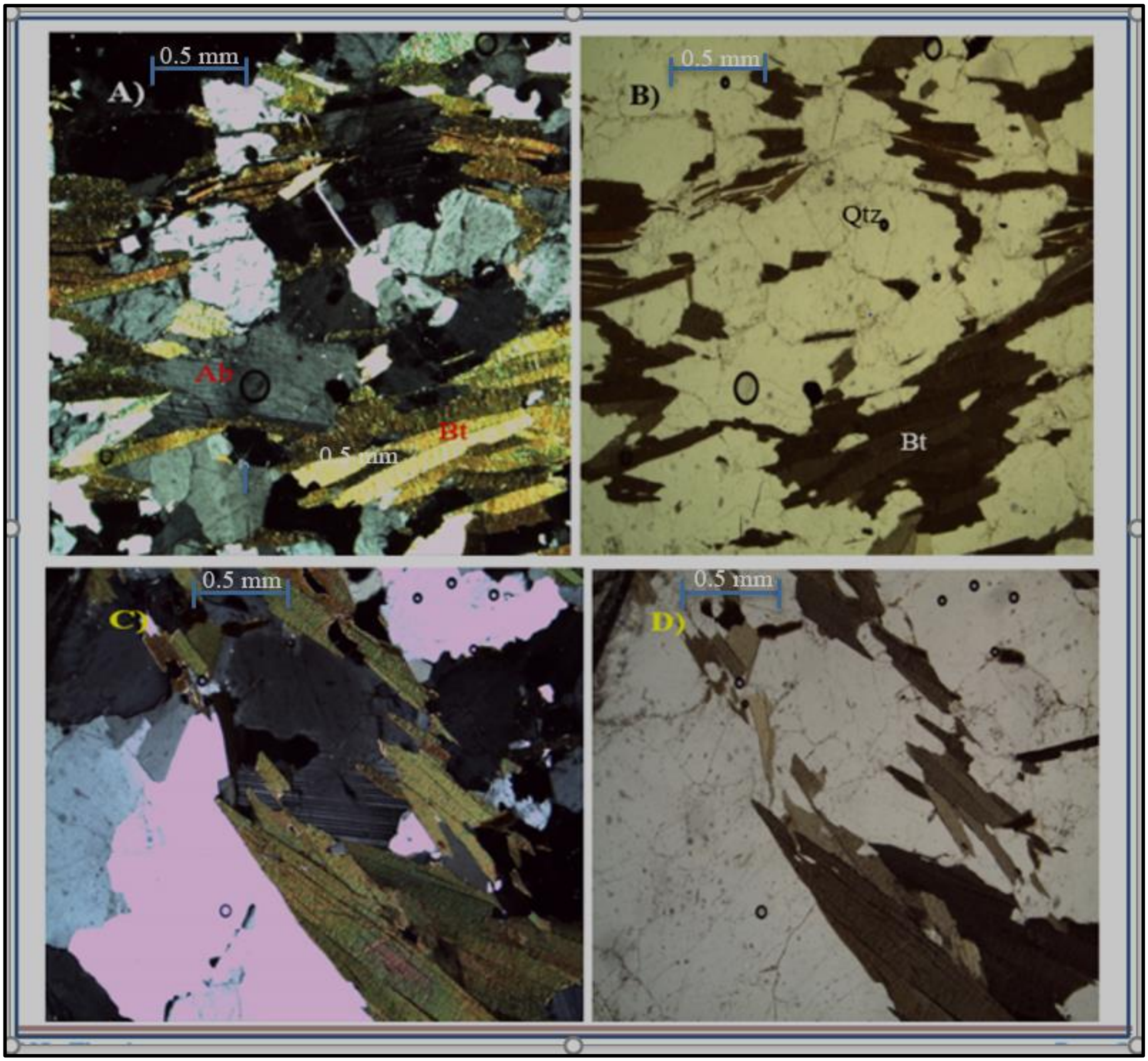

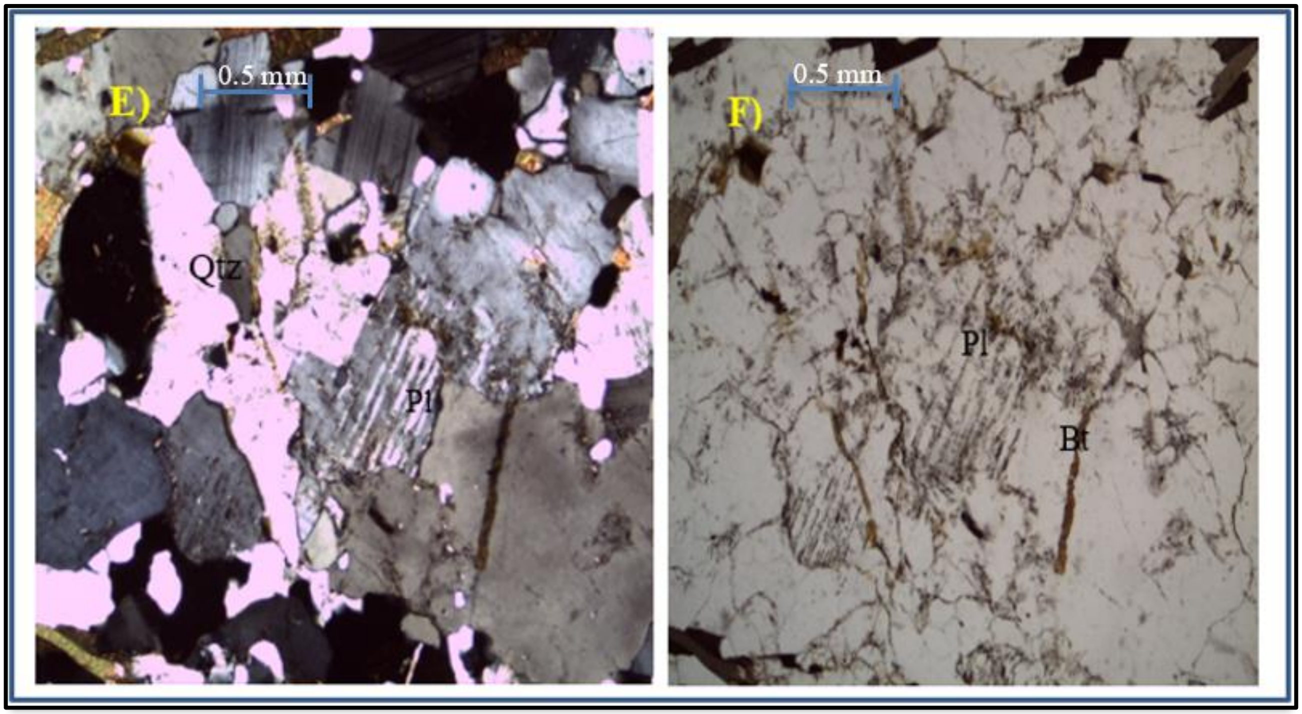

Figure 17: Photograph that shows quartz inclusion in poikilitic texture sample under XPL view **(**A**)** and PPL view **(**B**)** and microphotograph that plagioclase clearly shows polysynthetic twining and Elongated biotite crystals with a strong preferred orientation that shown under XPL view **(**C**)** and PPL view **(**D**)**. A photograph that shows Quartz inclusions in a large crystal of plagioclase under the XPL **(**E) view and PPL **(**F**)** view. The labels of the identified minerals are (Bt-Biotite, Qtz-Quartz, Pl-plagioclase, and Ab-Albite).

3.4. Geological Structures of the area

In the study area, the rocks have been affected by several phases of deformation as evidenced by the presence of both ductile and brittle structures in the area. The ductile geological structures foliation and lineation while the brittle geological structures joints, veins, dikes, and fractures have been observed in the study. These structures have been formed due to tectonic processes which resulted in different geological structures. The presence of various discontinuity planes on different geological units is responsible for these structures. An equal-area plot and rose diagram have been used to show the orientation of all fabric, which indicates multiphase deformation. The various orientations (strike and dip) of geological structures are shown in Appendix 2.

3.4.1. Foliation

Foliation is a planer structure dominantly found in a metamorphic rock resulting from the ductile flatting of grain. Foliation is the most common structure, which affects most of the rocks in the area. In the study area, this foliation is defined by slaty cleavage and alignment of elongate minerals which have a strike of NE to SW with gently to horizontal and dipping of NW and SE as shown in the stereographic projection. (Fig. 18) shows gneissic banding formed from the tectonic segregation of mafic and felsic minerals, which are formed before folding. The Equal-area and rose diagram shows the orientation of foliation. Various foliations orientations have been measured in the area with the strike of S20W and 70NW; S20W:70SE; S30W:60NW and the rest are attached in the appendices.

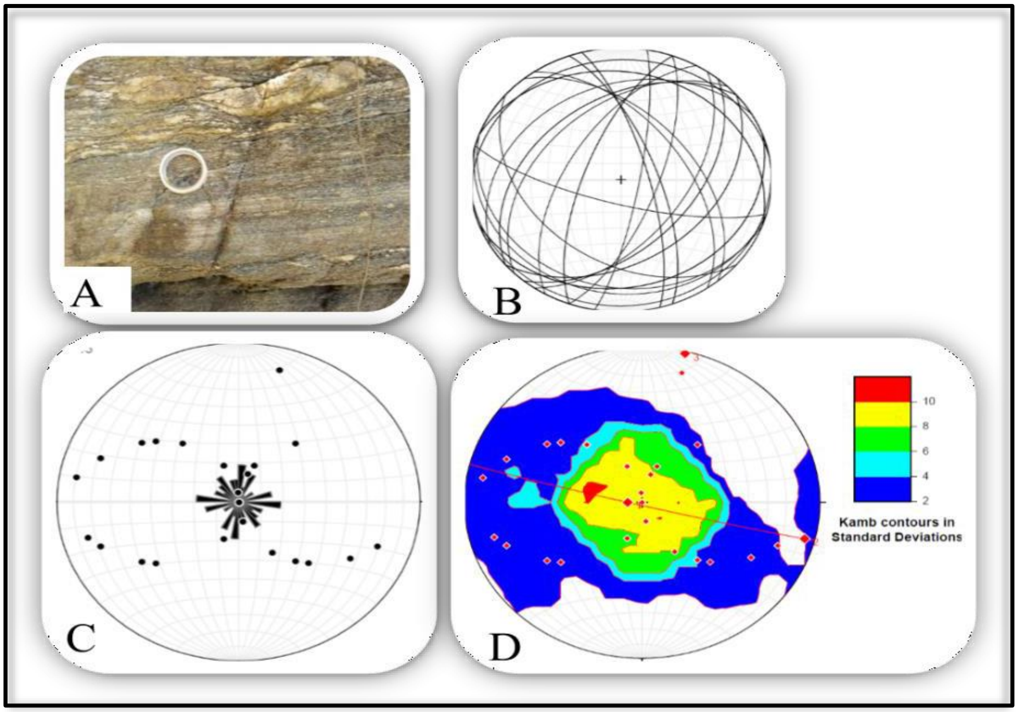

Figure 18: Shows **A)** foliation, **B)** Stereo plots of planes to the foliation, **C)** Stereo plots of the pole to foliation and rose diagram **D)** Kamb counters plot foliation of data.

3.4.2. Fold

There are many fold structures observed in the study area as shown in (Fig. 19**)**. Asymmetric, symmetric, Ptygmatic, recumbent, major, and minor fold structures are measured and present in the study area. Ptygmatic fold involves an irregularly folded, isolated layer, typically a quartzo-feldspathic vein is observed in a ductile amphibole gneisses rock unit.

By using a contoured equal-area point diagram the orientation of the axial trace of the fold is determined from a large number of data points of pole to foliation.

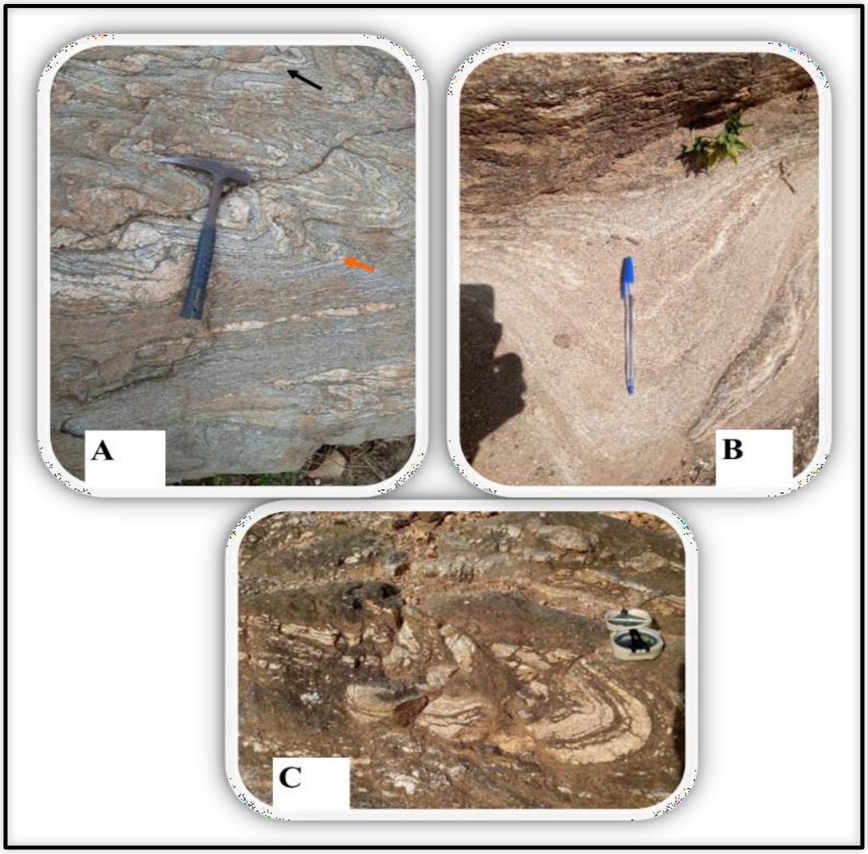

Figure 19: A**)** Red arrow shows ptygmatic fold and red arrows small scale M fold, B**)** Synformal fold, and C**)** Recumbent fold

Figure 20: Fold structure shows **A)** Antiformal fold and **B)** Recumbent fold

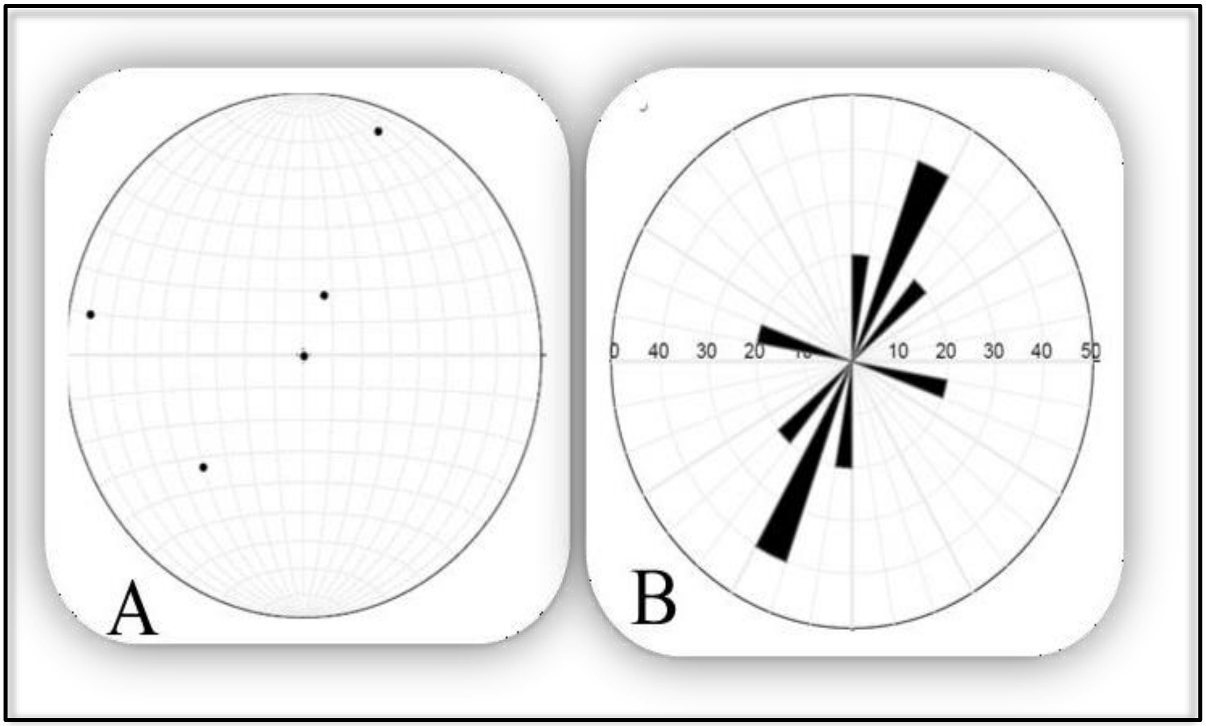

Figure 21: A) Point data of lineation and B) Rose diagram of lineation

3.4.3. Joint

Joints are fractures formed without any significant displacement. There are different generations of joints in different parts of the study area which are parallel or oblique to foliation as shown in (Fig. 22).

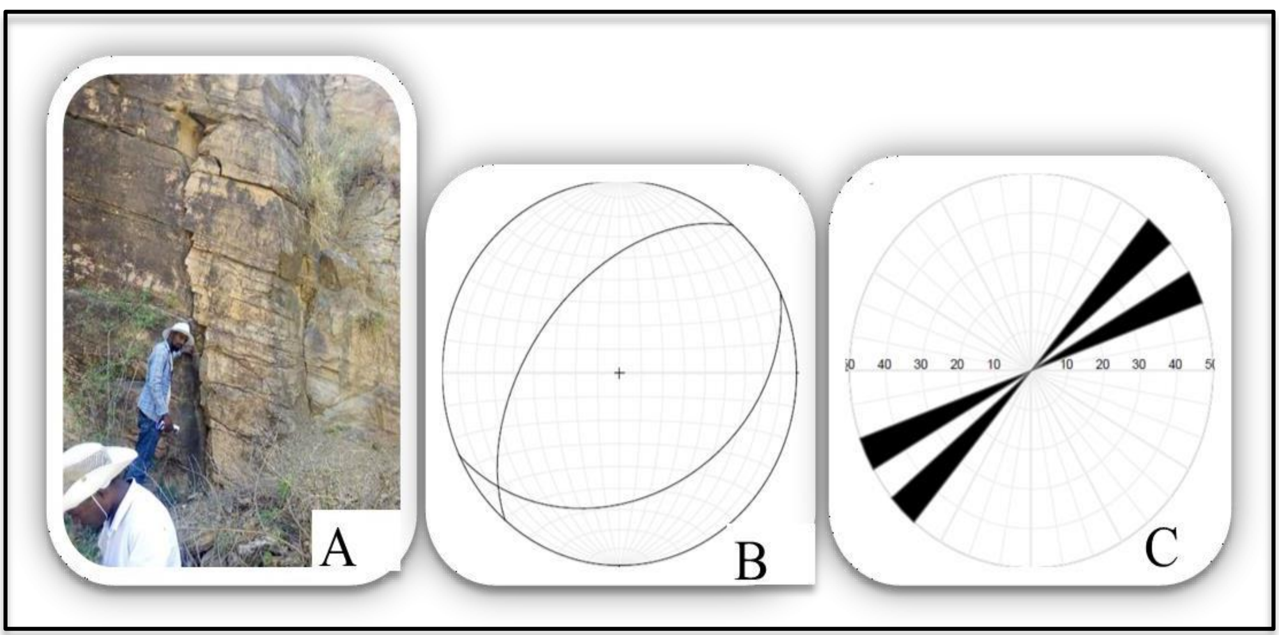

Figure 22: A) Field photograph of Joint structure B) Stereonet plot of a plane to joint and C) Rose diagram of joints

3.4.4. Boudinage

Boudins are formed when lengthening affects a layered rock formation involving competent felsic layers of boudinage within a less competent, easily deformable, host rock. Upon extension, the stronger layers which are competent are lengthened via heterogeneous thinning leading to the development of pinch and swell structures. Amplification of thinning in the pinched regions eventually led to the segmentation of the stronger layers into boudins separated by the necks. Thinning and necking in the stronger layers often initiate the development of extensional fractures as shown in (Fig. 23).

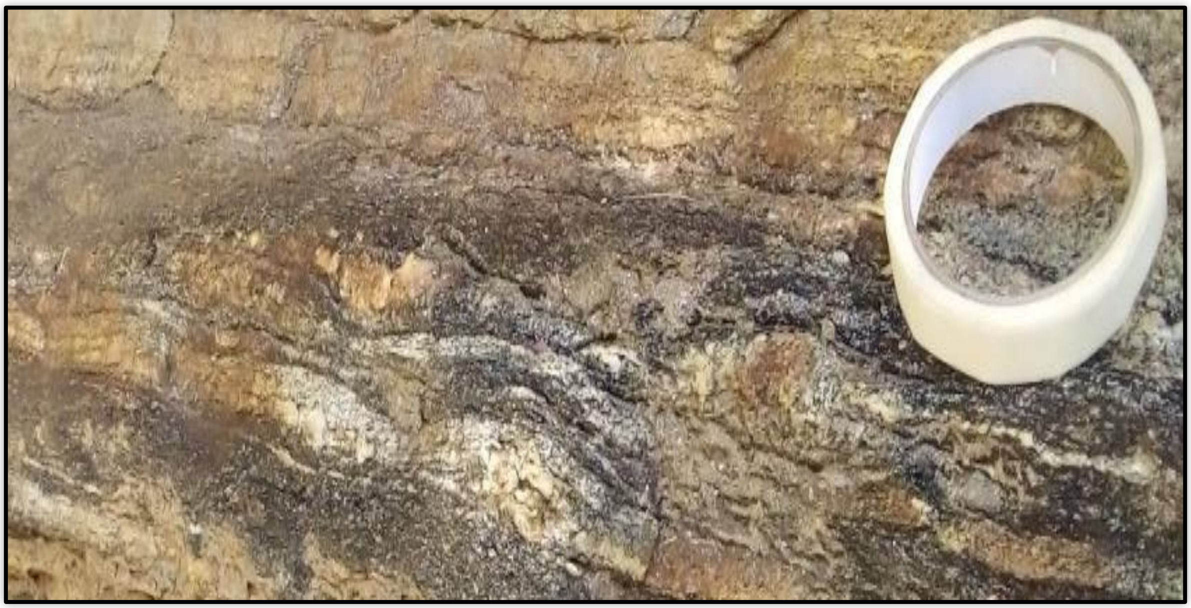

Figure 23: Boudinage structure

3.4.5. Ductile shear sense indicators

There are several ductile shear zone indicators features in the study area which is used to determine the sense of shearing. These shear sense indicators are asymmetric small-scale folds and mica fish as shown in (Fig. 24).

The geometry of mica fish structure is the result of dissolution, growth, and internal deformation. Commonly, trails of small mica fragments extend into the matrix from the tips of isolated mica fish. In general, (Fig. 25) clearly shows the geological map and structural view of the study area.

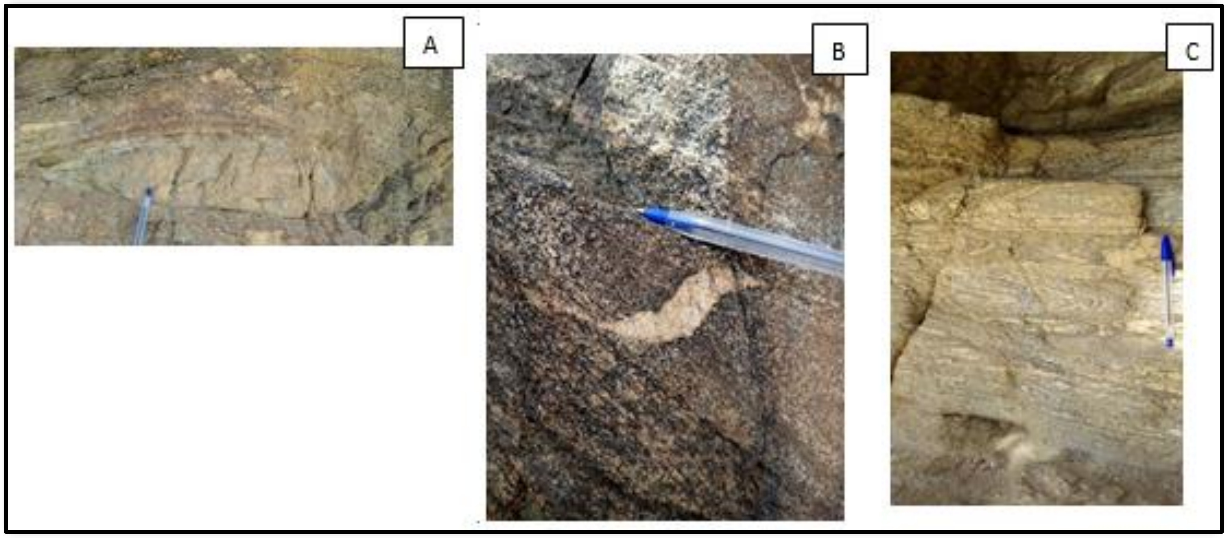

Figure 24: A) Mica fish structure showing dextral shearing, B and C) Small scale S fold structure showing sinistral shearing

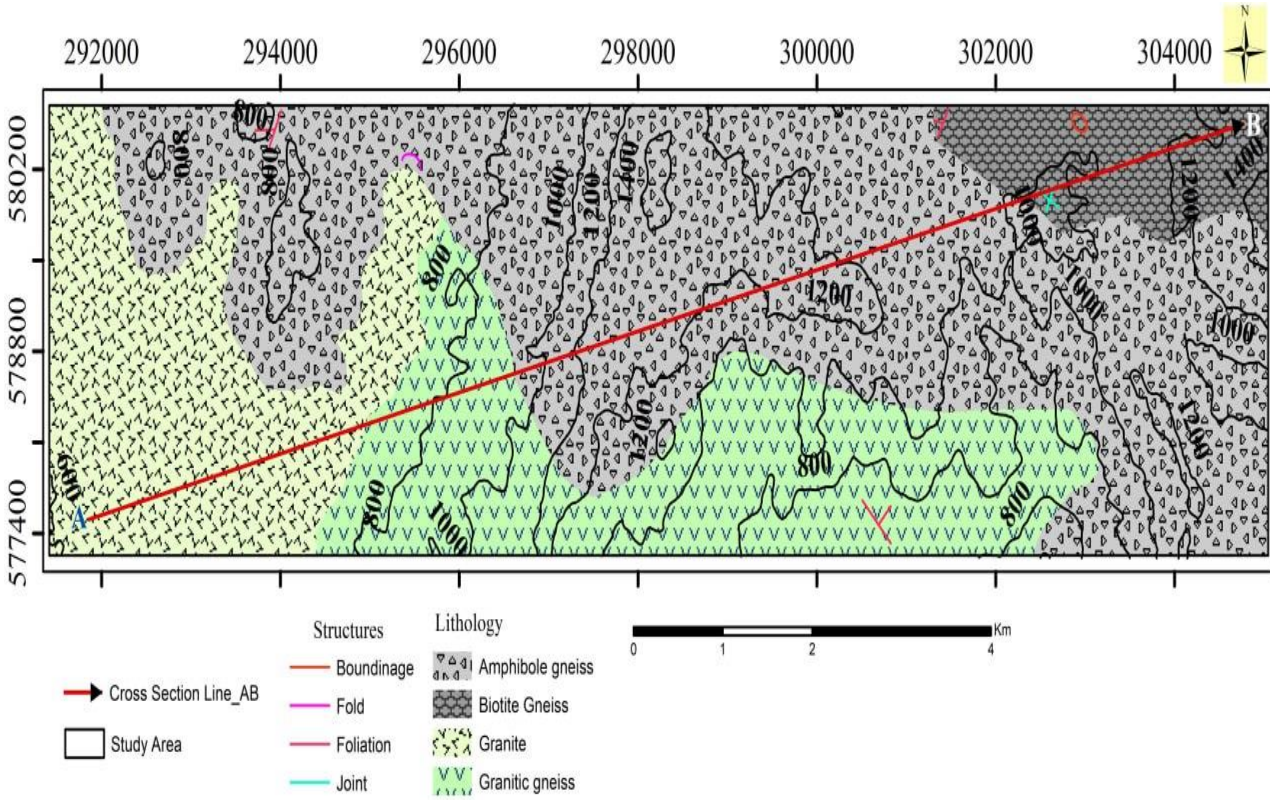

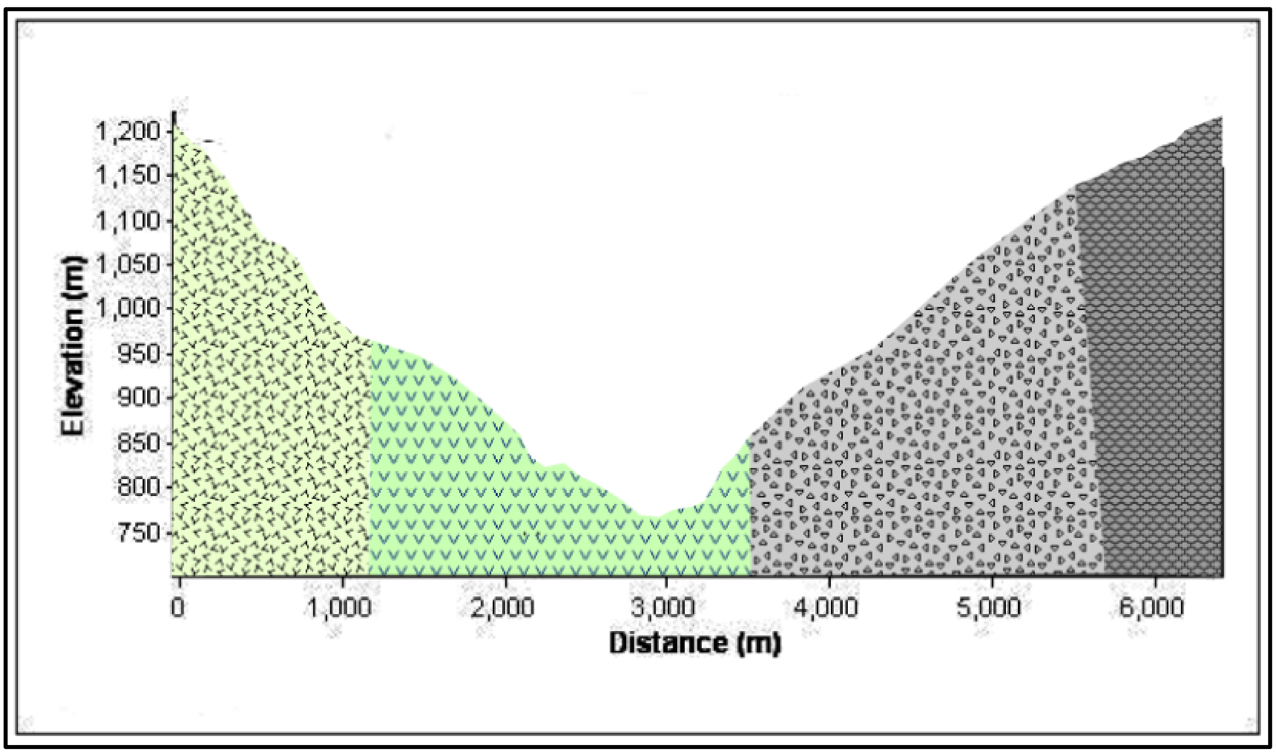

Figure 25: Geological map and Cross-sectional profile (A-B) of the study area

3.5. Metamorphism

By combining field observations, thin section analysis, and potentially geochemical data, all the rocks study area as a regional metamorphic event with a range of intensities**.** Medium-grade rocks like biotite gneiss and mica schist indicate moderate conditions, while high-grade rocks like amphibolite gneiss and granite gneiss suggest areas that experienced significantly higher temperatures and pressures. Additionally, the presence of granite rocks might suggest localized contact metamorphism, where the heat from intruding granite magma causes thermal alteration of surrounding rocks. The analyzed sample amphibolite gneiss is compositionally dominated by hornblende, biotite, chlorite, and with minor amounts of quartz. The dominance of mafic minerals and the chemistry of two samples from this unit typified as 48.8-49.1 wt. % SiO_2 indicates that the protolith of this rock is mafic igneous rock most probably basalt. On the contrary to this, samples KSGN1, KSGN2, KSGN3, and KSGN5 are compositionally dominated Quartz, K-feldspar microcline or orthoclase, plagioclase feldspar, biotite.; and the chemistry is characterized as 61.6-78.1 wt. % SiO2 This indicates that the protolith of this rock is felsic igneous rock most probably granite. The segregation of mafic and felsic-rich compositional bands both at the mesoscale and in the thin section; and the dominance of hornblende and plagioclase in the mineral assemblage indicates that rock has been subjected to high-grade metamorphism.

The Mineral assemblages of various rock units from the study area are described as follows:

1. **Biotite gneiss:** Biotite (mica) + quartz + feldspar ± muscovite ± opaque minerals.
2. **Amphibolite gneiss:** Hornblende + chlorite + quartz ± biotite ± opaque minerals.
3. **Granite gneiss:** K-feldspar (microcline) + quartz + plagioclase feldspar + biotite ± muscovite.
4. **Mica schist:** Muscovite + quartz + plagioclase feldspar ± garnet ± opaque minerals.
5. **Granite rock (unaltered):** Quartz + K-feldspar + plagioclase feldspar + biotite ± muscovite ± opaque minerals.

CHAPTER FOUR

4. GEOCHEMISTRY OF THE AREA

4.1. Introduction

The primary objective of the geochemical data was to investigate the paleo-tectonic setting, petrogenetic evolution, and the protolith of the basement rocks. Additionally, it aimed to understand the behavior of elements during alteration and metamorphism. Based on the analytical results obtained for the samples, the data were interpreted, plotted, and analyzed in terms of both major and trace elements. The major element data was recalculated to 100% on a volatile-free basis for presentation in the geochemical classification as shown in Table 1.

Table 1: chemical analysis of the selected samples where Major and minor oxides expressed in wt% and trace elements in ppm.

Major Oxides (wt. %)	**Metamorphic Rocks**						**Intrusive Rock**		
	Granitic Gneiss				**Amphibolitic gneiss**		**Granite**		
	KSGN1	KSGN2	KSGN3	KSGN5	KSAM11	KSAM12	KSG8	KSG9	KSG10
SiO_2	69.5	78.1	61.6	69.8	49.1	48.8	77.1	74.4	71.1
TiO_2	0.55	0.08	0.8	0.5	0.36	1.7	0.03	0.01	0.27
Al_2O_3	14.5	11	18.6	14.6	15.7	16	12.8	14.4	13.8
Fe_2O_3	4.53	1.62	7.36	4.16	11.8	13	1.21	1.07	2.71
MnO	0.08	0.01	0.11	0.06	0.09	0.28	0.01	0.1	0.05
MgO	1.01	0.04	1.53	1.5	8.07	6.42	0.03	0.09	0.39
CaO	2.33	0.32	1.4	3.16	9.24	10.4	0.2	0.51	1.32
Na_2O	2.86	2.81	2.49	3.8	2.76	2.51	2.51	4.3	4.22
K_2O	4.29	5.06	4.45	2.19	0.64	0.77	7.48	5.16	3.87
P_2O_5	0.09	<0.01	0.14	0.15	0.11	0.24	0.01	0.03	0.12
Cr_2O_3	0.006	<0.002	0.006	0.004	0.002	0.027	0.003	0.002	0.002
SrO	0.22	<0.01	0.01	0.05	0.03	0.04		0.01	0.03
BaO	0.13	0.02	0.08	0.07	0.02	0.01	0.01	0.01	0.1
LOI	0.71	0.35	2.14	1.15	0.29	1.35	0.37	0.48	0.37
Total	100.8	99.4	100.666	101.194	98.212	101.547	101.813	100.562	98.35
Trace element (ppm)	**Metamorphic Rocks**						**Intrusive Rock**		
	Granitic Gneiss				**Amphibolitic gneiss**		**Granite**		
	KSGN1	**KSGN2**	**KSGN3**	**KSGN5**	**KSAM11**	**KSAM12**	**KSG8**	**KSG9**	**KSG10**
Sc	8	1	18	6	32	39	1	14	4
V	59	5	95	75	361	349	<5	14	14
Cr	62	16	57	32	221	210	35	29	21
Co	7	1	12	7	45	37	<1	1	1
Ni	8	1	16	10	60	65	<1	2	1
Cu	19	3	23	26	115	117	<1	2	<1
Zn	54	26	131	34	171	168	4	9	46

Cs	3.67	1.14	6.99	1.27	0.23	0.47	15.8	48	0.91
Ga	19	19.6	27.2	18.2	20.3	21.8	25.8	62	19.2
Rb	71	138	115	69.5	23.4	22.6	457	259	80.6
Sr	1975	35.4	1755	448	402	381	48.3	76.6	295
Y	9.5	26.8	36.6	10.4	32.5	30.1	12.3	5.9	23.3
Zr	288	172	225	130	101.1	95	6	25	238
Nb	7.44	9.99	10.9	7.18	4.68	2.51	41.3	107	7.32
Ba	1120	169	651	637	85.9	79.8	63.6	114	911
La	8.3	14.5	35.1	18.8	5.02	7.1	1.1	2	30
Ce	8.1	103	61.3	31.7	18.1	17.3	1.2	4.8	56.4
Pr	1.16	4.51	8.52	4.28	3.06	2.87	0.22	0.93	7
Nd	5.1	19.8	34.1	16.1	17.4	14.6	1.1	4	27.6
Sm	1.08	5.37	6.63	2.95	5.12	4.57	0.49	2.64	5.28
Eu	0.39	0.23	1.54	0.8	1.09	1.6	0.2	0.07	0.91
Gd	1.14	5.43	6.56	2.53	6.24	5.07	0.91	2.5	4.1
Tb	0.17	1.1	1.06	0.36	0.73	0.81	0.2	0.35	0.58
Dy	1.44	6.65	6.7	1.74	6.78	5.19	1.62	1.25	4
Ho	0.35	1.31	1.33	0.4	0.9	1.16	0.47	0.15	0.85
Er	1.36	4.03	3.81	1	4.02	3.42	2.22	0.37	2.38
Tm	0.26	0.63	0.67	0.19	0.05	0.51	0.41	0.07	0.4
Yb	2.1	4.96	4.25	0.99	4.25	3.08	3.06	0.46	2.6
Lu	0.4	0.7	0.64	0.16	0.3	0.46	0.58	0.07	0.37
Hf	7.74	8.64	6.16	3.41	3.01	2.74	0.37	5.02	6.33
Ta	0.5	1	0.7	1.3	0.8	0.2	5.2	69.2	0.6
Pb	56	14	14	6	15	8	86	23	12
Th	6.29	20.4	9.78	7.42	0.62	0.34	6.97	5.37	8.65
U	2.54	2.6	2.15	1.44	0.05	0.09	9.1	11.6	1.55
∑REE	31.35	172.22	172.21	82	73.06	67.74	13.78	19.66	142.47
Eu/Eu *	1.07	0.13	0.71	0.89	0.2	1.01	0.91	0.08	0.6
LaN/Y bN	2.69	1.99	5.62	12.92	0.8	1.57	0.24	2.96	7.85
EuN/Y bN	0.53	0.13	1.04	2.31	0.74	1.49	0.19	0.44	1

4.2. Geochemistry of Rocks

4.2.1. Major Elements Geochemistry and Rock Classification

The purpose of utilizing major element variation diagrams is to characterize, analyze, and classify rock samples of the area which are plotted in a constructive variation diagram. The selected major element oxides of the studied rocks were plotted against SiO_2 concentrations in Harker variation diagrams (Fig. 26). In general, the samples in the study area exhibit a trend of decreasing Al_2O_3, TiO_2, MgO, CaO, and P_2O_5 as SiO_2 increase. The K_2O and Na_2O concentration shows an increasing pattern even though they show scattered and irregular distribution patterns (Fig. 26E). The TiO_2 shows a scattered negative correlation with SiO_2 content. The Na_2O shows good correlation in contrast to K_2O, hence, K_2O shows most data scatter and poor correlation. These irregular trends indicate magma contamination during the asthenosphere uprise. The major element oxides selected in intrusive rock were plotted against SiO_2 concentrations in Harker variation diagrams. Most of the rock samples are characterized by very high silica contents (71.1 to 78.6 wt. %); high contents of Al_2O_3 (11 - 14.4 wt. %); Fe_2O_3 (1.07 to 2.71 wt%); Na_2O (2.76 to 4.22 wt%); K_2O (3.87 to 5.39 wt%), low contents of CaO (0.32 to 1.32 wt%); MgO (0.02 to 0.39 wt%), TiO_2 (0.01 to 0.27 wt%), MnO (0.01 to 0.1 wt%), very low P_2O_5 (0.01 to 0.12 wt%).

In the total alkali-silica; SiO_2 (wt %) versus Na_2O + K_2O in (wt %) diagram (Middlemost, 1994), as shown in (Fig. 28A**)** most rock units of granite samples fall in the granite field. However, on the SiO_2 (wt %) Vs K_2O (wt%) diagram (Peccerillo and Taylor, 1976), all the granite rock unit samples occupy the high-K calc-alkaline series as shown in (Fig. 28D**)**. The Alumina Saturation index diagram proposed by Shand (1943) as shown in (Fig.28C) shows that the granite of the study area is exclusively peraluminous as indicated by the values of A/CNK and values of A/NK where A: Al_2O_3, CNK: CaO+ Na_2O+K_2O respectively. On the other hand, the Ab-An-Or classification diagram of (O'Connor, (1965) as shown in (Fig. 28B**)** can be applied to felsic rocks with more than 10% normative quartz. From this triangular diagram, those three sample rocks are occupied in the fields of granite and this proves the major element classification of those granite rocks is dominated in the Southwest of the Kholme area. The irregular trends may indicate the effects of crystals during fractional crystallization processes. The scattered trend is probably due to the alteration effect because the area is highly affected by the metamorphism process.

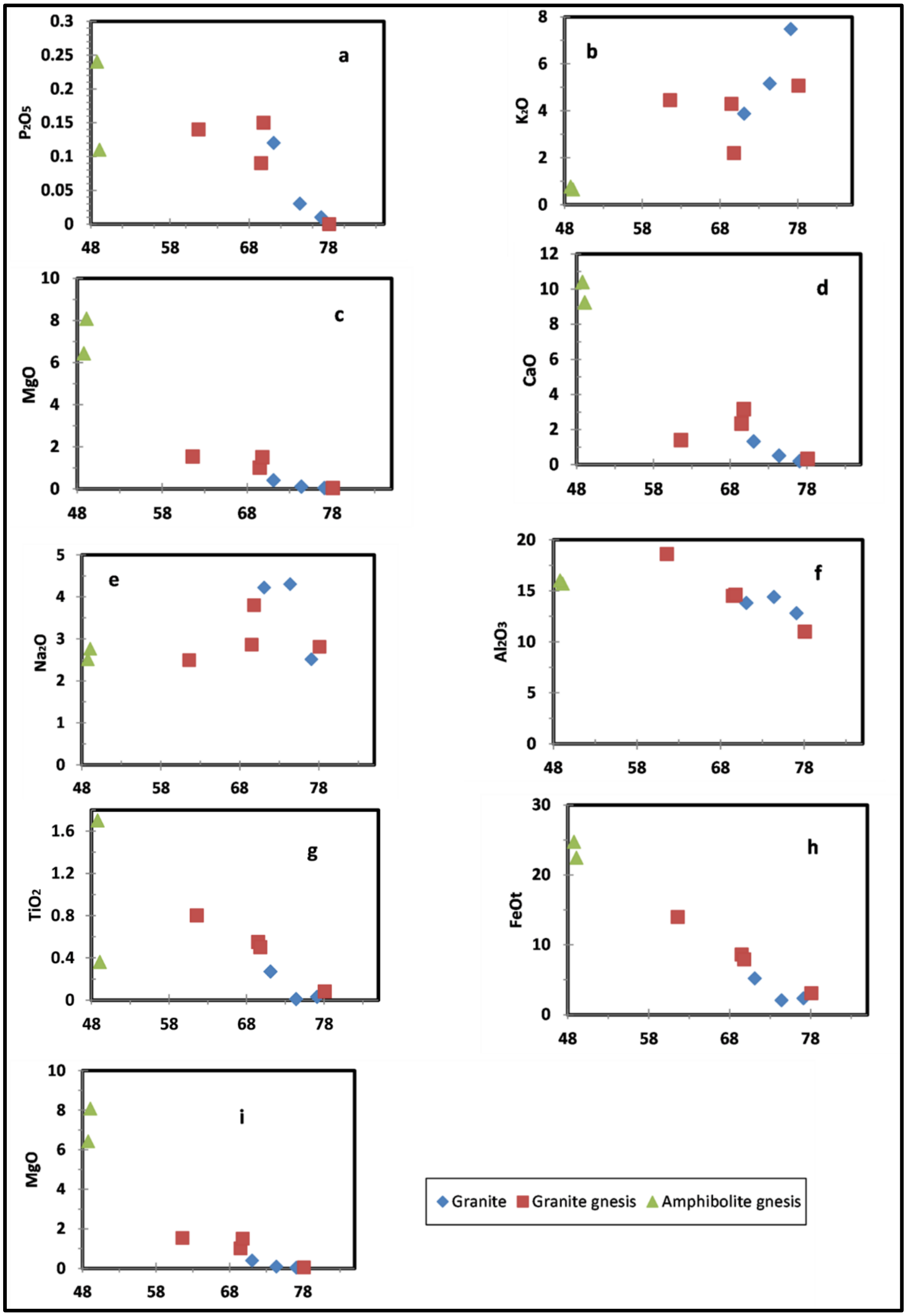

Figure 26: Harker variation diagram of SiO_2 vs major oxides for the studied rock

The AFM diagram is most commonly used to distinguish between tholeiitic and Calc-alkaline differentiation trends in the sub-alkaline magma series as shown in (Fig. 27**)**. Irvine and Baragar (1971) present the separation line of the rocks of the calc-alkaline series and rocks of the tholeiitic series. Thus, amphibolite gneiss rock units lie in the tholeiitic region of the AFM ternary diagram.

Classification of metamorphic rock

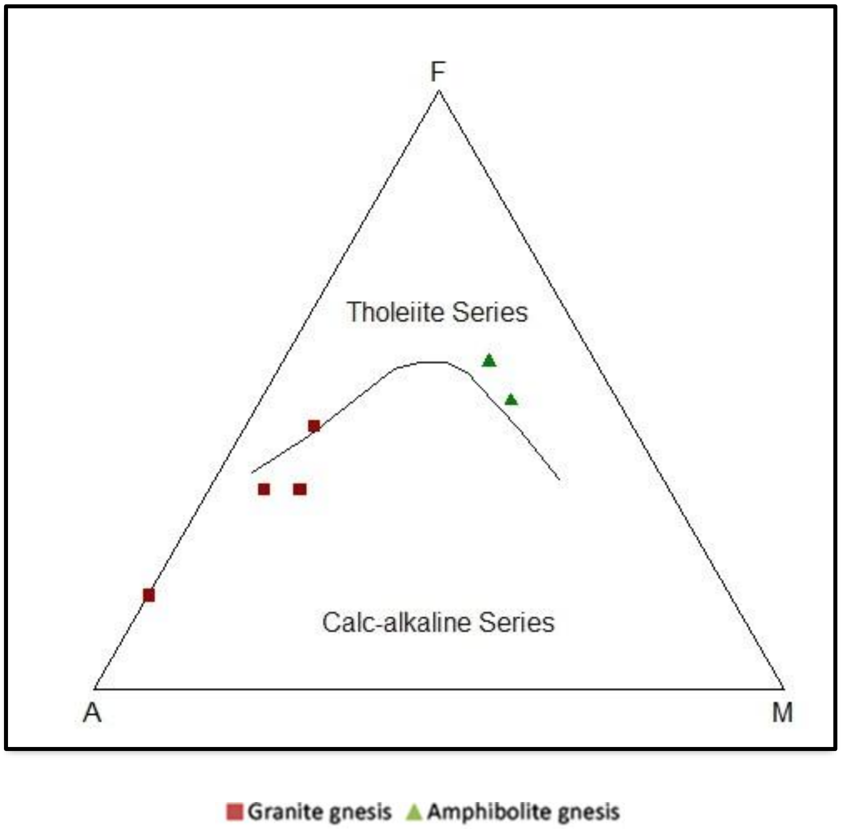

Figure 27: The AFM triangular diagram used to differentiate calc-alkaline series (CA) to tholeiitic series (TH) of orthogneiss rock of the study area: A=Na_2O+K_2O; F=FeO_2+0.9Fe_2O_3; M=MgO using the criteria of Irvine and Baragar (1971).

A

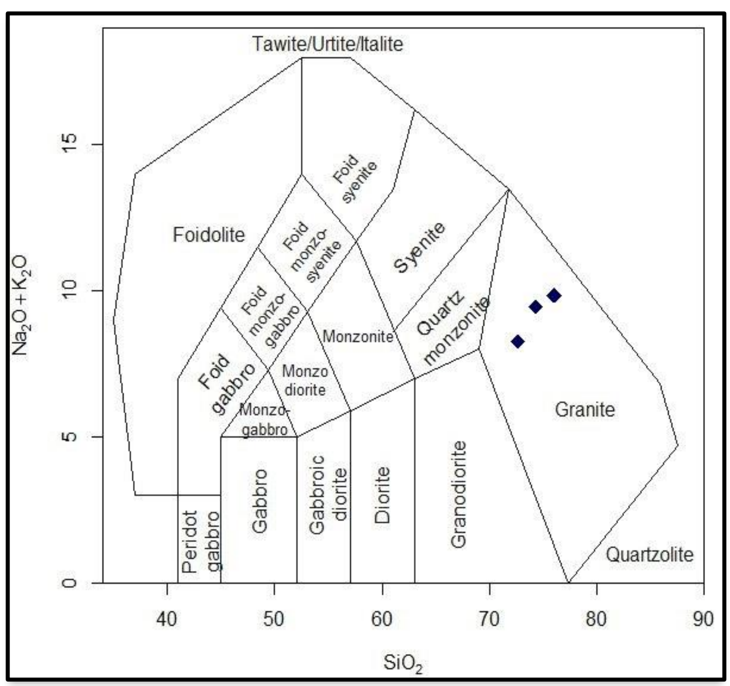

B

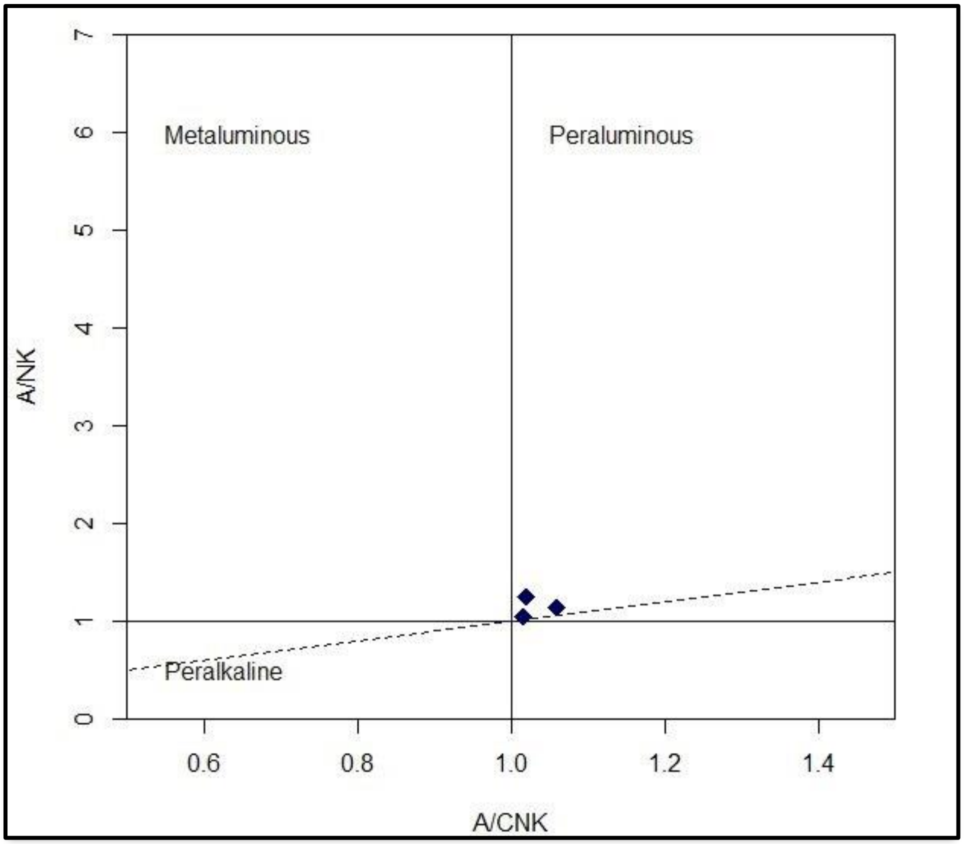
Metaluminous
Peraluminous
Peralkaline
A/NK
A/CNK
0
1
2
3
4
5
6
7
0.6
0.8
1.0
1.2
1.4

C

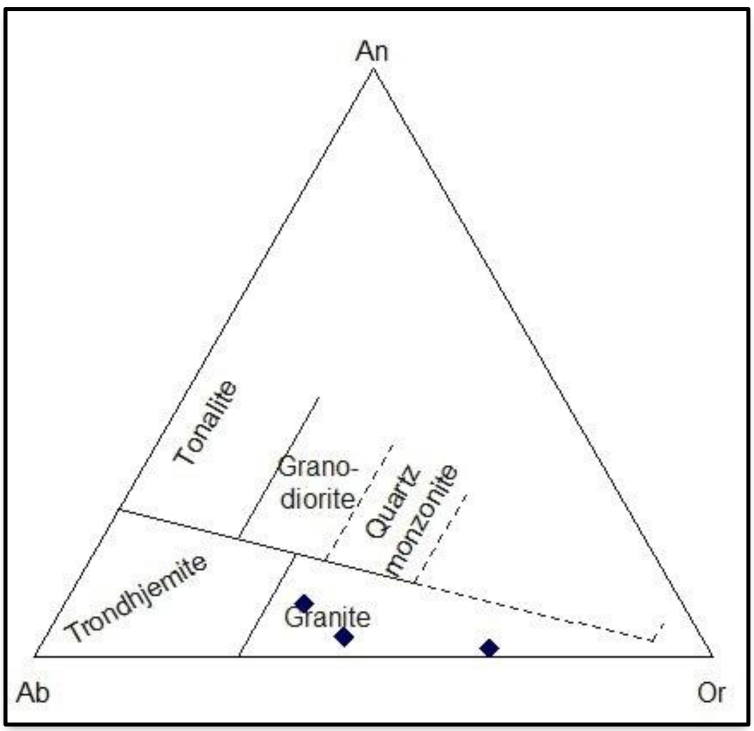
An
Tonalite
Grano-
diorite
Quartz
monzonite
Trondhjemite
Granite
Ab
Or

D

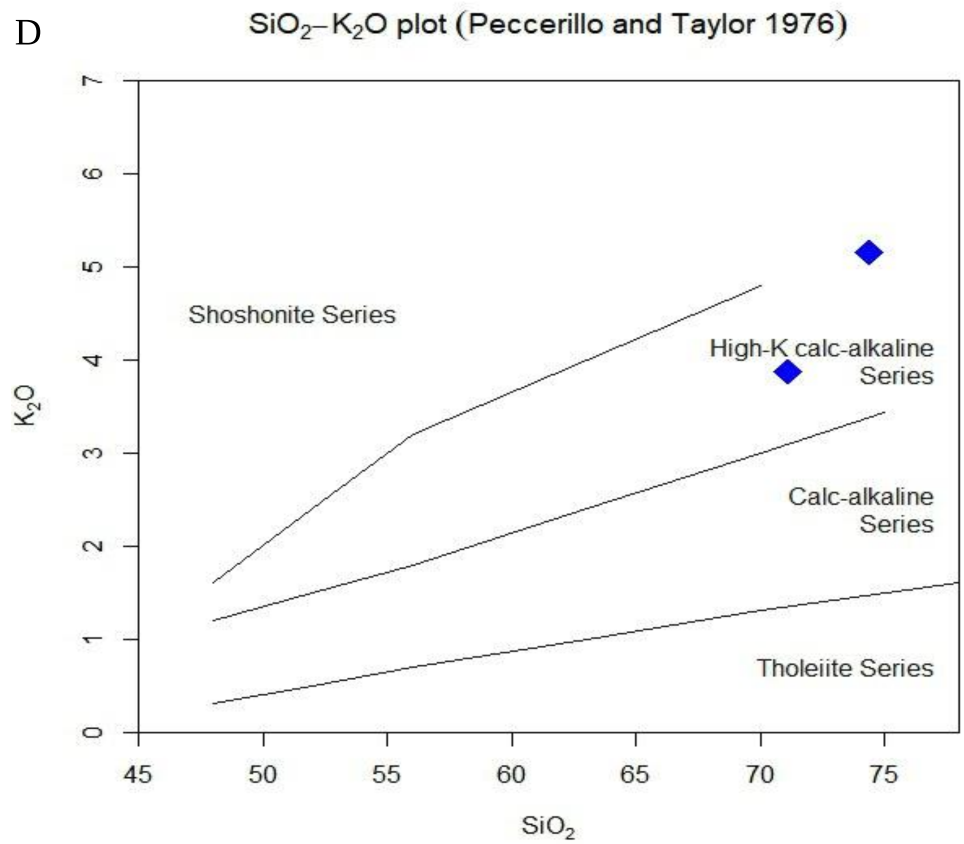

Figure 28: **(**A) Chemical classification diagram for granite rock of the study area based on TAS (SiO_2 Vs. Na_2O+K_2O) of (Middlemost,1994), **(**B**)** A/CNK (Al_2O_3/ ($CaO+Na_2O+K_2O$) Vs A/NK (Al_2O_3/ Na_2O+K_2O) (in molar proportions) plot (Shand, 1943) discriminating met aluminous, peraluminous and peralkaline compositions of the granites rock samples of the study area, **(**C**)** Chemical classification diagram for granite rock of the study area based on Feldspar triangle diagram for granite rock in the study area (Ab-An-Or) of (O'Connor, 1965 and **(**D**)** The K_2O vs SiO_2 plot showing nature of the granite rock (after Peccerillo and Taylor, 1976).

4.2.2. Trace Elements of Geochemistry

Trace elements are chemical elements present in minute quantities (less than 0.1 wt.%) within a rock. Their concentrations are typically expressed in parts per million (ppm) (Rollison, 1993). These elements play a crucial role in understanding the origin, evolution, and petrogenesis (rock formation processes) of rocks. They can constrain factors like the degree of partial melting and the composition of the source mantle.

Table 1 presents the trace element concentrations for the studied samples. These elements exhibit significant variation, with some samples showing exceptionally high values and others displaying very low values. Notably, the analyzed samples display low concentrations of compatible elements such as Cr, Ni, Co, V, Cu, Sc, Sn, and Zn. Their specific concentrations range from Cr (21-210 ppm) to Zn (4-168 ppm) (Fig .29**)** illustrates variation diagrams for selected compatible and incompatible trace elements plotted against SiO2 (silicon dioxide) content. The plot reveals a negative correlation between Ni and V with increasing SiO2. However, the trends for incompatible elements, particularly High Field Strength Elements (HFSE) and Large Ion Lithophile Elements (LILE), are more variable. The HFSE group (Ta, Hf, Zr, Y, Nb, Pb) exhibits a range of concentrations across the samples (Table 1), with Ta varying from 0.2 to 69.2 ppm and Zr from 6 to 288 ppm. In contrast, LILEs (Sr, Rb, Ba), known for their mobility during weathering processes, display moderate to high concentrations (Sr: 48.3-1975 ppm, Rb: 22.6-25.6 ppm, Ba: 63-1120 ppm).

The variation diagram (Fig. 29) further highlights these trends. HFSE elements like Zr, La, and Hf show a decreasing trend with increasing SiO2, whereas Sr (a LILE) exhibits a similar decrease. Notably, U (another selected element) doesn't display a well-defined linear trend. The study identified that high-silica granitic gneiss (KSGN2) and granite samples possess very low concentrations of certain elements. Especially, elements like Ni, V, Co, and Cu even fall below the instrument's detection limit in these samples. Conversely, the amphibole gneiss displays a higher concentration of these elements compared to the granite gneiss and granitic rocks.

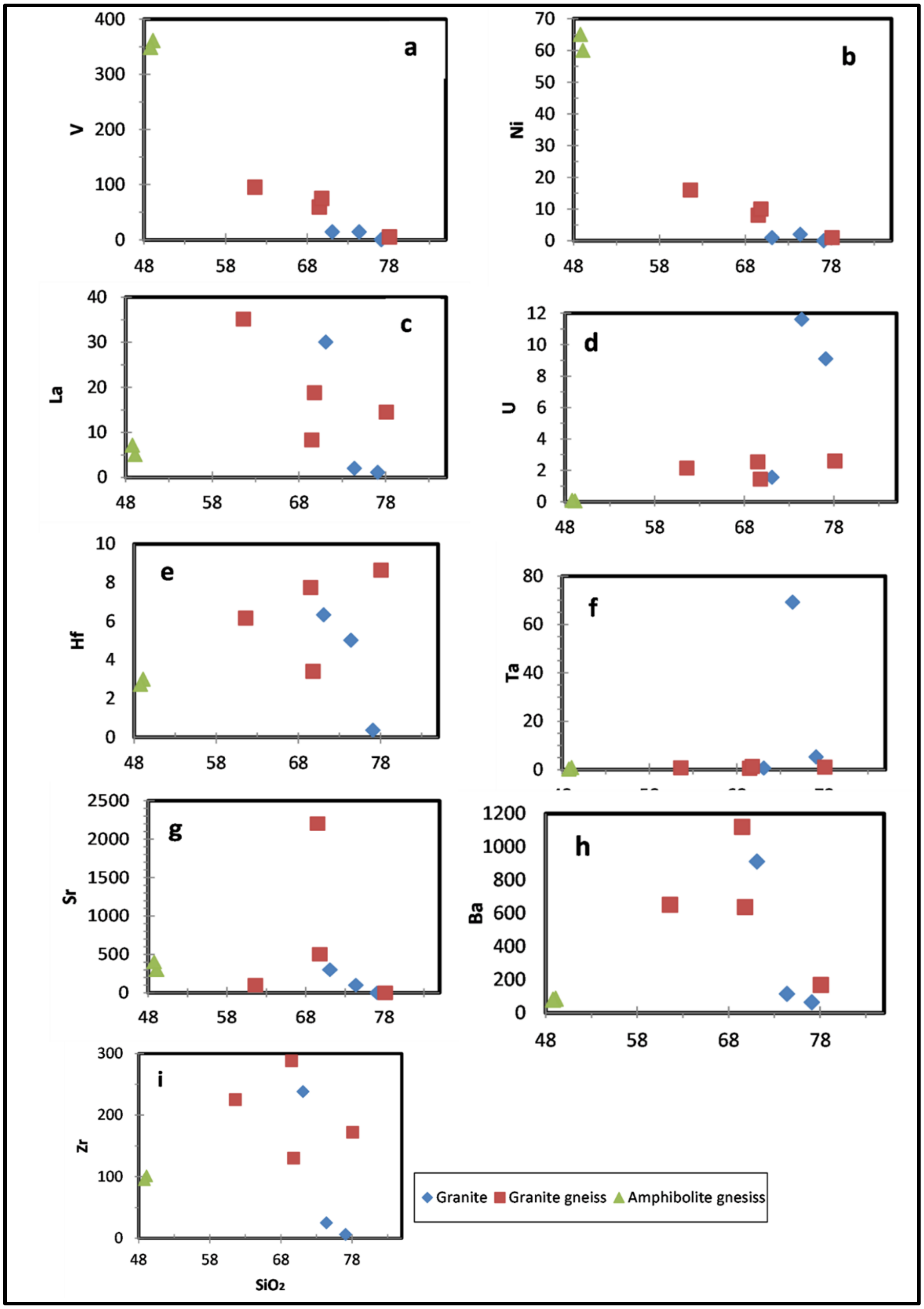

Figure 29: Variation diagram of SiO_2 vs selected trace elements for the studied rocks. The unit for the concentration is in ppm for trace elements and wt.% for the major element (SiO_2.)

4.2.3. Rare Earth Elements Geochemistry

Rare Earth element concentrations of the studied samples were given in detail in Table 1. According to the primitive mantle-normalized REE diagram (Fig. 30A), the granitic gneiss samples exhibit two distinct patterns. The first pattern shows weakly fractionated depletion of HREE with (La/Yb) N values ranging from approximately 5.62 to 12.92. The second pattern shows enriched LREE with (La/Yb) N values around 0.24. The enrichment of LREE and slight depleted pattern in HREE (Fig.30A) indicates fractionations plagioclase or plagioclase left as residual in the source rock. The weakly fractionated REE supports the absence of garnet or Amphibole in the source.

There are no Eu anomalies (Eu/Eu* = 0.89 - 1.07) among the samples, except for sample KSGN3 with a slight negative Eu anomaly (Eu/Eu* = 0.71). The Amphibolite gneiss on the primitive mantle normalized diagram has a very weak fractionation with (La/Yb) N ≈ 1.7 at about of the primitive mantle and no Eu anomaly (Eu/Eu* = 1.01). The enrichment in LREEs and a flat pattern in HREEs are indicative of the acidic properties of the studied rocks. They have a fractionated spectrum showing a very pronounced negative anomaly in Europium (Eu) when samples are normalized concerning the primitive mantle. Europium anomalies may be quantified by comparing the measured concentration (Eu) with an expected concentration obtained by interpolating between the normalized values of Sm and Gd= (Eu*). In the Chondrite-normalized Rare Earth Elements (REEs) spider diagrams (Boynton, 1984), (Fig. 30B) shows overall steep patterns characterized by negative slope with overall enrichment of LREE relative to flat Heavy Rare Earth Elements (HREEs). The studied samples exhibit similar Rare-Earth Elements (REE) distribution patterns.

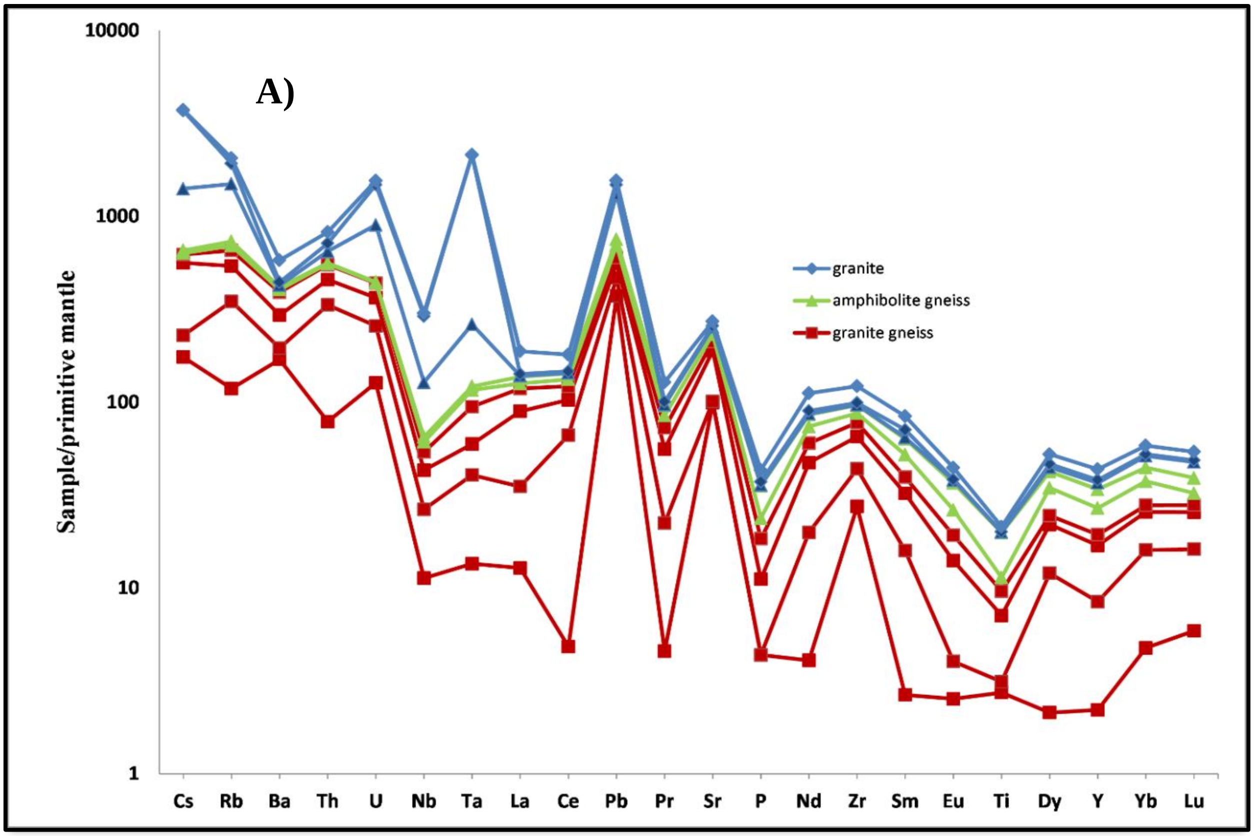
A)
Sample/primitive mantle
10000
1000
100
10
1
granite
amphibolite gneiss
granite gneiss
Cs Rb Ba Th U Nb Ta La Ce Pb Pr Sr P Nd Zr Sm Eu Ti Dy Y Yb Lu

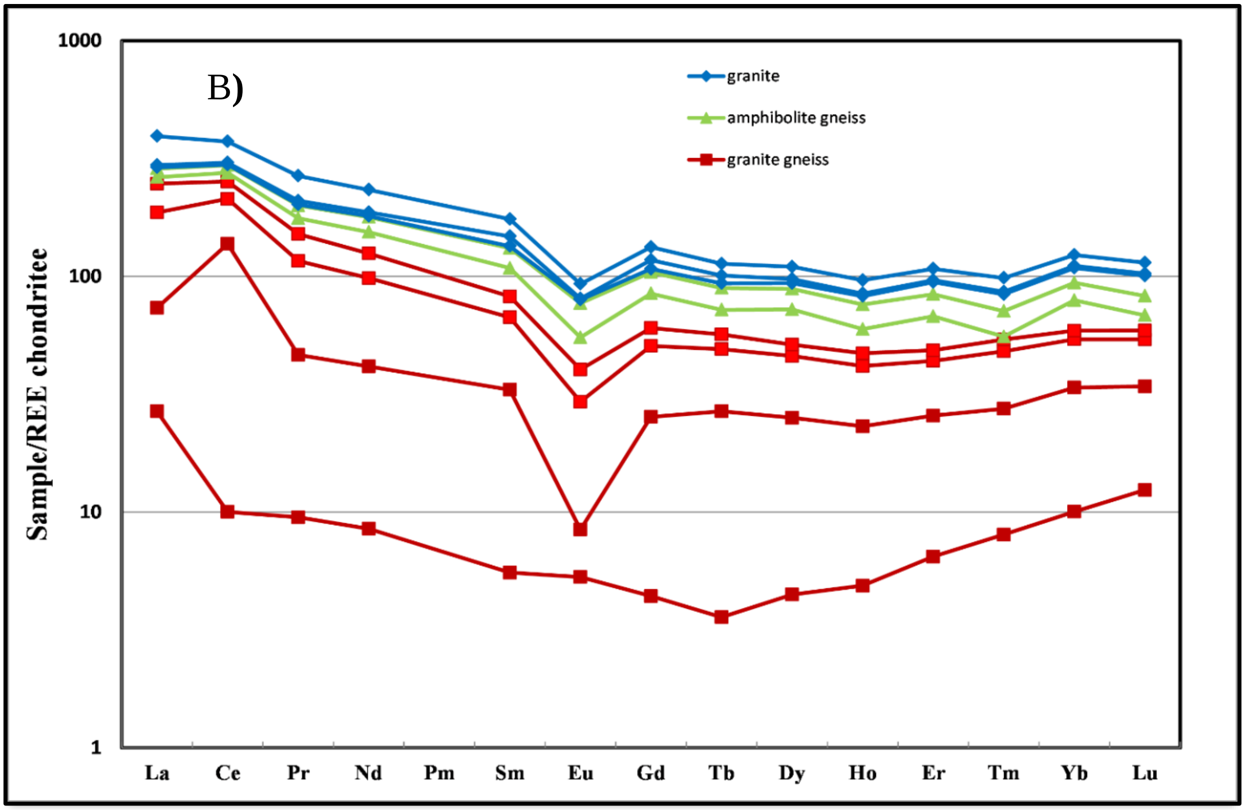

Figure 30: **A)** Primitive mantle-normalized trace elements diagrams from McDonough and Sun (1995). **B)** Chondrite-normalized REE spider diagrams used by Boynton (1984) of the studied rocks.

4.2.4. Protoliths of Metamorphic Rocks

4.2.4.1Alteration and Mobility of Elements

The construction of protoliths in a metamorphic rock requires a systematic study of the mobility of elements during weathering and alteration processes. It is important to assess element mobility before interpreting the protolith of metamorphic rocks. According to Drury (1978), Floyd and Winchester (1978), and Taylor et al. (1986), it is widely accepted that HFSE and REE remain immobile during secondary alteration and metamorphism. Therefore, these elements can be used to determine the origin of metamorphic rocks. The mobility of LILE such as Ba, K, Rb, Th, and U can affect the metamorphic rocks (Smalley et al., 1983; Lan et al., 2014). The assessment of this mobility in metamorphic rocks can be done through K/Rb, Th/U, and La/Th ratios (Shaw, 1968; Rudnick et al., 1985). K/Rb ratios in high-grade metamorphic rocks typically range between 250 and 500, and over 500 when the K concentration is <1 wt% (Rudnick et al., 1985). In un-metamorphosed rocks and shales, these K/Rb ratios are low, at 230 and 200, respectively (Shaw, 1968; Rudnick et al., 1985). The K/Rb ratios of the studied metamorphic rocks in the area fall within the trend of K/Rb observed in granulite rocks (Fig. 31A), indicating significant K and Rb loss.

4.2.4.2. Photolith reconstruction

Thus, LILE samples are relatively unstable and could not be considered for protolith reconstruction. Based on the Al_2O_3 vs. (Na_2O + K_2O) diagram (Wang et al., 1987), it was observed that all the studied metamorphic rocks in the area fall within the field of magmatic rocks as shown in (Fig. 31B). This indicates that the protoliths of these rocks are likely to be igneous in nature. Several discrimination diagrams were utilized to decode the protoliths of different metamorphic rocks, and this particular diagram helped to confirm the igneous protolithic character of the studied rocks. However, KSGN3 exclusively plots outside of the magmatic rocks and also has MgO>CaO, K2O>NaO, and normative corundum >5% deemed to be the sedimentary origin. Winchester (1984) proposed a geological and geochemical approach to distinguish igneous and sedimentary parentage for amphibolite gneiss, by comparing TiO_2 with MnO contents (Fig. 31C). The studied amphibole gneiss sample KSAM12 falls in the field of ortho-amphibolite indicating a magmatic origin whereas sample KSAM11 fall in the field of para-amphibolite indicating sedimentary origin.

4.2.4.3. Source Characteristics

In the Th/Yb vs. Zr/Y plot (Ross and Bédard, 2009), these amphibolite gneisses and granite gneisses show transitional to calc-alkaline affinity (Fig. 31D). The transitional to calc-alkaline affinity of most amphibolite and granite gneisses suggests their source rocks could be linked to subduction zones or volcanic arcs. Subduction zones occur where oceanic crust subducts beneath the continental crust or another oceanic crust. Volcanic arcs are chains of volcanoes formed above these subduction zones due to the melting of the subducted material (Britannica, 2011) Magmas in these subduction zones can have a range of compositions depending on the subduction dynamics and the subducted material's nature. The transitional affinity observed in the plot might reflect this variability in the source magmas for these gneisses.

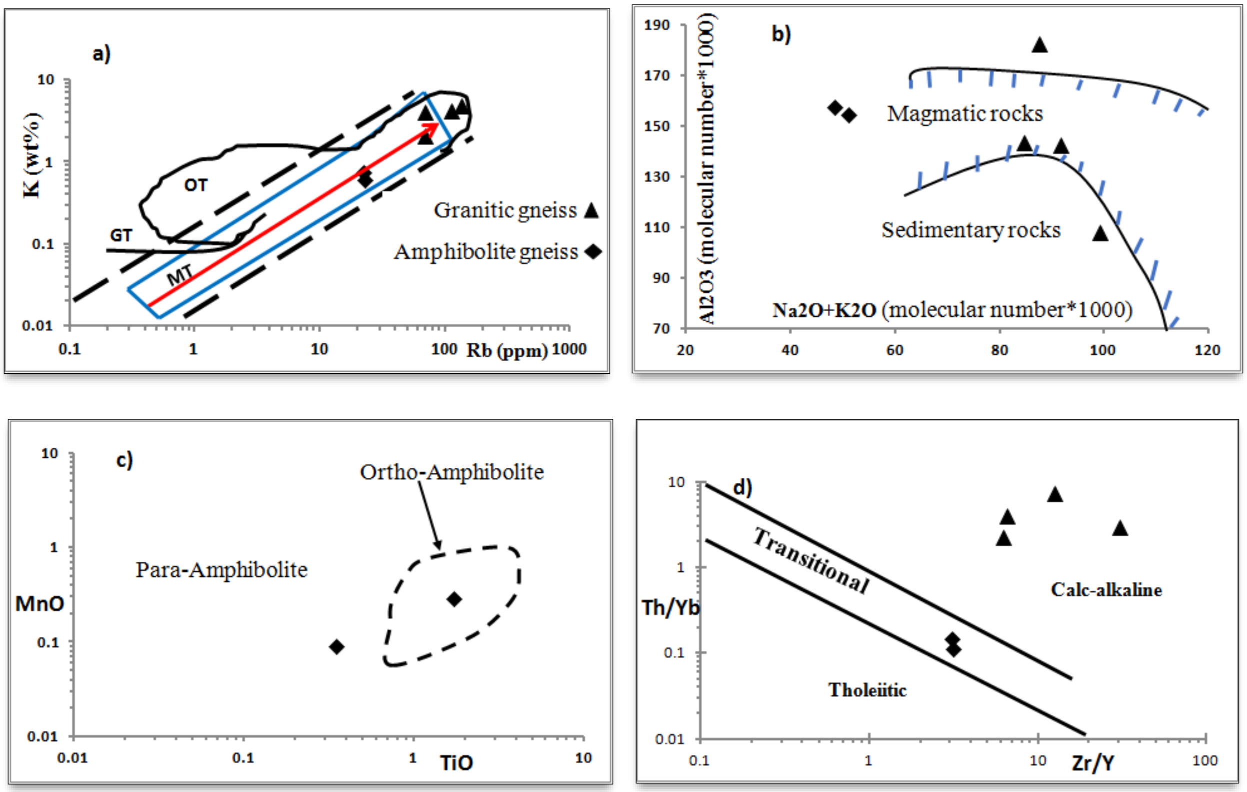

Figure 31: Element mobility and protolith reconstruction diagrams for the Kolme metamorphic rocks. (A) K (wt.%) vs. Rb (ppm) diagram (Rudnick et al., 1985) for element mobility evaluation. MT, main trend obtained from igneous rocks; OT, ocean tholeiite trend; GT, granulite trend. The field surrounding the MT line represents a field of 12 linear regressions averaged by Shaw (1968) to obtain the MT line. (B) Al_2O_3 vs. Na_2O + K_2O diagram for protolith reconstruction (Wang et al., 1987). (C) TiO_2 vs. MnO diagram for the Kolme amphibole gneiss (Winchester, 1984). (D) Th/Yb vs. Zr/Y plot (Ross and Bédard, 2009) .

4.2.5. Tectonic Setting of Intrusive Rock

Several discrimination diagrams of trace elements were used to constrain the tectonic settings of plutonic rocks. Based on the geochemical data, the tectonic-magmatic discriminant diagrams, (Pearce et al.,1984) granites are classified into oceanic ridge granite (ORG), within plate granite (WPG), volcanic arc granite (VAG) and Collisional granite (COLG).

Taking all the tectonic setting discrimination diagrams of the granite (Pearce et al. 1984) all the analyzed samples plotted on three major tectonic settings; the volcanic arc granite (VAG), Syncollisional granite (syn-COLG), and within plate granite (WPG) as shown on (Fig 32**)**. On the Rb-(Y+Nb) and Rb-(Ta+Yb) diagram granite samples were plotted on the volcanic arc granite field, syn –COLG field, and within plate granite (WPG). On the other hand, on the Nb-Y and Ta-Yb binary diagram one granite sample is plotted on the volcanic arc granite (VAG), and two granite sample are plotted on the within plate granite (WPG). In conclusion according to all the above tectonic setting diagrams adopted by (Pearce et al. 1984) all the analyzed samples are plotted on the VAG field and Syn-COLG field, and within plate granite (WPG) indicating that the granite of the study area emplaced during a syn-orogenic event continues to the orogenic events and post-orogenic events (Liu et al., 2019) and indicates the continuation of magmatism after the end of the collisional stage.

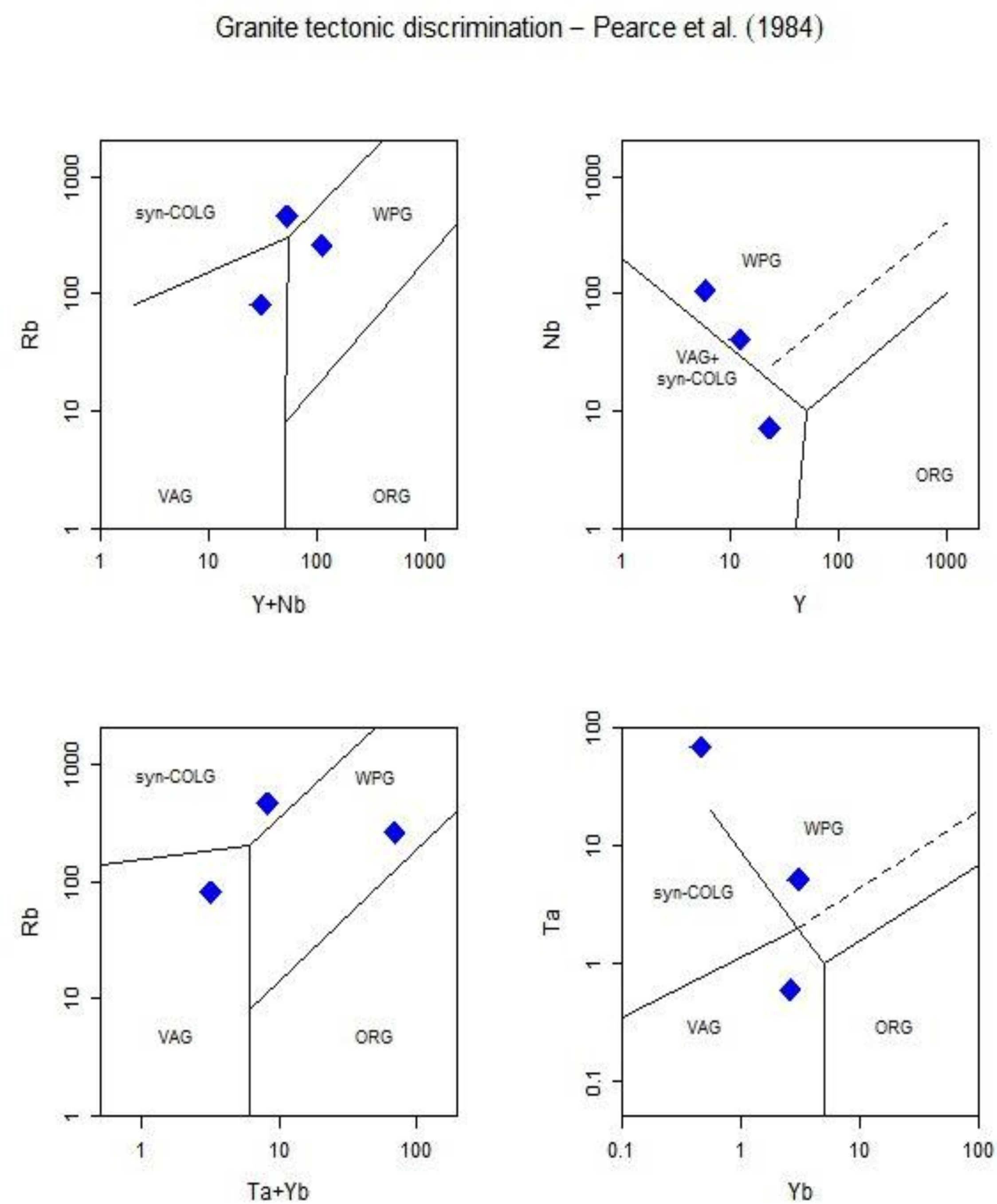

Figure 32: Y+Nb vs Rb; Y vs Nb; Ta+Yb vs Rb, and Yb vs Ta tectonic discrimination diagrams of Pearce et al. (1984). Abbreviations of fields; VAG: volcanic arc granites; WPG: within plate granites; Syn-COLG: Syn-collisional granites; ORG: ocean ridge granites; post-COLG: post-collision granites. All the units are in wt. %

CHAPTER FIVE

5. DISCUSSION

5.1. Fractional Crystallization

The Harker variation diagram is described by using the relationships between the concentration of SiO_2 versus all major oxides wt. % (Fig. 26 a-i) to describe the origin and behavior of magma. Some major oxides such as P2O5, MgO, CaO, Al2O3, TiO2, and Feo_t (Fig.26 a, c, d, f, g, h) show a decreasing trend with increasing SiO2 suggesting commencement of plagioclase fractionation or magmatic differentiation trends (Clarke et al., 2005). Other major oxides such as Na_2O and K_2O show a positive correlation with SiO_2 even if they are scattered. Their low concentration of compatibility with most of them below the detection limit and high SiO2 content indicates the rock has evolved from a depleted mantle source. Furthermore, Hf, Sr, La, and Ba show an appositive trend with SiO_2 which suggests that they have not been affected by metamorphism and hydrothermal alteration processes as shown in (Fig. 29). There is a negative correlation between Ni and V with SiO_2. This suggests that these elements were concentrated during the early fractionation of ferromagnesian minerals such as olivine, clinopyroxene, and spinel (Alene et al. 2000). On the primitive mantle-normalized rare earth elements diagram the two samples (KSGN3, KSGN5) show a weak fractionation of REE indicating the garnet-free source. Those samples also have relatively negative Eu anomaly (0.71- 0.89**)** and proportionally higher Sr concentration indicating the absence of plagioclase fractionation. Plagioclase is the main phase that controls Sr concentrations and Eu anomalies in granitoids (Springer and Seck, 1997). On the same diagram, the Amphibole gneiss shows a very low fractionation of REE with 10x concentrations of the primitive mantle showing the absence of garnet in the source. Negative anomalies of Nb, P, and Ti are considered to be a characteristic feature of a subduction-related environment. Most of the granite has negative Eu anomaly in the RRE primitive mantle normalized diagram (Fig. 30a). These Eu anomalies suggest fractionation of plagioclase or plagioclase left as residual in the source rock. The weakly fractionated REE supports the absence of garnet or Amphibole in the source.

5.2. Mantle Source Characteristics

The geochemical signatures of the studied samples suggest contributions from two distinct mantle sources (Fig. 30a & b). the patterns in the plots resemble those of enriched mid-ocean ridge basalts (E-MORB) and ocean island basalts (OIB) (Sun and McDonough, 1989). This is supported by the enrichment of the samples in large ion lithophile elements (LILEs, e.g., Pb, Sr) and moderate-to-high abundances of light rare earth elements (LREEs) in the primitive mantle-normalized plot. These features are difficult to reconcile solely with a depleted mid-ocean ridge basalt (MORB) source. The same plot (Fig. 30) also reveals a significant depletion in high-field strength elements (HFSEs, e.g., Nb, Ta, Ti). This, along with the negative anomalies for Nb, Pr, and Ti, is a hallmark of subduction-related granites (Pearce et al., 1984; Condie, 1998). This suggests varying degrees of magma contamination during subduction events, contributing to the compositional variations observed in the granite samples. Further supporting this idea, the La/Nb ratio for most samples is greater than 1 (De Paolo and Daley, 2000). Therefore, the compositional variation of the granite samples is possibly caused by varying contamination of magma in subduction-related tectonics. Similarly, De Paolo and Daley (2000) suggest that the ratio of La/Nb is ~0.24 for the asthenosphere source, and if the ratio is > 1, it indicates a lithospheric source. Therefore, it is concluded that the geochemical data based on trace element variation of rocks, which are alternating in the lithological sequence, suggest two different sources, a lithospheric mantle, and an asthenosphere mantle.

5.3. Degree of Partial Melting and Depth of Melting

The composition of rare earth elements (REEs) in rocks helps to understand the conditions under which the rock formed in the Earth's mantle (Lassiter et al., 1995). The key lies in how much melting occurred (degree of partial melting) and the type of mineral present spinel or garnet in the mantle source region (Furman et al., 2016). These minerals play a crucial role because they preferentially incorporate certain REEs. Garnet, for example, tends to grab onto heavy REEs like Yb, while leaving lighter REEs like La and mid-range REEs like Sm and Gd behind. This selective behavior affects the ratios of these elements (La/Yb and Sm/Yb) in the resulting melt (Rollinson, 1993). Therefore, using the ratios of certain elements within rocks (like La/Yb or Tb/Yb) to estimate the depth at which those rocks formed (Ayalew et al., 2016; Dostal et al., 2019). Generally, higher ratios indicate deeper formation. In this study, samples KSG9 and KSG10 have higher La/Yb of 2.96-7.85, and Tb/Yb ratios compared to KSG8 is 0.24, suggesting that the KSG9 and KSG10 samples originated at a relatively greater depth than the KSG8 samples. Furthermore, the relative abundance of rare earth elements (REEs) is influenced by the rock's source material and can indicate the presence of specific minerals like garnet or spinel (Furman et al., 2016).

5.4. Crustal Contamination

The studied samples exhibit a significant enrichment in light rare earth elements (LREEs) and highly incompatible trace elements. This enrichment could be attributed to two possible origins: Magma interacting with continental crust during its ascent can become enriched in these elements (Thompson, 1984; Dereje Ayalew et al., 1999). The mantle source itself may have been inherently enriched in LREEs and incompatible elements (e.g., similar to sources of ocean island basalts, OIBs). The La/Nb ratio is a key indicator of crustal contamination. The specific La/Nb ratio for the studied area indicates slight contamination (Thompson,1984). Accordingly, samples KSG8 and KSG9 have high values of the Nb/La ratio of Nb/La of 37.5 and 53.5 respectively whereas sample KSG10 is 0.24. This shows that sample KSG10 is affected by crustal material, however; samples KSG8 and KSG9 are not affected by crustal contamination.

Magma rising through thick continental crust, especially in slow-spreading rift zones, is more susceptible to contamination (Furman, 2007). This is because slower magma ascent allows for longer interaction with the crust, increasing the chance of material incorporation. Crustal contamination can occur through several mechanisms: Bulk assimilation: Magma physically incorporates chunks of crustal rock. Assimilation of partial melts: Magma absorbs melted portions of the crust.

Selective element exchange: Fluids transfer specific elements from the crust to the magma (Rollinson, 1993). Distinguishing between crustal contamination and an enriched mantle source for high levels of light rare earth elements (LREEs) and incompatible elements in the analyzed samples can be challenging (Thompson, 1984). Additionally, negative anomalies of some use variations in certain incompatible elements in the primitive mantle-normalized multi-element variation diagrams (Fig. 30a**)** Nb, Ce, Pr as tracers to identify crustal contamination present during magma formation of the study area. These variations reflect processes like magma-crust interaction, crustal recycling, and subduction (Pearce, 2008). Notably, depletion of (Nb) and (Ti) is a signature of arc magmas, continental crust, and crustal sediments (Taylor & McLennan, 1995).

CHAPTER SIX

6. CONCLUSION AND RECOMMENDATION

6.1. Conclusion

Based on the combination of the field, petrographic, and geochemical results, the metamorphic and associated intrusive igneous rocks of the study area have been well discussed. Thus, the study area is covered by medium to high-grade metamorphic rocks (granitic-gneiss, amphibole gneiss, biotite gneiss, and unmappable mica schist units at the scale of 1:25,000) and associated intrusive igneous rocks (granite unit).

The gneiss rock units clearly show the segregation of mafic and felsic-rich compositional banding. The petrographic microscope perceptibly displays hornblende, biotite, microcline, plagioclase with a lesser amount of sericite, and opaque minerals as the dominant mineral assemblage in the area. From the field investigation and structural measurement, the study area is characterized by various geological structures (ductile, brittle) formed by tectonic processes operating throughout the earth's history including foliation, folds, joints, dikes, veins, boudinage, and veinlets.

According to the AFM plot diagram, the Kholme granitic gneisses are primarily displayed on the Calc-alkaline series, except for one sample that falls under the tholeiitic series. Hence, the amphibole gneiss displays on the tholeiitic series. The high LILE relative to HFSE in gneisses and granitoids points to the subduction-zone enrichment and/or crustal contamination of the source region. On the REE diagram, the amphibole gneiss shows a very low fractionation of REE with 10x concentrations of the primitive mantle thus, showing the absence of garnet in the source. The Al_2O_3 vs. (Na_2O + K_2O) diagram (Wang et al., 1987), shows the metamorphic rocks in the study area fall in the field of magmatic rocks suggesting their igneous protolithic character. Yet, the KSGN3 sample exclusively displays outside of the magmatic rocks and it is considered to be of a sedimentary origin.

Petrographically, the studied granite rock samples are mainly composed of K-feldspar (microcline), quartz, plagioclase, and biotite besides constituting some accessory minerals such as apatite and opaque. The overall geochemical characteristics of the granite rock units in the study area are characterized by high K, Calk-Alkaline series, and peraluminous affinity. Moreover, on the chondrite normalized REE abundance plot, the granite rock relatively shows slight to moderate enrichment of light rare earth elements (LREE) and flat heavy rare earth elements (HREE) patterns. Thus, the tectonic setting of granite rocks in the area is typical of intrusion in a destructive plate margin. The enrichment in LREEs and a flat pattern in HREEs are indicative of the acidic properties of the studied rocks. The fractionated spectrum shows a very pronounced negative Europium (Eu) anomaly when samples are normalized with respect to the primitive mantle. The discrimination diagrams of Rb-(Y+Nb), Ta-Yb, Rb-(Y+Nb), and Nb-Y suggest the granite rock units were developed in a volcanic arc and syn-COLG tectonic setting environment. Except for one sample which was positioned in the field of within plate granite (WPG).

6.2 Recommendation

The present study has addressed the petrogenetic evolution, geochemical characteristics, tectonic setting, and protolith of the area based on field observation, petrographic description, and geochemical data interpretation. However, to fully understand the metamorphic history and associated intrusive rocks of the Konso, Kholme area, it needs further investigation. Therefore, the following studies are recommended for future work.

- A detailed Geothermobarometric study of minerals is needed to determine the pressure and temperature conditions in which the rocks formed.
- Isotopic geochemistry analysis is required to clarify the petrogenesis, source rock of metamorphic rock, and dating. For example, stable isotopes are geochemical tracers, which are used for evolution, geochronologic history, and alteration in addition to the petrographic and geochemical analysis.
- Studies on mineral chemistry are also required to determine the qualitative and quantitative mineral composition of the rock.
- It is recommended that in the study area, more detailed integrated geophysical methods should be employed and borehole logging data needed for correlation.

REFERENCE

Abbate, E., Bruni, P. and Sagri, M. (2015). Geology of Ethiopia: A Review and Geomorphological Perspectives, *Springer Netherlands*, 33-64pp.

Abdelsalam, M. G., & Stern, R. J. (1996). Sutures and shear zones in the Arabian-Nubian Shield. *Journal of African Earth Sciences*, *23*(3), 289-310.

Abraham, A. (1996). The Precambrian of southern Ethiopia. Unpublished Ep., EIGS, Addis Ababa, Note No. 397, 6pp.

Alene, M., & Barker, A. J. (1993). Tectonometamorphic evolution of the Moyale region, southern Ethiopia. *Precambrian research*, *62*(3), 271-283.

Almond D.C. (1983). The concept of the Pan African Episode and Mozambique belt, in relation to the geology of East and Northeast Africa. King Abdulaziz University, Jeddah, Saudi Arabia. Faculty of Earth Science Bulletin 6, 71-78.

Asrat, A., & Barbey, P. (2003). Petrology, geochronology and Sr–Nd isotopic geochemistry of the Konso pluton, south-western Ethiopia: implications for transition from convergence to extension in the Mozambique Belt. *International Journal of Earth Sciences*, *92*, 873-890..

Asrat, A., Barbey, P., & Gleizes, G. (2001). The Precambrian geology of Ethiopia: a review. *Africa Geoscience Review*, *8*(3/4), 271-288.

Avigad, D., & Gvirtzman, Z. (2009). Late Neoproterozoic rise and fall of the northern Arabian–Nubian Shield: the role of lithospheric mantle delamination and subsequent thermal subsidence. *Tectonophysics*, *477*(3-4), 217-228.

Ayalew, D., Jung, S., Romer, R. L., Kersten, F., Pfänder, J. A., & Garbe-Schönberg, D. (2016). Petrogenesis and origin of modern Ethiopian rift basalts: Constraints isotope and trace element geochemistry. *Lithos, 258, 1-14*

Ayalew, D., Yirgu, G., & Pik, R. (1999). Geochemical and isotopic (Sr, Nd and Pb) characteristics of volcanic rocks from southwestern Ethiopia. *Journal of African Earth Sciences*, *29*(2), 381-391.

Ayalew, T., Bell, K., Moore, J. M., & Parrish, R. R. (1990). U-Pb and Rb-Sr geochronology of the western Ethiopian shield. *Geological Society of America Bulletin*, *102*(9), 1309-1316.

Behrmann, J. H. and Weldehaimanot, B. (1995). A study of metabasite and Meta granite chemistry in Adola region (South Ethiopia): Implication for the evolution of East African Orogeny *Afr Earth Sic* 21:459-476.

Berhe, S. M. (1990). Ophiolites in Northeast and East Africa: implications for Proterozoic crustal growth. *Journal of the Geological Society*, *147*(1), 41-57.

Blades, M. L., Collins, A. S., Foden, J., Payne, J. L., Xu, X., Alemu, T., ... & Taylor, R. J. (2015). Age and hafnium isotopic evolution of the Didesa and Kemashi Domains, western Ethiopia. *Precambrian Research*, *270*, 267-284.

Bonavia, F. F., & Chorowicz, J. (1992). Northward expulsion of the Pan-African of northeast Africa guided by a reentrant zone of the Tanzania craton. *Geology*, *20*(11), 1023-1026.

Britannica,T.(2011,June29).Subductionzone.Retrievedfromhttps://www.britannica.com/science/subduction-zone

Burke, K., & Sengör, C. (1986). Tectonic escape in the evolution of the continental crust. *Reflection seismology: the continental crust*, *14*, 41-53.

Davidson, A. (Compiler), (1983). Reconnaissance geology and geochemistry of parts of Illubabor, Keffa, Gemu Gofa, and Sidamo Ethiopia. *Ethiopian Institution of Geological Surveys*, 89p.

De Wit, M. J., & Chewaka, S. (1981). Plate tectonic evolution of Ethiopia and the origin of its mineral deposits: an overview. *Plate tectonics and metallogenesis: some guidelines to Ethiopian mineral deposits. Abbis Ababa, Ethiopian Institute of Geological Survey*, 115-129.

Dostal, J., Keppie, J. D., & Church, B. N. (2019). Generation of E ocene volcanic rocks from the C ordilleran arc of south-central B ritish C olumbia (C anada) during subduction of the F arallon and R esurrection plates and Y ellowstone oceanic plateau. *Geological Journal*, *54*(1), 590-604.

Fritz, H., Abdelsalam, M., Ali, K. A., Bingen, B., Collins, A. S., Fowler, A. R., ... & Viola, G. (2013). Orogen styles in the East African Orogen: A review of the Neoproterozoic to Cambrian tectonic evolution. *Journal of African Earth Sciences*, *86*, 65-106.

Furman, T., Nelson, W. R., & Elkins-Tanton, L. T. (2016). Evolution of the East African rift: Drip magmatism, lithospheric thinning and mafic volcanism. *Geochimica et Cosmochimica Acta*, *185*, 418-434.

Ghebreab, W. (1992). The geological evolution of the Adola Precambrian greenstone belt, southern Ethiopia. *Journal of African Earth Sciences (and the Middle East)*, *14*(4), 457-469.

Gichile, S. (1991). *Structure, metamorphism and tectonic setting of a gneissic terrane, the Sagan Afelata area, southern Ethiopia*. University of Ottawa (Canada).

Gichile, S. (1992). Granulites in the Precambrian basement of southern Ethiopia: geochemistry, PT conditions of metamorphism and tectonic setting. *Journal of African Earth Sciences (and the Middle East)*, *15*(2), 251-263.

Hargrove, U. S., Stern, R. J., Kimura, J. I., Manton, W. I., & Johnson, P. R. (2006). How juvenile is the Arabian–Nubian Shield? Evidence from Nd isotopes and pre-Neoproterozoic inherited zircon in the Bi'r Umq suture zone, Saudi Arabia. *Earth and Planetary Science Letters*, *252*(3-4), 308-326.

Illubabor, Kefa, Gemu Gofa, and Sidamo, Ethiopia. The Omo River Project. Ethiopian Institute of Geological Surveys, Bulletin 2. Addis Ababa.

Kazmin, V. (1972). Some aspects of Precambrian development in East Africa. *Nature*, *237*(5351), 160-160.

Kazmin, V., (1975). The Precambrian of Ethiopia and some aspects of the geology of the Mozambique Belt. *Geophysical Observatory* Bulletin, vol. 1. Addis Ababa, Ethiopia, 14 p.

Kazmin, V., (1979). Stratigraphy and correlation of volcanic rocky in Ethiopia. Ethiopian Institute of Geological Surveys, Note No. 106, 26p.

Kazmin, V., Shifferaw, A., & Balcha, T. (1978). The Ethiopian basement: stratigraphy and possible manner of evolution. *Geologische Rundschau*, *67*, 531-546.

Key, R. M., Charsley, T. J., Hackman, B. D., Wilkinson, A. T., & Rundle, C. C. (1989). Superimposed Upper Proterozoic collision-controlled orogenies in the Mozambique orogenic belt of Kenya. *Precambrian Research*, *44*(3-4), 197-225.

Kroner, A. and Stern, RJ. (2004). Pan-African Orogeny, Encyclopedia of Geology, Elsevier, map of Ethiopia. Ethiopian Institute of Geological Surveys, Addis Ababa, Ethiopia, 1:1–12.

Lai, S., Qin, J., Li, Y., Li, S. and Santosh, M. (2012). Permian high Ti/Y basalts from the eastern part of the Emeishan Large Igneous Province, southwestern China: petrogenesis and tectonic implications. *Journal of Asian Earth Sciences*, **47**: 216-230

Lassiter, J.C., DePaolo, D.J. and Mahoney, J.J. (1995). Geochemistry of the Wrangellia Flood Basalt Province: implications for the role of continental and oceanic lithosphere in Flood Basalt Genesis. *Journal of Petrology,* **36**: 983-1009.

Liu, X., Liu, W., Si, C., 2019. Petrogenesis and source rocks of the high-K calc-alkaline and shoshonitic I-type granitoids in the northwestern part of East Junggar, NW China. Lithos 326–327, 298–312. https://doi.org/10.1016/j.lithos.2018.12.033.

Meert, J. G. (2003). A synopsis of events related to the assembly of eastern Gondwana. *Tectonophysics*, *362*(1-4), 1-40.

Mengesha, T., Tadiwos, C. and Workneh, H. (1996). The Geological Map of Ethiopia, 1:2,000,000 scale, (2nd eds), EIGS, Addis Ababa.

Mohr, P. (1967)., Ethiopian rift system. Bull. *Geophys. Obs.* Addis Ababa 11,1-65.

Robinson, F, Foden, J, Collins, A, Payne, J., (2014). Arabian Shield magmatic cycles and their relationship with Gondwana assembly: insights from zircon U–Pb and Hf isotopes. *Earth Planet Sci*.408: 207-225.

Rollinson H. (1993). Using geochemical data: evaluation, presentation, interpretation. *Pearson, prentice hall*, 380pp.

Rooney, T., Furman, T., Bastow, I., Ayalew, D., & Yirgu, G. (2007). Lithospheric modification during crustal extension in the Main Ethiopian Rift. *Journal of Geophysical Research: Solid Earth*, *112*(B10).

Shackleton, R. M. (1978). Precambrian tectonics of north-east Africa. *Evolution and mineralization of the Arabian-Nubian Shield*, *2*, 1-6.

Solomon, G., (2000). A short introduction to the geology of Ethiopia, *Chronique de la Recherche* minerals Na 540, 2000, 3-10**.**

Stern, R. J. (1994). Arc assembly and continental collision in the Neoproterozoic East African Orogen: implications for the consolidation of Gondwanaland. *Annual review of earth and planetary sciences*, *22*(1), 319-351.

Stern, R. J. (2002). Crustal evolution in the East African Orogen: a neodymium isotopic perspective. *Journal of African Earth Sciences*, *34*(3-4), 109-117.

Stern, R. J., Avigad, D., Miller, N. R., & Beyth, M. (2006). Evidence for the snowball Earth hypothesis in the Arabian-Nubian Shield and the east African Orogen. *Journal of African Earth Sciences*, *44*(1), 1-20.

Stoeser, D. B., & Frost, C. D. (2006). Nd, Pb, Sr, and O isotopic characterization of Saudi Arabian shield terranes. *Chemical Geology*, *226*(3-4), 163-188.

Tadesse, A., and Tsegaye, A., (2007). Geology and Tectonic Evolution of the Pan-African of the Pan-African Tulu Dimtu Belt, Western Ethiopia. *Online Journal of Earth Sciences,* 1:24-42.

Tadesse, Y., (2003). Chemical Th-U-total Pb Isochron Ages of Zircon & Monazite from Granitic Rocks of the Negele Area, Southern Ethiopia. Geological Survey of Ethiopia.

Taylor, S.R. and McLennan, S.M. (1985). The Continental Crust: Its Composition and Evolution. Oxford. *Blackwell Scientific publications, London*, 312 p.

Teklay, M., Kröner, A., Mezger, K., & Oberhänsli, R. (1998). Geochemistry, Pb□ Pb single zircon ages and Nd□ Sr isotope composition of Precambrian rocks from southern and eastern Ethiopia: implications for crustal evolution in East Africa. *Journal of African Earth Sciences*, *26*(2), 207-227.

Thompson, R. N., Morrison, M. A., Hendry, G. L., & Parry, S. J. (1984). An assessment of the relative roles of crust and mantle in magma genesis: an elemental approach. *Philosophical*

Transactions of the Royal Society of London. Series A, Mathematical and Physical Sciences, *310*(1514), 549-590.

Vail, J. R. (1985). Pan-African (late Precambrian) tectonic terrains and the reconstruction of the Arabian-Nubian Shield. *Geology*, *13*(12), 839-842.

Warden, A. J., & Horkel, A. D. (1984). The geological evolution of the NE-branch of the Mozambique Belt (Kenya, Somalia, Ethiopia). *Aust. J. Earth Sci*, *77*, 161-184.

Worku, H. (1996). Structural control and metamorphic setting of the shear zone-related Au vein mineralization of the Adola Belt (southern Ethiopia) and its tectono-genetic development. *Journal of African Earth Sciences*, *23*(3), 383-409.

Worku, H., & Yifa, K. (1992). The tectonic evolution of the Precambrian metamorphic rocks of the Adola Belt (southern Ethiopia). *Journal of African Earth Sciences (and the Middle East)*, *14*(1), 37-55.

Yaxley, G. M. (2000). Experimental study of the phase and melting relations of homogeneous basalt+ peridotite mixtures and implications for the petrogenesis of flood basalts. *Contributions to Mineralogy and Petrology*, *139*(3), 326-338.

Yibas, B., Reimold, W. U., & Anhaeusser, C. R. (2000). The geology of the Precambrian of southern Ethiopia: I—the tectonostratigraphic record. Information Circular 344. *Economic Geology Research Institute, University of the Witwatersrand, Johannesburg*.

Yibas, B., Reimold, W. U., Armstrong, R., Koeberl, C., Anhaeusser, C. R., & Phillips, D. (2002). The tectonostratigraphic, granitoid geochronology and geological evolution of the Precambrian of southern Ethiopia. *Journal of African Earth Sciences*, *34*(1-2), 57-84.

APPENDICES

Appendix 1: Location of rock samples

No	Sample code	Sample name	Location		Elevation (m)
			Easting (m)	Northing(m)	
1	KSGN1	Kholme granite gneiss1	293895	580454	788
2	KSGN2	Kholme granite gneiss 2	303502	580402	1019
3	KSGN3	Kholme granite gneiss3	297382	578172	1270
4	KSGN5	Kholme granite gneiss5	300996	579109	1140
5	KSG8	Kholme granite8	300239	580066	1107
6	KSG9	Kholme granite9	279560	579257	1277
7	KSG10	Kholme granite0	305229	581571	1327
8	KSAM11	Kholme amphibole gneiss11	303087	580270	1000
9	KSAM12	Kholme amphibole gneiss 12	303489	579388	1021
10	KSBN4	Kholme biotite gneiss4	298646	579257	1254
11	KSBN6	Kholme biotite gneiss	301268	579483	1093
12	KSM13	Kholme mica schist	301401	580479	1111

Appendix 2: Geological Structural Measurements

Geological Structure Measurements					
Geological Structure	Location			Orientation	
	Northing	Easting	Elevation	Strike	Dip

Foliation						
1	Foliation	305229	580490	1327	N15W	75NE
2	Foliation	304241	580495	1181	105	NE
3	Foliation	303500	580403	1018	S50W	40SE
4	Foliation	303502	580402	1016	N20E	70SE
5	Foliation	303062	580442	1012	N70E	20NW
6	Foliation	303087	580270	1000	090	N
7	Foliation	303872	579479	1110	N-S	E
8	Foliation	301405	580499	1108	S20W	70NW
9	Foliation	301444	580184	1072	N-S	W
10	Foliation	301444	580184	1072	E-W	N
11	Foliation	301710	579831	1051	N70E	20NW
12	Foliation	301728	579733	1067	S50E	40NE
Pegmatite Dyke and Pegmatite vein						
1	Pegmatite Dyke	305229	580491	1327	N15W	75NE
2	Pegmatite Dyke	301314	579626	1070	S20W	70SE
3	Pegmatite Dyke	300720	580184	1066	N20W	70SW
4	Pegmatite Dyke	299973	580213	1175	S30W	60NW
5	Pegmatite Dyke	298972	579481	1306	S50W	40NW
6	Pegmatite Dyke	298700	579384	1268	S80W	10NW
7	Pegmatite Dyke	297560	578474	1277	S75W	15NW
8	Pegmatite Dyke	298252	578908	1246	S60W	30SE
9	Pegmatite Dyke	293421	580331	774	N40E	50NW
10	Pegmatite Vein	301410	579662	1064	260	NW
11	Pegmatite vein	297817	580047	1273	N40E	50SW

Quartz Vein						
1	Quartz Vein	298652	579263	1259	S45W	45NW
2	Quartz vein	297424	578326	1263	S60W	30SE
3	Quartz vein	297817	580047	1273	N40E	50SW
4	Quartz vein	300654	580468	1016	N40W	50NE
5	Quartz vein	300278	577835	804	N70W	20NE
6	Quartz vein	300234	577823	810	N30W	60SW
Joint						
1	Joint	302865	580277	990	5cm	1.5m
2	Joint	302601	579919	980	5cm	1.5m
3	**Boudinage**	303062	580442	1012	N-S	
Fold						
1	Fold Limb1	301410	579662	1064	N40W	50NE
	Fold Limb2	301410	579662	1064	N40E	50NW
	Fold (Lineation)	301410	579662	1064	N20E	10
2	Fold Limb1	298652	579263	1259	S45W	45SE
	Fold Limb2	298652	579263	1259	S45W	45NW
	Fold (Lineation)	298652	579263	1259	S45W	40
3	Fold Limb1	294920	577653	597	N40E	50NW
	Fold Limb2	294920	577653	597	S60W	30NW
	Fold (Lineation)	294920	577653	597	N20E	70
4	Fold Limb1	294920	577653	597	N70W	20NE
	Fold Limb2	294920	577653	597	S70W	20NW

	Fold (Lineation)	294920	577653	597	N80W	10

Appendix 3: Total iron

Fe_2O_3	FeO	FeOt
4.53	4.077	8.607
1.62	1.458	3.078
7.36	6.624	13.984
4.16	3.744	7.904
11.8	10.62	22.42
13	11.7	24.7
1.21	1.089	2.299
1.07	0.963	2.033
2.71	2.439	5.149
	= 0.9* **Fe_2O_3i**	= **Fe_2O_3 + FeO**